First phytoplankton community assessment of the Kong Håkon VII Hav, Southern Ocean during austral autumn

Hanna M. Kauko[1], Philipp Assmy[1], Ilka Peeken[2], Magdalena Różańska[3], Józef M. Wiktor[3], Gunnar Bratbak[4], Asmita Singh[5,6], Thomas J. Ryan-Keogh[5], Sebastien Moreau[1]

[1] Norwegian Polar Institute, Fram Centre, Tromsø, Norway

[2] Alfred Wegener Institute Helmholtz Centre for Polar and Marine Research, Bremerhaven, Germany

[3] Institute of Oceanology, Polish Academy of Sciences, Sopot, Poland

[4] Department of Biological Sciences, University of Bergen, Bergen, Norway

[5] Southern Ocean Carbon- and Climate Observatory (SOCCO), Council for Scientific and Industrial Research (CSIR), Cape Town, South Africa

[6] Department of Earth Sciences, Stellenbosch University, Stellenbosch, South Africa

Correspondence: Hanna M. Kauko, hanna.kauko@npolar.no; hanna.kauko@alumni.helsinki.fi

Key words: phytoplankton, chemotaxonomy, biodiversity, Weddell Gyre, carbon and silicon cycles

Key points:

1) A typical Southern Ocean open ocean phytoplankton community dominated by heavily silicified diatoms was observed in the Kong Håkon VII Hav in autumn 2019
2) Blooms dominated by the diatom *Chaetoceros dichaeta* were observed in two of the sampling areas
3) The other areas, mainly in a post-bloom phase, had high relative contribution from flagellates, predominantly from the Chl *c* -lineage

Abstract

We studied phyto- and protozooplankton community composition based on light microscopy, flow cytometry and photosynthetic pigment data in the Atlantic sector of the Southern Ocean during March 2019 (early austral autumn). Sampling was focused on the area east of the prime meridian in the Kong Håkon VII Hav, including Astrid Ridge, Maud Rise and a south-north transect at 6° E. Phytoplankton community composition throughout the studied area was characterized by oceanic diatoms typical of the iron-deplete High-Nutrient Low-Chlorophyll (HNLC) Southern Ocean. Topography and wind-driven iron supply likely sustained blooms dominated by the centric diatom *Chaetoceros dichaeta* at Maud Rise and at a station north of the 6° E transect. For the remainder of the 6° E transect diatom composition was similar to the previously mentioned bloom stations but flagellates dominated in abundance suggesting a post-bloom situation and likely top-down control by krill on the bloom-forming diatoms. Among flagellates, species with haptophyte-type pigments were the dominating group. At Astrid Ridge, overall abundances were lower and pennate were more numerous than centric diatoms, but the community composition was nevertheless typical for HNLC areas. The observations described here show that *C. dichaeta* can form blooms beyond the background biomass level and fuels both carbon export and upper trophic levels also within HNLC areas. This study is the first thorough assessment of phytoplankton communities in this region and can be compared to other seasons in future studies.

1. Introduction

Phytoplankton play an important role for marine food webs and biogeochemical cycles as primary producers and important mediators of the biological carbon pump. They are represented by a vast diversity of species that occupy various ecological niches and play different ecological and biogeochemical roles, with diatoms and haptophytes generally the main bloom-forming taxa at high latitudes (Arrigo et al., 1999; Assmy et al., 2013; Deppeler and Davidson, 2017; Tréguer et al., 2018). Hence, for a full characterization of an ecosystem and its biogeochemical function, it is important to investigate the phytoplankton species composition.

In the Southern Ocean, phytoplankton communities have been coarsely divided into two broad categories (Smetacek et al., 2004). Communities characteristic of iron-replete regions such as in coastal polynyas and near the Antarctic Peninsula and subantarctic islands (e.g. Blain et al., 2007; Pollard et al., 2009) are dominated by bloom forming species with a 'boom and bust' life cycle and high carbon export, and largely composed of weakly-silicified diatoms and *Phaeocystis antarctica*. The iron-limited High-Nutrient Low-Chlorophyll (HNLC) areas of the Antarctic Circumpolar Current (ACC) on the other hand are characterized by communities dominated by heavily silicified diatoms that largely drive the selective export of silicon (Assmy et al. 2013). Hence the impact on biogeochemical cycles differs dramatically depending on phytoplankton community composition. It however needs to be noted that within the diatom community representative of the iron-limited ACC certain species can support enhanced carbon export upon relief of iron limitation (Assmy et al., 2013; Smetacek et al., 2012). Outside of the bloom periods the community composition in areas such as the Weddell Gyre is typically characterized by smaller cells such as haptophyte flagellates (Vernet et al., 2019). The communities also have a varying role as prey and in the marine food webs: the large and heavily silicified bloom-forming species can be grazed by krill but are avoided by microzooplankton grazers, which can control the abundance of smaller prey (e.g. Irigoien et al., 2005; Löder et al., 2011; Smetacek et al., 2004).

This study was carried out as part of an ecosystem cruise in March 2019 to the Kong Håkon VII Hav, an area off Dronning Maud Land mainly east of the prime meridian that encompasses parts of the Eastern Weddell Gyre. The cruise observations and satellite chlorophyll *a* (Chl *a*) data have shown distinct phytoplankton phenologies in the region, such as between Astrid Ridge and Maud Rise (Kauko et al., 2021). Knowledge on the community composition complements our understanding of this regional variability. As Vernet et al. (2019) highlighted in their review about the Weddell Gyre, thorough characterizations of the phytoplankton community in this area are sparse, particularly in the area east of the prime meridian. This area is poorly studied, while spatial management processes require improved knowledge of the ecosystem. We used different methods, with each giving a complementary, though not complete picture of the phytoplankton community composition: light microscopy (enabling identification to species level for some taxa), flow cytometry (providing data on abundance of the smallest size classes) and algal pigment analysis (informing on the taxa that are hard to identify in microscopy) via High Performance Liquid Chromatography (HPLC) and the statistical method CHEMTAX (Mackey et al., 1996). The objectives of this study are to characterize the phytoplankton and other protists communities in Kong Håkon VII Hav in late summer – early autumn, delineate their spatial variability, and to discuss the environmental control of community composition.

2. Methods

2.1 The cruiseField sampling and laboratory analyses

The data for this study were collected during a research cruise with RV Kronprins Haakon to Kong Håkon VII Hav, in the Atlantic sector of Southern Ocean, from February to April 2019 (cruise number 2019702). Sampling stations were located at 64.8 – 69.5° S and 2.3 – 13.5° E with Maud Rise, Astrid Ridge and a south-north transect at 6° E as the main focus areas (Fig. 1). In addition, two stations were sampled in between the areas: station 53 at 68.1° S, 6.0° E and station 54 at 68.5° S, 8.3° E. Station 53, though geographically close to the 6° E transect, showed much higher biomass and a distinct bloom event (Kauko et al., 2021; Moreau et al., in prep.) and was therefore considered separately. We also investigated the different sampling areas separately based on topography and associated hydrography (e.g., (Kauko et al., 2021; Le Paih et al., 2020; de Steur et al., 2007) and differing phytoplankton bloom phenology patterns (Kauko et al., 2021) to study whether these areas differ in phytoplankton community composition.

Selected environmental variables are presented in Kauko et al. (2021). In short, macronutrients (silicic acid, nitrate, and phosphate) were above limiting concentrations (33.0–93.8, 20.7–32.9 and 1.4–2.3 µM, respectively). Mixed layer depth (MLD) was on average 36 (±13) m. Krill swarms occurred especially at the northern part of the 6° E transect and to a lesser extent at Astrid Ridge, while mesozooplankton was most abundant at Maud Rise. Carbonate chemistry in the region is presented in (Ogundare et al., (2021).

2.2 Water sampling and laboratory analyses

Water samples were collected from multiple depths in the upper 100 m at a total of 37 stations (station numbers starting with 53) between 12 and 31 March in connection with CTD (conductivity-temperature-depth) casts with a 24-bottle or 12-bottle SBE 32 carousel water sampler.

100 Samples for phytoplankton microscopy analyses (190 mL) were collected from 3 different depths (typically 10,

101 25 or 40, and 75 m), filled into 200 mL brown glass bottles and fixed with glutaraldehyde and 20%

102 hexamethylenetetramine-buffered formalin~~formaldehyde~~ at final concentrations of 0.1 and 1%, respectively, and

103 thereafter stored cool and dark. For analysis, 10–50 mL subsample were settled in Utermöhl sedimentation

104 chambers (HYDRO-BIOS©, Kiel, Germany) for 48 h and counted with a Nikon Ti-U inverted light microscope

105 using the Utermöhl method (Edler and Elbrächter, 2010). Protists cells were counted in fields of view located

106 along transects crossing the bottom of the chamber. In each sample, at least 50 cells of the dominant species

107 were counted (95% confidence limit~~error~~ of ±28% according to Edler and Elbrächter, 2010).

108 Flow cytometry (FCM) samples (4.5 mL) for counting cells in small algal size classes (pico- and

109 nanophytoplankton, 0.7 to 2 µm and 2 to 20 µm, respectively) were collected in cryovials from 5-6 different

110 depths, fixed with glutaraldehyde (0.5% final concentration) and stored in -80° C until analyses at the University

111 of Bergen. In the laboratory, samples were thawed, mixed gently, and analysed in an Attune™ NxT Acoustic

112 Focusing Cytometer (Invitrogen™, Thermo Fisher Scientific Inc. USA) equipped with a 50 mW 488 nm (blue)

113 laser. Quantification and discrimination of the different phytoplankton size classes was done with the help of

114 biparametric plots based on side scatter and red fluorescence.

115 Samples for algal pigment analysis (usually 1 L) were collected from 3 different depths (typically 10, 25 or 40,

116 and 75 m), filtered on 0.7 µm GF/F filters (GE Healthcare, Little Chalfont, UK) with a gentle vacuum pressure

117 (approximately −30 kPa), and immediately stored in the dark at -80° C. Pigments were measured and quantified

118 with a Waters Alliance 2695 HPLC Separation Module connected to a Waters photodiode array detector (2,996).

119 HPLC-grade solvents (Merck) and an Agilent Technologies Microsorb-MV3 C8 column (4.6 × 100 mm) was

120 used for peak separation. The auto sampler module was kept at 4°C during the measurements. In total 100 µl

121 sample were injected with an auto addition function of the system between sample and a 1 molar ammonium

122 acetate solution in the ratio of 30:20:30:20. Peak identification and quantification was obtained with the

123 EMPOWER software. More details about the solvents and gradient can be found in Tran et al. (2013). Overview

124 of the taxonomical distribution of pigments is given in Jeffrey et al. (2011), Higgins et al. (2011) and the data

125 sheets of Roy et al. (2011).
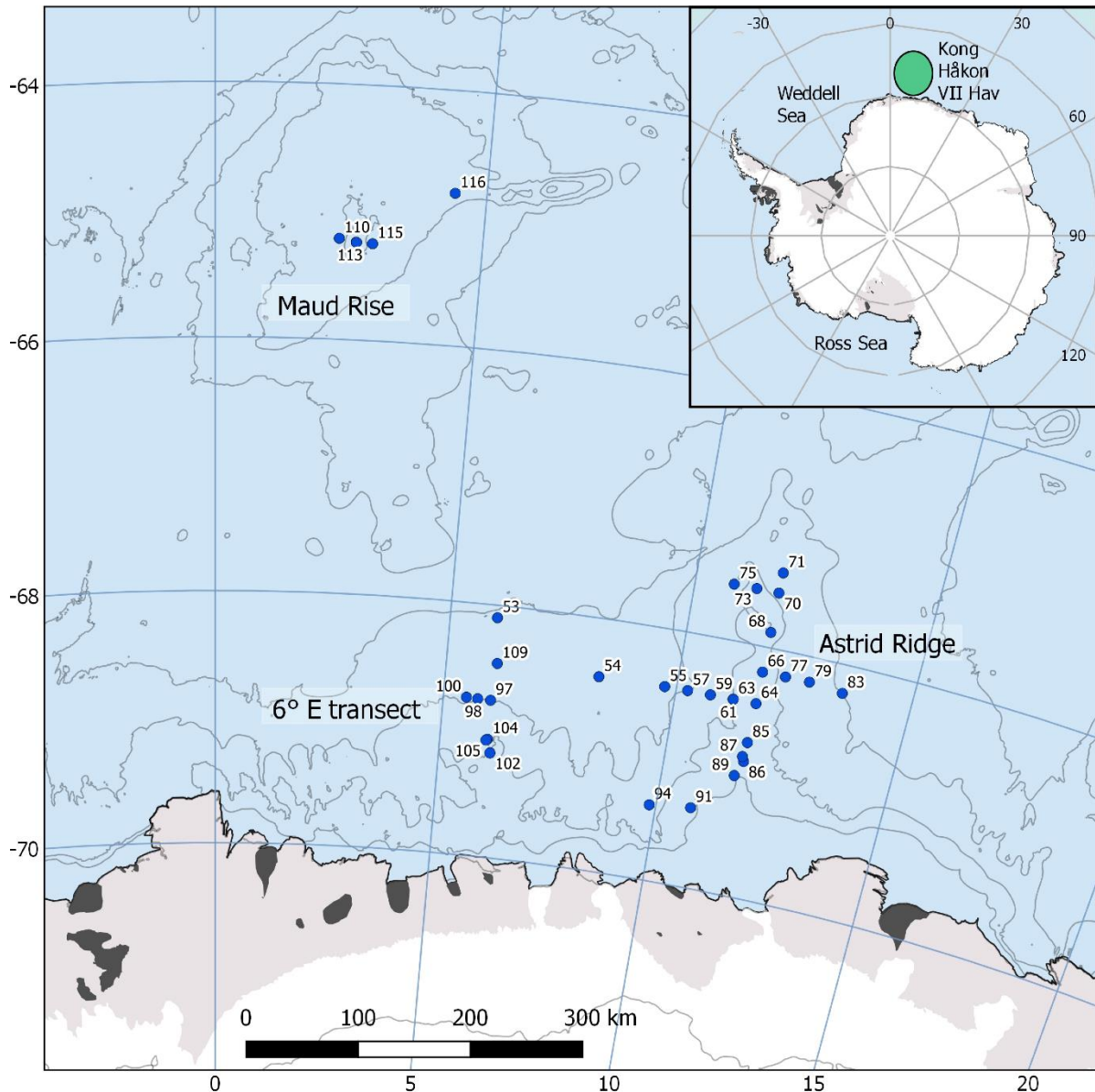
126

127 **Figure 1: Map of the study area. The CTD stations with water sampling are marked with blue circles. The sampling**
128 **area is marked with a green ellipse in the insert. <u>Contour interval is 1000 m.</u> Map created with the help of**
129 **Quantarctica (Norwegian Polar Institute, 2018).**

130 **2.3~~2~~ Statistical analyses**

131 Similarity <u>and separation</u> between the sampling areas in terms of the microscopy counts was evaluated with non-

132 metric multidimensional scaling (NMDS) using the *isoMDS* function in the MASS package (Venables and

133 Ripley, 2002) and the R software (R Core Team, 2017). <u>Water</u>~~CTD~~ samples down to 100 m depth with full

134 taxonomical resolution were used for the analysis. Bray-Curtis dissimilarities (vegan package in R; Oksanen et

135 al., 2017) were used for the scaling and abundances were square-root transformed prior to that to reduce the

136 effect of high and uneven abundances. The dissimilarities between the groups were further tested statistically

137 with the *anosim* function from the vegan package. Test result values (R values) close to 0, as opposed to 1,

138 indicate random grouping. For the test considering differences between the sampling areas, the assumptions of

5

139 heterogeneity and similar sample size were not met, however, due to the lower range of dissimilarities occurring
140 in the smaller-sized sample group Maud Rise (Fig. A1), the test tends to be overly conservative (Anderson and
141 Walsh, 2013) and thus a significant result appears reliable.

142 To study the relationship of abiotic environmental variables and the community composition, a canonical
143 correspondence analysis (CCA) was used from the vegan package. The included environmental variables were:
144 silicate and nitrate (Chierici and Fransson, 2020; Kauko et al., 2021), MLD, temperature and salinity (Kauko et
145 al., 2021; Hattermann and de Steur, 2022). Phosphate correlated highly (0.90) with nitrate and was therefore not
146 included; nitrate thus can be considered representative of both macronutrients. Missing environmental data were
147 filled with the mean of that variable, and all environmental data were standardized by subtracting the mean of the
148 data and dividing by the standard deviation. Phytoplankton species count data were mainly grouped into upper-
149 level categories (corresponding to the main geographical features observed in the data and discussed in this
150 paper) and included the following taxa: flagellates, dinoflagellates, pennate diatoms, centric diatoms and
151 *Chaetoceros dichaeta*. These data were then square-root transformed. Originally, the analysis was conducted
152 with full taxonomical resolution, but in this configuration only a small portion of the variance (11 %) was
153 explained (figures not shown). The orientation of the figure was, however, largely similar.

154 Diversity in the phytoplankton community was investigated with the Shannon's diversity index (H; function
155 *diversity* in the vegan package) and species richness (number of species, genera and size groups of unidentified
156 taxa). Differences between the areas and sampling depths were tested with one-way Analysis of Variance
157 (ANOVA; function *aov* in R). The assumptions of homoscedasticity were met in the models.

158 **2.43 CHEMTAX analysis**

159 Phytoplankton community composition was further investigated by applying a factor analysis program called
160 CHEMTAX (Mackey et al., 1996), which allows to calculate the abundance of the various algal groups based on
161 the measured marker pigments. As we had a large number of samples and no experimental or field information
162 on local pigment ratios, the original approach (Mackey et al., 1996) was concluded to be more suitable than the
163 Bayesian approach (Van den Meersche et al., 2008), according to Higgins et al. (2011). The software package
164 CHEMTAX was obtained from Wright (2008).

165 The initial ratio matrix was based on literature. Pigment to Chl *a* ratios for prasinophytes, chlorophytes,
166 cryptophytes, two pigment types of diatoms and peridinin-containing dinoflagellates were taken from the table in
167 Wright et al. (2010), a study that was conducted close to our study area (between 30° to 80° E and south of 62°
168 S), with the following modifications. Chl c_1 was changed to Chl c_{1+2} (which is the resolution of our
169 chromatographic results) with values taken from the CHEMTAX material (geometric means of reported ratios
170 from the literature collected in Higgins et al., 2011). The values for 19'-butanoyloxyfucoxanthin (but-fuco),
171 ratios for haptophytes pigment type 6 and for dinoflagellates pigment type 2 (microscopy revealed dominance of
172 *Gymnodinium* spp.) were taken from Table 6.1 in Higgins et al. (2011). Zeaxanthin was observed in only one
173 sample and was omitted from the analysis. Diadinoxanthin, diatoxanthin and β,β-carotene were excluded
174 because they are not very group-specific. Neoxanthin, prasinoxanthin and violaxanthin were not observed in the
175 samples and were removed from the ratio matrix.

176 Haptophytes belong to several (8) different pigment types (Zapata et al., 2004) and in addition change their

177 marker pigment content according to environmental conditions such as iron availability (van Leeuwe and Stefels,

178 1998; Wright et al., 2010). Therefore, all haptophyte pigment types were initially tested with CHEMTAX runs

179 on all samples (20 randomized ratio matrices, using the pigment ratios from the CHEMTAX material mentioned

180 above as initial ratios). The pigment type 8 is typical in the Southern Ocean including the species *P. antarctica*,

181 whereas coccolithophores belong to pigment type 6. Out of the eight different pigment types tested, including

182 pigment types 6, 7 or 8 resulted in the lowest root mean square errors (RMSE; below 0.2). Pigment type 7

183 includes e.g. the genus *Chrysochromulina* which is not typical in the Southern Ocean. Including both haptophyte

184 type 6 and 8 (in different ratio range categories according to the CHEMTAX instructions) also resulted in a low

185 RMSE, and for the categories with high ratio range for haptophyte type 6 the error was lowest and similar to

186 when including only haptophyte type 6 (<0.15). However, coccolithophores should not be abundant this far

187 south (Balch et al., 2016; Saavedra-Pellitero et al., 2014; Trull et al., 2018) and were not observed in the

188 microscopy samples. Other prymnesiophytes were not abundant either – only *P. antarctica* was observed in only

189 three CTD samples. This taxon has a characteristic appearance and, if present in large quantities, would likely

190 have been identified, whereas the majority of flagellates in the microscopy samples were classified as

191 unidentified flagellates in the 3 to 7 µm size range. Therefore, to simplify the analysis (e.g. to avoid having too

192 many algal groups compared to pigments, Mackey et al., 1996) and to account for the unidentified status of this

193 group, we have included only one haptophyte group in the final runs with the best-performing i.e. type 6 pigment

194 ratios and called this "Haptophytes-6 -like". Silicoflagellates and chrysophytes, that were observed at low

195 abundances in microscopy samples (maximum abundances of 3900 and 18200 cells L^{-1}, respectively), will also

196 be included in the haptophyte pigment group, as they contain similar pigments, e.g., Chl *c*, fucoxanthin and its

197 derivatives (Jeffrey et al., 2011).

198 In the preliminary analysis, it was also tested to separate the samples into different clusters. With all samples

199 combined, including only the surface samples down to 10 m, or successively adding depth ranges one at a time

200 did not improve the result in terms of the RMSE, compared to including all depths. Separating Maud Rise from

201 the rest reduced the error, when different area clusters were tested with all samples. Trials indicated that dividing

202 the Maud Rise samples into depth clusters may bring further improvements but as the number of samples was

203 relatively small (in total 12 CTD samples from Maud Rise) they were kept as one cluster. Astrid Ridge had a

204 larger number of samples (55 in total) and was divided into two clusters (above and below including 40 m;

205 average mixed layer depth (MLD) was 34 m, Kauko et al., 2021) and separated from the rest, which reduced the

206 error. For the 6° E transect, separating the surface samples did not reduce the error.

207 In total there were 98 samples from the CTD casts. In the clusters Maud Rise, Astrid Ridge surface, Astrid Ridge

208 deep and other stations (stations 53, 54 and 6° E transect) there were 12, 26, 29 and 31 samples, respectively.

209 After the 60 first runs for each of the clusters (using 60 randomized pigment ratio matrices based on the initial

210 ratio matrix), the average output ratio matrix of the 6 best runs was used as the initial ratio matrix for the next 60

211 runs. The reported results are the averaged output from the six best runs of this second step.

3. Results

3.1 Microscopy

The microscopy data are shown here as averages per sampling area and for the most important taxa separately, whereas others are summed together into higher-level categories such as "Pennate diatoms (other)". All taxa are listed in Table B1 together with median abundances and occurrence in the different sampling areas, and variance in data used for the averages (i.e., data from all samples) is shown in Fig. A2 and A3.

Two of the sampling locations stood out in terms of higher diatom abundances. ~~had an active diatom bloom, with a~~Average diatom abundances at station 53 and Maud Rise reach~~ed~~ing 5.2×10^5 and 7.5×10^5 cells L^{-1}, respectively (Fig. 2a), and Chl *a* data show~~ed~~ing that these locations had the highest biomass in the area (Fig. 3; Kauko et al., 2021). Most of the sampling areas were dominated by diatoms in terms of average abundances, most notably for the area represented by station 53 and Maud Rise (74 and 89 %, respectively), whereas at station 54 or Astrid Ridge the dominance was less pronounced (62 and 56 %), and the area along the 6° E transect was slightly dominated by flagellates (45 % flagellates compared to 36 % diatoms). At Maud Rise flagellates and dinoflagellates occurred in similar abundances whereas in the other areas, flagellates were more abundant than dinoflagellates, most notably so along the 6° E transect. Ciliates and cyanobacteria (unidentified filamentous blue-green algae cf. *Anabaena* sp., see photo in Fig. A4) were also observed at very low abundances, especially the latter mainly at Astrid Ridge and along the 6° E transect. FCM biplots (Fig. A5) using orange fluorescence indicated the presence of cyanobacteria in the corresponding samples, however abundances were low and the filamentous nature of the cyanobacteria complicates interpretations for this method.

The dominance patterns were similar when abundances were averaged per depth interval (Fig. A6)~~, but at Astrid Ridge diatoms formed less than half of the community (about 30 %) below 45 m where dinoflagellates were slightly more prominent (32 to 37 %). In contrast, along the 6° E transect diatoms dominated at 75 m and formed about half of the community at 50 m~~. In terms of abundances, phytoplankton were concentrated in the upper 40 m at station 53 and Astrid Ridge, whereas along the 6° E transect the generally low abundances were more evenly distributed with depth and at Maud Rise the bloom extended deeper with relatively high cell numbers (4 $\times 10^5$ cells L^{-1}) until 75 m.

Among the diatoms, *C.~~haetoceros~~ dichaeta* clearly dominated station 53 and Maud Rise communities down to 40 and 50 m, respectively (Fig. 2b-c, 4 and A7). *Chaetoceros dichaeta* formed 59 % of the diatom community at 10 m and 40 % at 40 m at station 53, i.e. it was the most abundant species at these depths. At Maud Rise, besides the surface samples, *C. dichaeta* dominated the diatom community at 100 m depth (at station 110; Fig. A8). This species was also an important component of the 6° E transect diatom community although at much lower abundances. In these other sampling areas ~~not characterized by an active bloom~~ (the 6° E transect, station 54 and Astrid Ridge), the abundances of various diatom species were more evenly distributed. Other important taxa were *Fragilariopsis* spp., *F. nana*, *F. kerguelensis*, *F. cylindrus*, *Dactyliosolen antarcticus*, *Chaetoceros* spp. and *Pseudo-nitzschia* spp. At Astrid Ridge and station 54, pennate diatoms (particularly *Fragilariopsis* spp. and *Pseudo-nitzschia* spp.) were more abundant than centric diatoms, with shares of 72 and 56 %, respectively. In other areas pennate diatoms contributed 14 to 34 %. Overall, there were 89 diatom taxa (at the genus or species level) identified during this research campaign.

250   Maximum average abundances of flagellates were observed at station 53 and along the 6° E transect, with $1.0 \times$

251   10^5 and 1.1×10^5 cells L^{-1}, respectively (Fig. 2d). Among the flagellates, a majority was categorized as

252   unidentified flagellates in the size range 3 to 7 µm. Cryptophytes and especially the genus *Telonema* were also a

253   notable component of the flagellate community in many of the areas (in Fig. 2d cryptophytes and the genus

254   *Telonema* are presented separately). Choanoflagellates (heterotrophic flagellates) were observed at relatively

255   high numbers at station 53 and Maud Rise. *Phaeocystis antarctica* (the only prymnesiophyte species identified)

256   was found at station 54 mainly at 40 m, but it was not an abundant species during the cruise, which was also

257   confirmed by microscope analysis of live material from net samples taken from the upper 20 m at every CTD

258   station during the cruise. Chlorophytes, chrysophytes, prasinophytes and silicoflagellates were also observed in

259   minor numbers. The depth distribution of flagellates (figures not shown) was largely similar to the composition

260   of the whole area averages~~, but choanoflagellates were most prominent at 25 m at Maud Rise~~.

261   Dinoflagellates belonged mainly to different, unidentified species of the genus *Gymnodinium* in all areas (Fig.

262   2e) and at all depths (figures not shown). Additionally, the genera *Prorocentrum, Gyrodinium, Alexandrium,*

263   *Amphidinium, Polarella* and *Protoperidinium* were also present. The maximum average dinoflagellates

264   abundance was observed at station 53 (8.2×10^4 cells L^{-1}).

265   Ciliates were present in lower numbers (the maximum average abundance was 1500 cells L^{-1} at Maud Rise; Fig.

266   2f) but with several species (16 species or higher level taxa; Table B1). The most notable species were

267   *Salpingella costata, Strombidium* spp., and *Lohmanniella oviformis*, as well as *Uronema marinum* at station 53

268   and *Mesodinium rubrum* at station 54. At Astrid Ridge and along the 6° E transect, aloricate (naked) ciliates

269   dominated in abundance (at station 54 the dominance was less pronounced), whereas at Maud Rise the

270   abundances were even and at station 53 loricate ciliates (tintinnids) dominated (Fig. 2f). ~~Ciliate abundances were~~

271   ~~lowest at station 54 (125 cells L⁻¹).~~
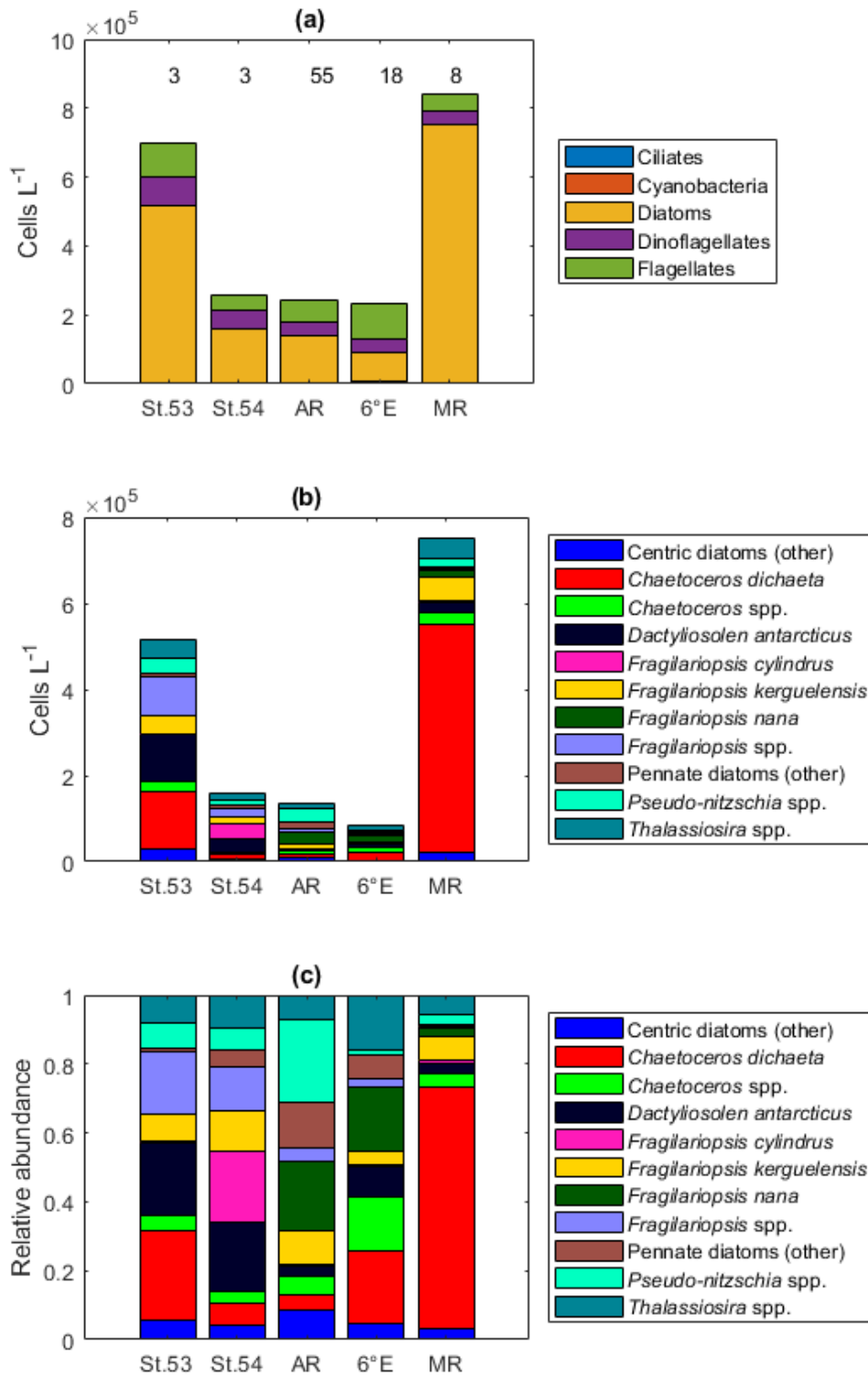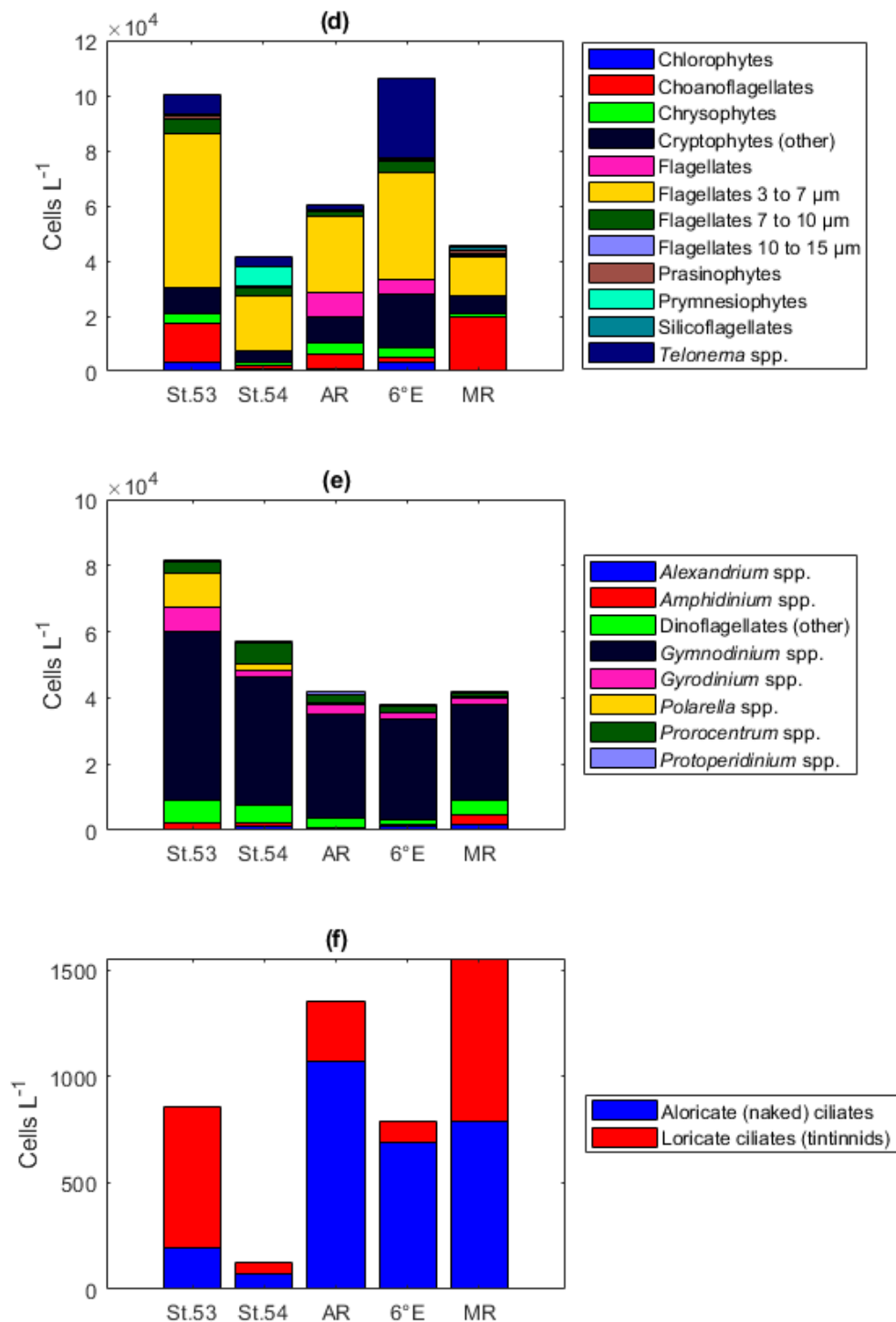
Figure 2: Abundance of different protist groups and species for (a) main taxa, (b) diatoms, (c) relative abundance of diatoms, (d) flagellates, (e) dinoflagellates and (f) ciliates. In (a), the number of samples used for the average abundances is shown in the top of the figure (the numbers apply to all figures). In (c) and (d), the genera *Fragilariopsis* and *Pseudo-nitzschia* belong to pennate diatoms, thus pennate diatoms are shown with colours pink/yellow to cyan. St.53=station 53, St.54=station 54, AR=Astrid Ridge, 6E=6° E transect, MR=Maud Rise.

279
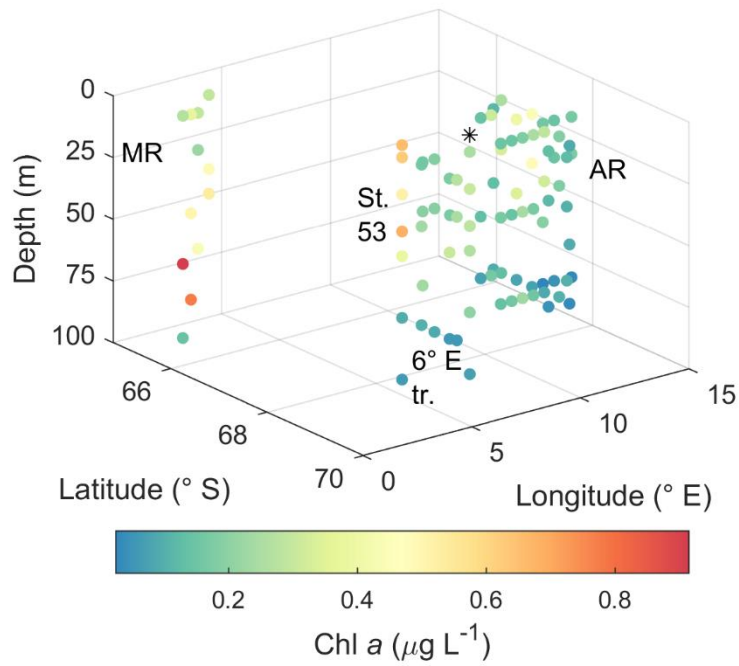
Figure 3: Horizontal and vertical distribution of phytoplankton biomass expressed as Chl *a* concentration. MR=Maud Rise, St. 53=station 53, AR=Astrid Ridge, 6° E tr.= 6° E transect. Station 54 is marked with a black asterisk.

282
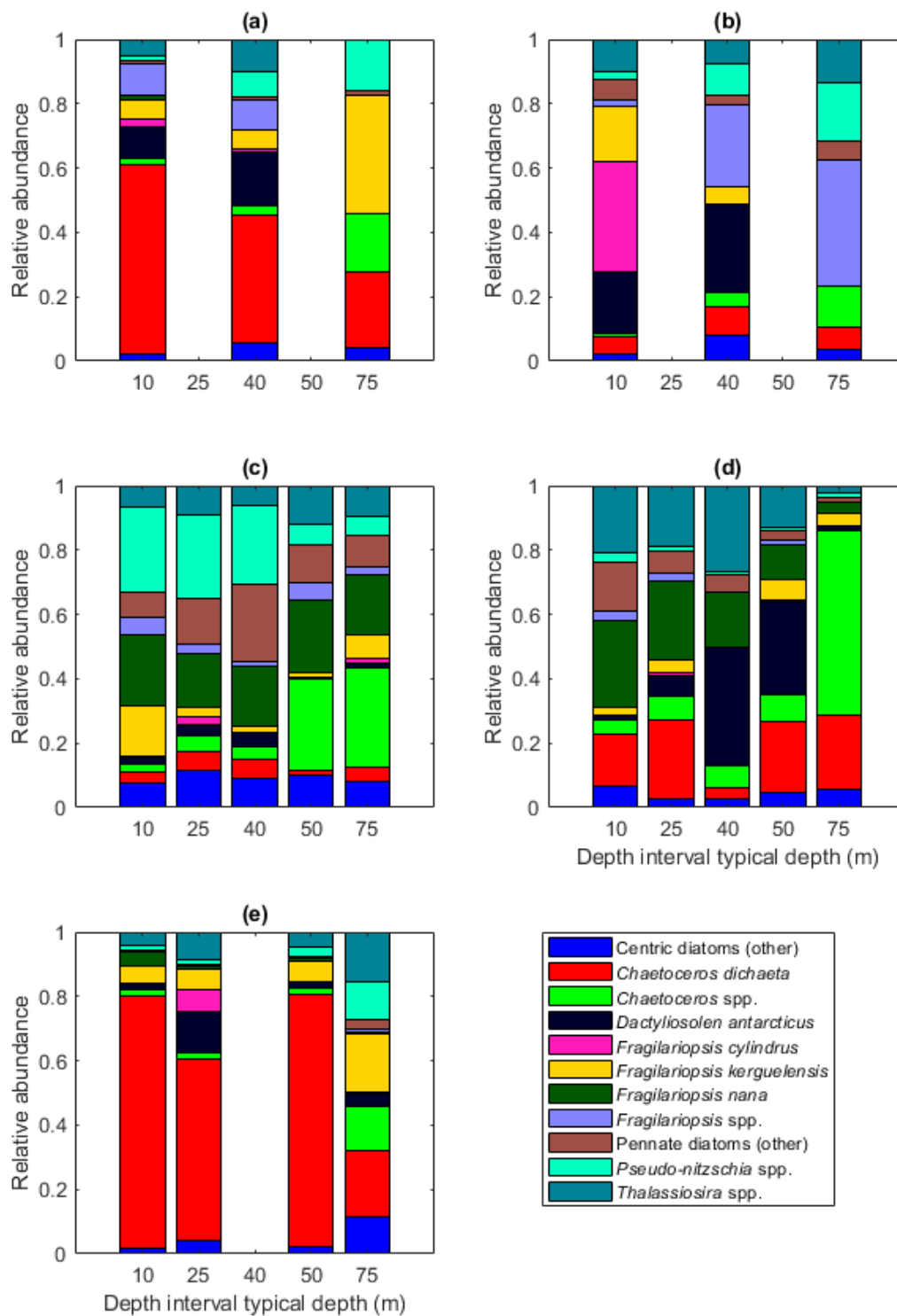
Figure 4: Diatom relative abundance in the different sampling areas averaged per depth interval for (a) station 53, (b) station 54, (c) Astrid Ridge, (d) 6° E transect and (e) Maud Rise. Depth intervals (with typical sampling depth in brackets): 5-10 (10); 25-35 (25), 35-45 (40), 50-60, 65-85 (75) m.

286

287 ~~Clustering (NMDS) of the abundance results from the microscopy analysis showed that the communities in the~~
288 ~~different sampling areas (marked with different symbols in Fig. 5) did not separate into distinct clusters, but they~~
289 ~~appear located at different sides of the cluster, with station 53 and 54 and Maud Rise samples on one side and the~~
290 ~~Astrid Ridge and 6° E transect samples predominantly on the other side. In addition to the diatom blooms in the~~
291 ~~first two mentioned areas, this could also reflect a coastal to offshore pattern. However, the low R value of 0.15~~
292 ~~from the *anosim* test (significance 0.017) indicated overall a high similarity between the areas.~~

293 ~~In addition, a separation along the sampling depth gradient (colour scale in Fig. 5) is clearly visible, with the~~
294 ~~surface samples (typically sampled at 25 m depth) and the deep samples (typically sampled at 75 m depth)~~
295 ~~located on different sides of the cluster. The *anosim* test indicated a somewhat higher degree of differentiation~~
296 ~~between the depth clusters (R value 0.27, significance 0.001) than between the sampling areas. In addition, when~~
297 ~~the NMDS analysis is performed on presence-absence data (Fig. A9), it is difficult to separate the areas, but the~~
298 ~~sampling depth pattern is still visible, though the samples are very condensed on the plot. Other categorizations~~
299 ~~included in the analysis, such as according to bottom depth, latitude or separation of Astrid Ridge into different~~
300 ~~areas (north, south, west and east parts of the Ridge), did not yield such clear patterns (figures not shown).~~

301 The Shannon's diversity index varied between 0.9 and 3.4, and the species richness between 11 and 65
302 species/taxa. The biodiversity between the areas was relatively similar, but the most notable geographical
303 patterns were that most depths at Maud Rise had a low diversity index, and that species richness in the other
304 sampling areas was lower at depth than in the upper part of the water column (Fig. 5~~6~~a and b). This was also
305 visible in the statistical analysis of differences between groups: regarding the diversity index, the differences
306 between areas were highly significant (p-value <0.001), but not between depth categories (p-value 0.32; the
307 same depth categories were used as in the Fig. 4). A post-hoc Tukey test confirmed that Maud Rise differed from
308 all other areas (p-value <0.02 for all comparisons). For species richness the inverse was found, differences
309 between depth categories were significant (p-value <0.001) and not between the areas (0.69). A post-hoc Tukey
310 test showed that the surface depth categories (10, 25 and 40 m) differed from the deeper categories (50 and 75 m;
311 p-value for all comparisons <0.02, except for between 50 and 25 m where the p-value was 0.06), that is, species
312 richness was significantly lower at depth (50 m and deeper). The means for the different areas were 2.7, 3.0, 2.7,
313 2.6 and 1.9 for the diversity index and 49, 47, 44, 45 and 49 for species richness for station 53, station 54, Astrid
314 Ridge, 6° E transect and Maud Rise, respectively. The mean diversity index was thus significantly lower at
315 Maud Rise. The diversity index did not have a clear correlation with biomass, but species richness increased with
316 increasing biomass up to maximum values of around 55–65 (Fig. 5~~6~~c and d).
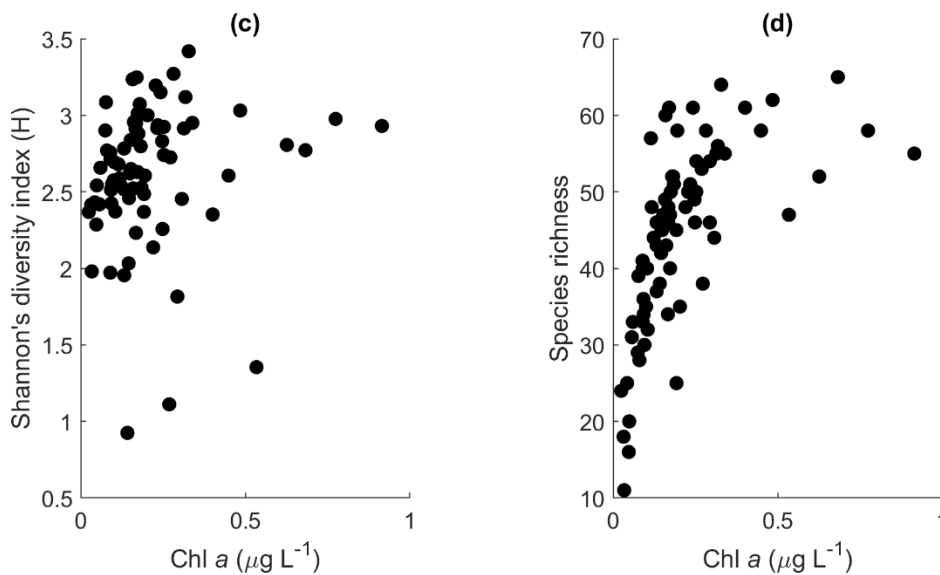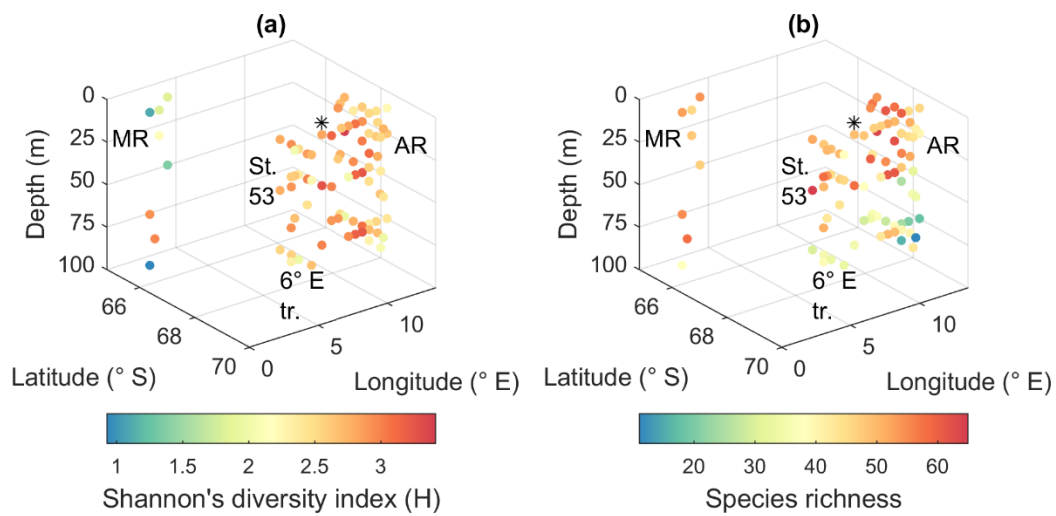
Figure 56: Biodiversity according to the microscopy samples. (a) Shannon's diversity index, (b) species richness, (c) relationship between algal biomass (expressed in Chl a concentration) and Shannon's diversity index and (d) algal biomass and species richness. MR=Maud Rise, St. 53=station 53, AR=Astrid Ridge, 6° E tr.= 6° E transect. Station 54 is marked with a black asterisk.

3.2 Statistical analysis of the sampling areas

Clustering (NMDS) of the species abundance results from the microscopy analysis showed that the communities in the different sampling areas (marked with different symbols in Fig. 6) did not separate into distinct clusters, but they appear located at different sides of the cluster, with station 53 and 54 and Maud Rise samples on one side and the Astrid Ridge and 6° E transect samples predominantly on the other side. In addition to the diatom

327 blooms in the first two mentioned areas, this could also reflect a coastal to offshore pattern. However, the low R

328 value of 0.15 from the *anosim* test (significance 0.017) indicated overall a high similarity between the areas.

329 In addition, a separation along the sampling depth gradient (colour scale in Fig. 6) is clearly visible, with the

330 surface samples (typically sampled at 25 m depth) and the deep samples (typically sampled at 75 m depth)

331 located on different sides of the cluster. The *anosim* test indicated a somewhat higher degree of differentiation

332 between the depth clusters (R value 0.27, significance 0.001) than between the sampling areas. In addition, when

333 the NMDS analysis is performed on presence-absence data (Fig. A9), it is difficult to separate the areas, but the

334 sampling depth pattern is still visible, though the samples are very condensed on the plot. Other categorizations

335 included in the analysis, such as according to bottom depth, latitude or separation of Astrid Ridge into different

336 areas (north, south, west and east parts of the Ridge), did not yield such clear patterns (figures not shown).
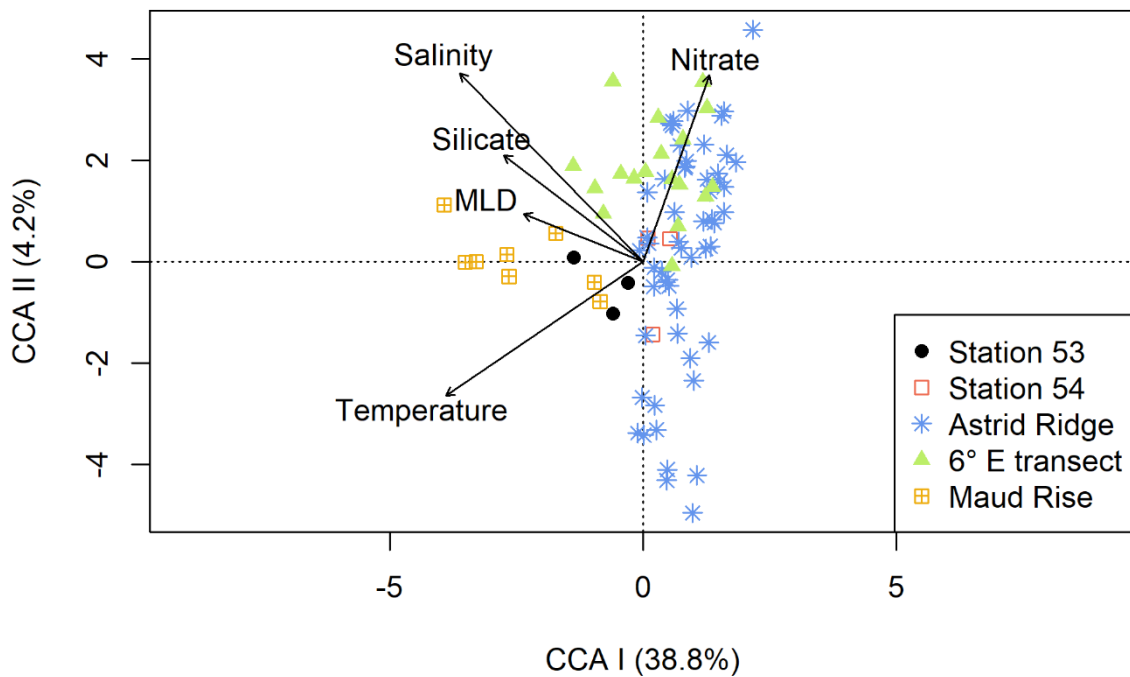
337 Similarly, in the CCA analysis (Fig. 7), the sampling areas are distributed along the first axis (explaining 38.8 %

338 of the variance), although not completely separated. The environmental variables that best explain the first axis

339 are silicate and MLD. Maud Rise and station 53 (in addition to some stations at the 6° E transect) are thus

340 associated with deeper MLD and higher silicic acid concentrations, as well as higher salinity and temperature.

341 Nitrate best explains the second axis, although this axis only explains a small portion of the variance (4.2 %).

342 The different stations especially at Astrid Ridge, and to a lesser extent at the 6° E transect, are spread along the

343 second axis.
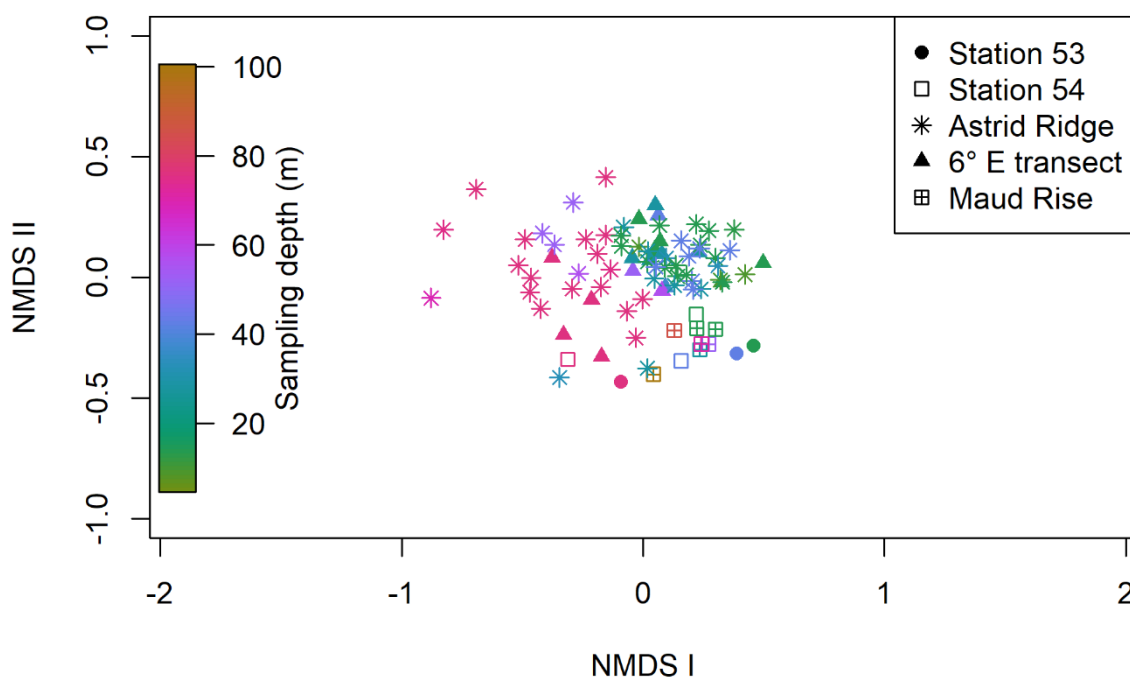
344

345 **Figure 65: Results of the NMDS clustering of the microscopy count samples. The colour shows the sampling depth**
346 **and the different sampling areas are shown with different symbols, see legend. The stress value of the plot is 22 %.**

16

3.3 Flow cytometry

Smaller nanophytoplankton (Nanophytoplankton 1; Fig. A5) showed the highest abundances along the 6° E transect, with abundances up to 4.7×10^6 cells L^{-1} (Fig. 87a), and lowest at Maud Rise. On the contrary, larger nanophytoplankton (Nanophytoplankton 2) were associated with Maud Rise and station 53 (up to 4.2×10^6 cells L^{-1}; Fig. 87b). Maud Rise had high abundances also at depth, contrary to station 53. Some larger cells (Nanophytoplankton 2) were also observed on top of Astrid ridge (stations 66, 68 and 73), near the surface.

Picophytoplankton abundance was lower than for nanophytoplankton (up to 0.7×10^6 cells L^{-1}; Fig. 87c), but a few stations on the west side of Astrid ridge (57, 59, 61) showed a distinct picophytoplankton population in the FCM biplots (Fig. A5).

(a)

(b)

(c)
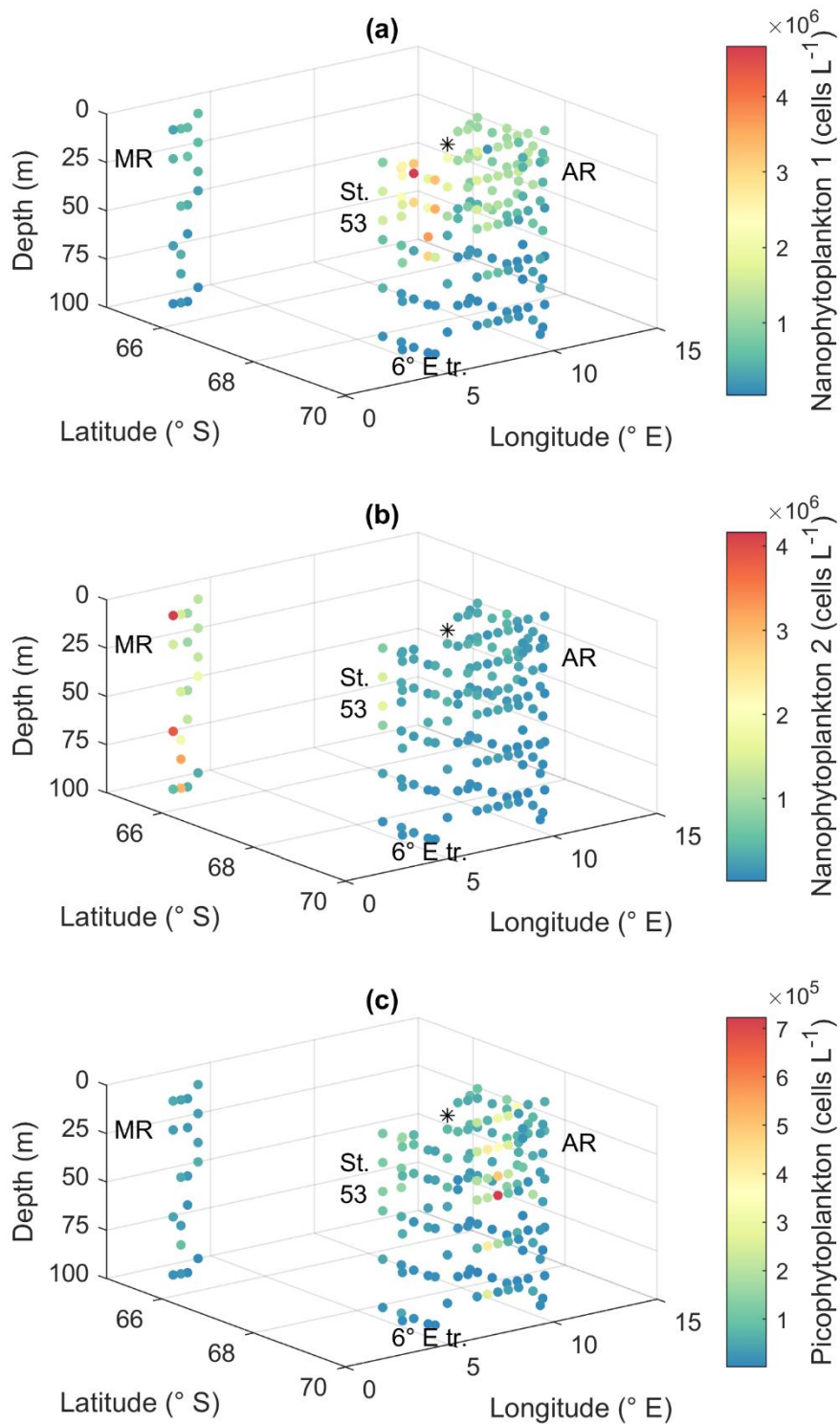
360

361 **Figure 8̶7̶: Flow cytometry results. Cell abundances of two groups of nanophytoplankton (a, b) and**
362 **picophytoplankton (c). MR=Maud Rise, St. 53=station 53, AR=Astrid Ridge, 6° E tr.= 6° E transect. Station 54 is**
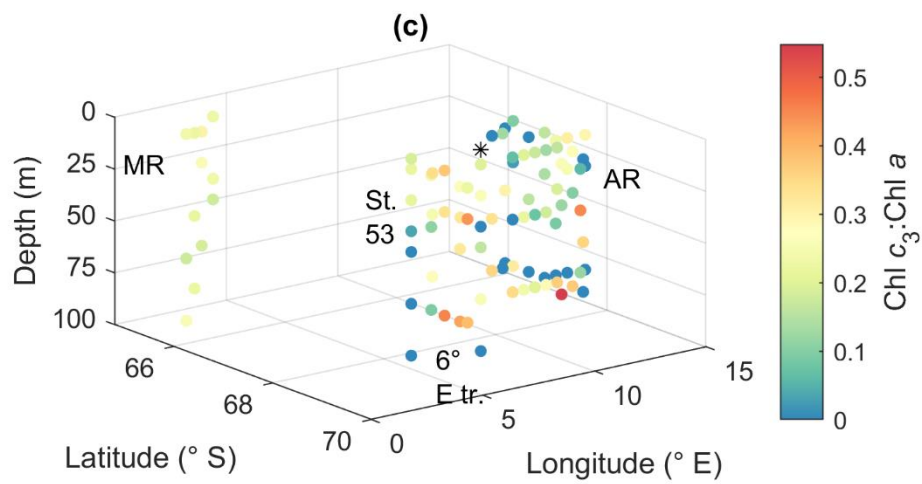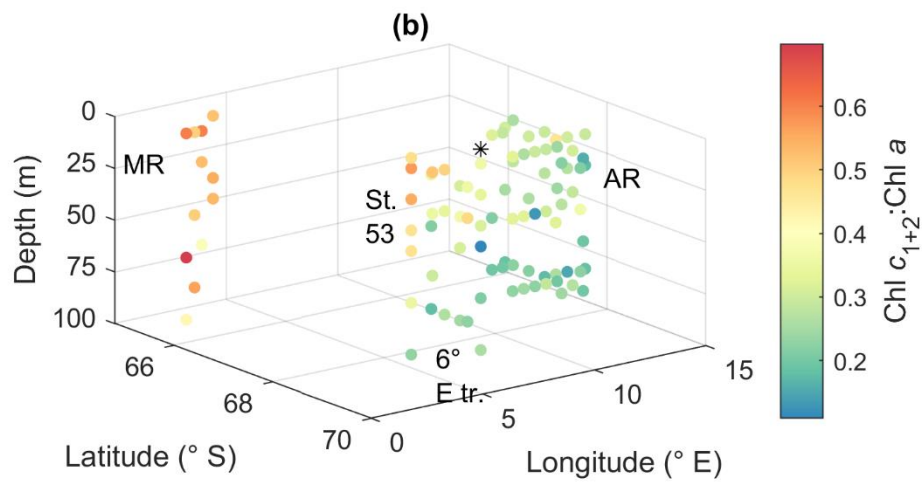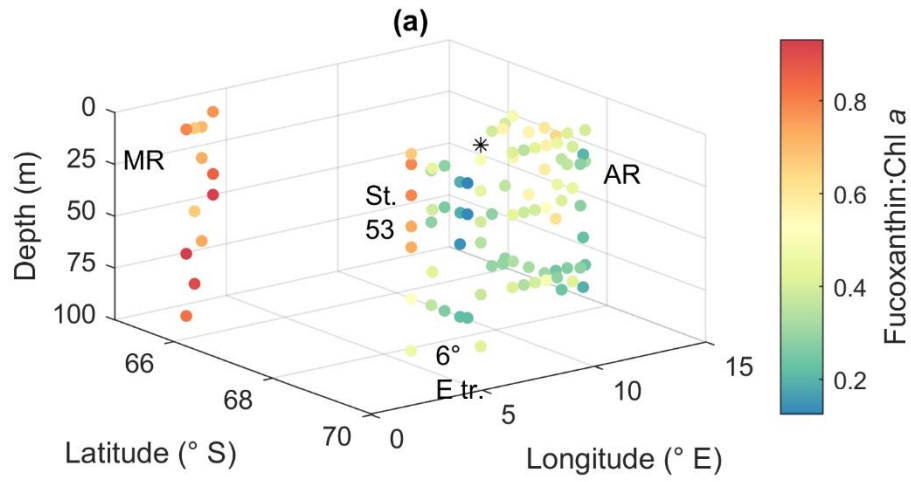363 **marked with a black asterisk.**

3.43 Marker pigments

Pigment to Chl *a* ratios are presented in Fig. 98 and A109 and reported here, whereas the pigment concentrations are shown in Fig. A110 and A121. Pigment to Chl *a* ratios indicate the relative community composition better than the absolute concentrations. Chl *a* concentration ranged between 0.02 and 0.92 µg L^{-1} (Fig. 3). The diatom blooms at Maud Rise and station 53, and the importance of flagellates at the 6° E transect were also visible in the pigment data.

Ratios of fucoxanthin, a typical pigment in diatoms, to Chl *a* were very high at Maud Rise and station 53, up to 0.93 (Fig. 98a). The ratios were the lowest at the 6° E transect, with a minimum of 0.12. At Astrid Ridge the ratios were in between these values at around 0.5. The ratios of Chl c_{1+2} to Chl *a* were also the highest at Maud Rise and station 53, up to 0.70 and seemed thus to be primarily associated with fucoxanthin and diatoms (Fig. 98b). However, other Chl c_{1+2} containing groups were also likely present, as the ratios at the flagellate-dominated 6° E transect did not differ from the other areas as much as for fucoxanthin.

Chl c_3 showed the highest pigment to Chl *a* ratio values at the 6° E transect and at depth at Astrid Ridge, up to 0.55 (Fig. 98c). It was also found at Maud Rise at all depths, in the surface waters at station 53 and station 54, and at Astrid Ridge mainly in the middle of the ridge, from the surface to mid-depths. This pigment thus further indicates that flagellates were an important part of the 6° E transect community, as it is a major pigment e.g. in haptophytes. In addition, 19'-hexanoyloxyfucoxanthin (hex-fuco), another important pigment in haptophytes, showed clearly its highest pigment to Chl *a* ratio values at the 6° E transect, up to 1.01, and the lowest at Maud Rise (Fig. 98d). Another fucoxanthin derivative, but-fuco, that is mainly found in pelagophytes, silicoflagellates and some haptophytes, showed the highest pigment to Chl *a* ratio values at depth at the 6° E transect and Astrid Ridge, but values were low (Fig. 98e).

Diadinoxanthin, a carotenoid participating in the photoprotective xanthophyll cycle, occurred in the highest pigment to Chl *a* ratios close to the surface in all areas (up to 0.25), but at Maud Rise relatively high ratios were observed throughout the sampling depths (Fig. 98f). Diatoxanthin, its counterpart in the xanthophyll cycle, was observed in five samples at a much lower concentration (5–16 % of diadinoxanthin). It should be noted that although the samples were processed as quickly as possible, they were part of a larger sampling effort, and conversion from diatoxanthin to diadinoxanthin may have happened during the storage under dark conditions.

Peridinin (a major pigment in one of the dinoflagellate pigment classes), alloxanthin (a major pigment in cryptophytes), lutein (Chl *b*-lineage, e.g. chlorophytes and prasinophytes) and Chl *b* were observed in minor amounts in certain areas (Fig. A109): peridinin on the west side of Astrid Ridge (pigment to Chl *a* ratio up to 0.15), alloxanthin at the surface at a few stations of the 6° E transect and Astrid Ridge (up to 0.01), and lutein and Chl *b* at the 6° E transect (up to 0.04 and 0.06, respectively). β,β-carotene is not very taxon-specific and did not show clear geographical patterns (pigment to Chl *a* ratio up to 0.05; Fig. A132). Zeaxanthin was only observed in one sample, in the surface (5 m) at station 70 at Astrid Ridge, in low concentration (ratio to Chl *a* was 0.02).

401

(d)

(e)

(f)

402
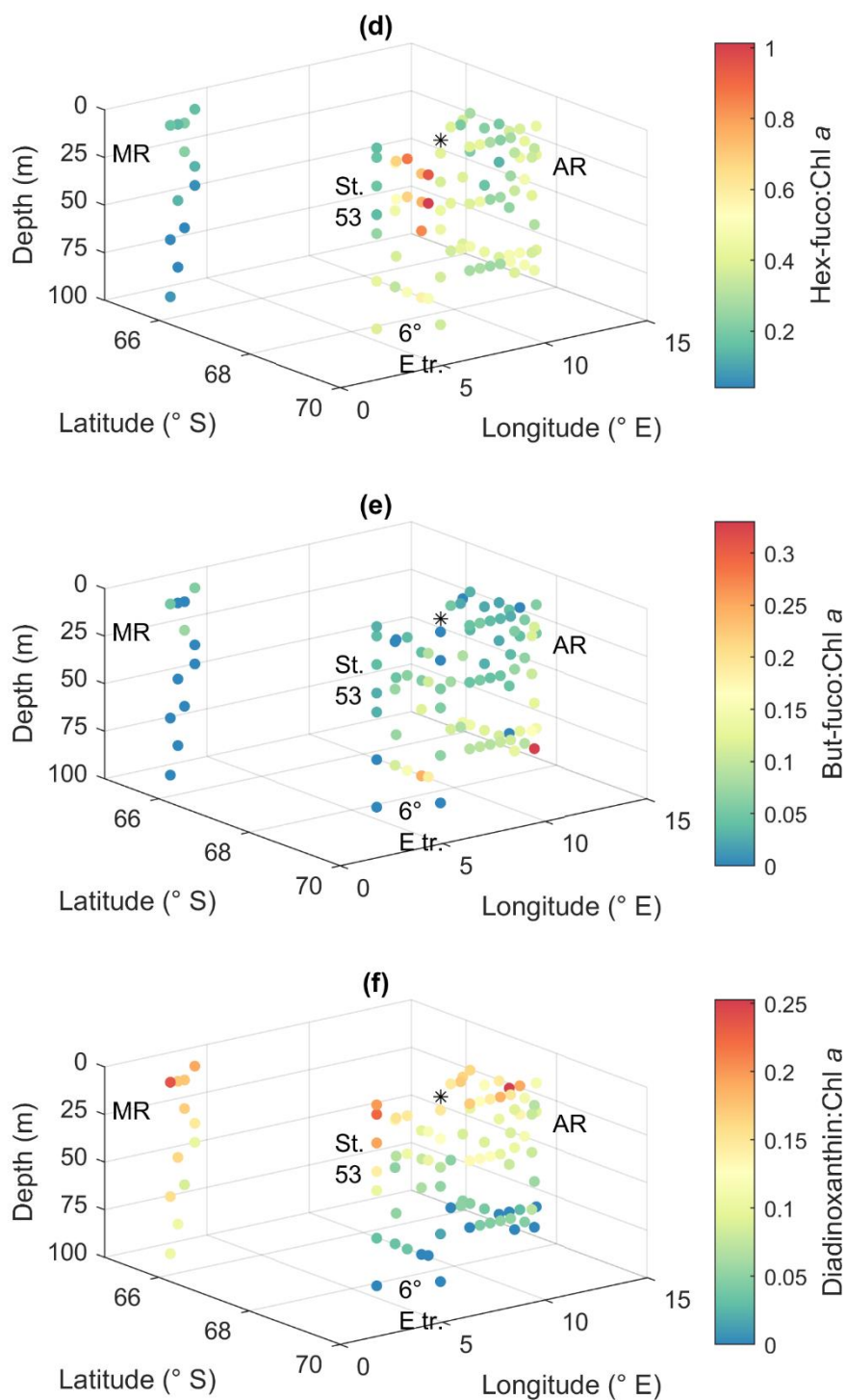
Figure 98: Ratios of algal pigments to Chl a for (a) fucoxanthin, (b) Chl c$_{1+2}$, (c) Chl c$_3$, (d) hex-fuco, (e) but-fuco and (f) diadinoxanthin. MR=Maud Rise, St. 53=station 53, AR=Astrid Ridge, 6° E tr.= 6° E transect. Station 54 is marked with a black asterisk.

3.54 CHEMTAX analysis

The CHEMTAX analysis is a way to distinguish and quantify the contribution of various phytoplankton groups based on the measured marker pigment concentrations. In total eight phytoplankton groups were included in the analysis based on prior knowledge from the microscopy results and the literature. Clear geographical patterns were observed in the distribution of the groups in line with the other phytoplankton data sources. Diatoms pigment type 2 (diatoms containing Chl c_3) had the highest biomass, followed by diatoms type 1 and the haptophyte-like group (Fig. 10). Diatoms type 1 ranged up to 0.17 µg Chl a L^{-1} and had the highest values in the upper water column at Astrid Ridge and Maud Rise. Diatoms type 2 were most prominent at station 53 and at depth at Maud Rise with a maximum value of 0.78 µg Chl a L^{-1}. The haptophytes-6 -like had the highest values at Maud Rise and the upper water column at the 6° E transect with a maximum value of 0.18 µg Chl a L^{-1}, but clear presence also at Astrid Ridge. Of the dinoflagellate groups, type 2 had higher biomass and was present in all areas, though only at the surface at Maud Rise, with a maximum value of 0.10 µg Chl a L^{-1}. Occurrence of dinoflagellates type 1 (peridinin-containing dinoflagellates), prasinophytes, chlorophytes and cryptophytes in the CHEMTAX results (Fig. 10) followed closely the distribution of their respective marker pigments (Fig. A10 and A129) and was correspondingly scattered and scarce. A maximum value of 0.04 µg Chl a L^{-1} was found for dinoflagellates type 1 and 0.03 µg Chl a L^{-1} for the other three groups. From the Chl b-containing groups, chlorophytes were more abundant than prasinophytes with a clear presence along the 6° E transect.

The final RMSE for the clusters Maud Rise, Astrid Ridge surface, Astrid Ridge deep and other stations (stations 53, 54 and 6° transect) was 0.017, 0.064, 0.080 and 0.069, respectively (average RMSE of the best 6 runs). The final output ratio matrices for each of the clusters are presented in Table B21 for potential use as initial ratio matrices in future studies in the area. It is noteworthy that differentiating the data between the sampling areas, and in some cases along the depth gradient, improved the results.

428
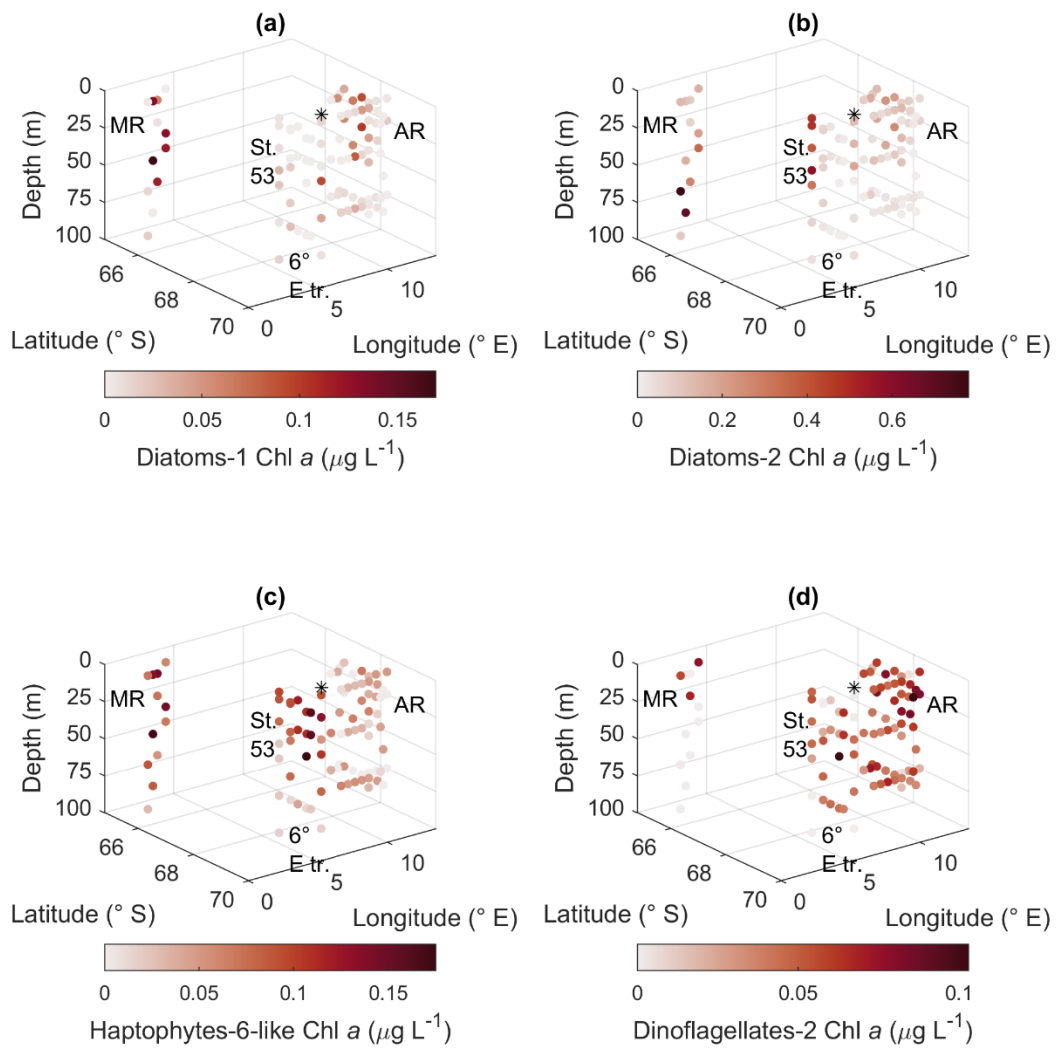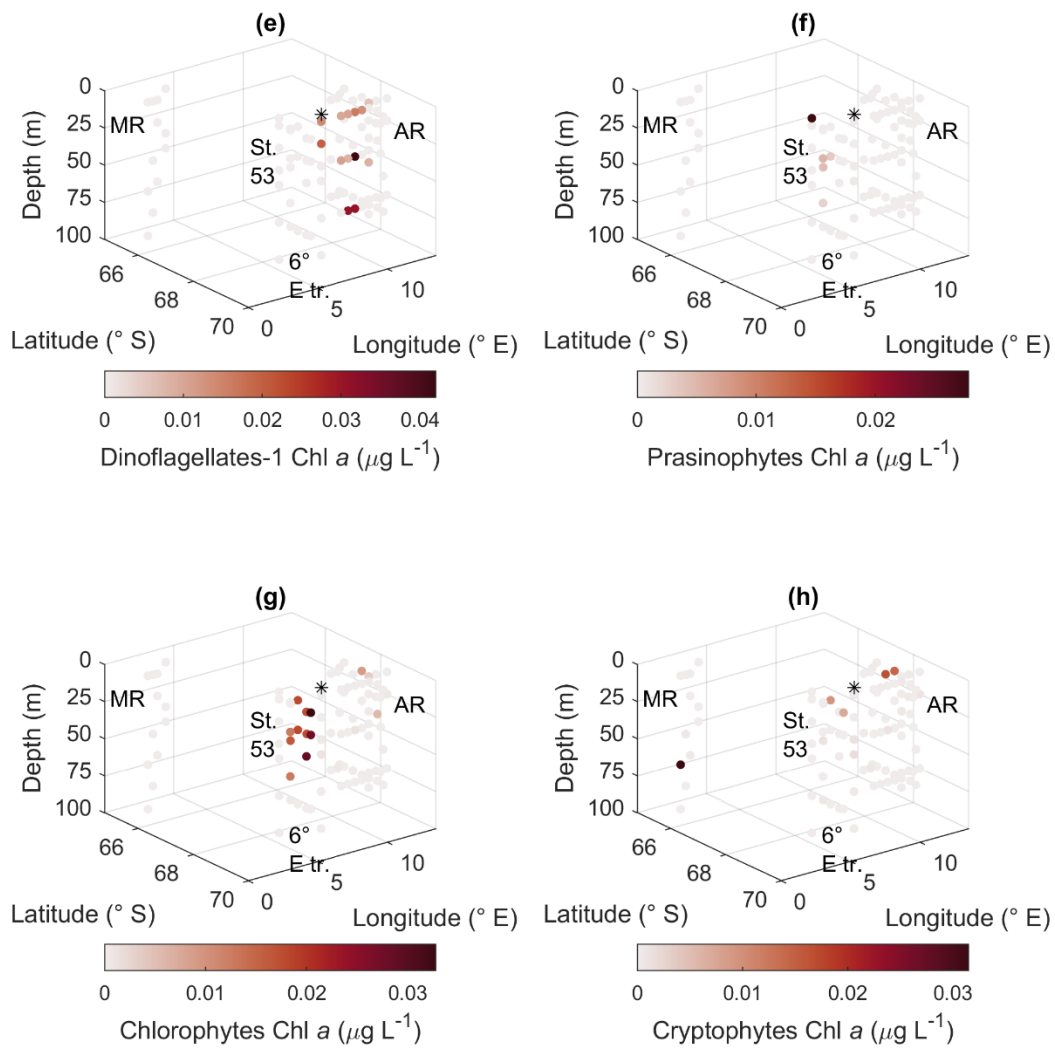
Figure 10: CHEMTAX results for the different algal groups. (a) Diatoms type 1, (b) diatoms type 2, (c) haptophytes type 6 -like, (d) dinoflagellates type 1, (e) dinoflagellates type 2, (f) prasinophytes, (g) chlorophytes and (h) cryptophytes. MR=Maud Rise, St. 53=station 53, AR=Astrid Ridge, 6° E tr.= 6° E transect. Station 54 is marked with a black asterisk.

Initial ratios	Chl_c3	Chlc_1_2	Peri	But-fuco	Fuco	Hex-fuco	Allo	Lut	Chl_b	Chl_a
Prasinophytes	0	0	0	0	0	0	0	0.0066	0.55	1
Chlorophytes	0	0	0	0	0	0	0	0.23	0.15	1
Cryptophytes	0	0.17	0	0	0	0	0.21	0	0	1
Diatoms-1	0	0.09	0	0	1.04	0	0	0	0	1
Diatoms-2	0.016	0.22	0	0	0.83	0	0	0	0	1
Dinoflagellates-1	0	0.23	0.82	0	0	0	0	0	0	1
Dinoflagellates-2	0.04	0.12	0	0.06	0.19	0.18	0	0	0	1
Haptophytes-6-like	0.18	0.18	0	0.005	0.23	0.47	0	0	0	1

Final ratios										
Maud Rise	Chl_c3	Chlc_1_2	Peri	But-fuco	Fuco	Hex-fuco	Allo	Lut	Chl_b	Chl_a
Prasinophytes	0	0	0	0	0	0	0	0.006	0.533	1
Chlorophytes	0	0	0	0	0	0	0	0.239	0.157	1
Cryptophytes	0	0.163	0	0	0	0	0.191	0	0	1
Diatoms-1	0	0.101	0	0	0.624	0	0	0	0	1
Diatoms-2	0.187	0.561	0	0	0.974	0	0	0	0	1
Dinoflagellates-1	0	0.221	0.714	0	0	0	0	0	0	1
Dinoflagellates-2	0.100	0.284	0	0.227	0.588	0.304	0	0	0	1
Haptophytes-6-like	0.495	0.809	0	0.003	0.557	0.404	0	0	0	1
Astrid Ridge surface	Chl_c3	Chlc_1_2	Peri	But-fuco	Fuco	Hex-fuco	Allo	Lut	Chl_b	Chl_a
Prasinophytes	0	0	0	0	0	0	0	0.006	0.507	1
Chlorophytes	0	0	0	0	0	0	0	0.260	0.153	1
Cryptophytes	0	0.179	0	0	0	0	0.211	0	0	1
Diatoms-1	0	0.112	0	0	1.232	0	0	0	0	1
Diatoms-2	0.015	0.324	0	0	0.429	0	0	0	0	1
Dinoflagellates-1	0	0.219	0.802	0	0	0	0	0	0	1
Dinoflagellates-2	0.031	0.209	0	0.142	0.256	0.576	0	0	0	1
Haptophytes-6-like	0.943	0.392	0	0.012	0.502	0.795	0	0	0	1
Astrid Ridge deep	Chl_c3	Chlc_1_2	Peri	But-fuco	Fuco	Hex-fuco	Allo	Lut	Chl_b	Chl_a
Prasinophytes	0	0	0	0	0	0	0	0.007	0.475	1
Chlorophytes	0	0	0	0	0	0	0	0.220	0.136	1
Cryptophytes	0	0.156	0	0	0	0	0.226	0	0	1
Diatoms-1	0	0.088	0	0	1.014	0	0	0	0	1
Diatoms-2	0.016	0.276	0	0	0.463	0	0	0	0	1
Dinoflagellates-1	0	0.233	0.765	0	0	0	0	0	0	1
Dinoflagellates-2	0.035	0.219	0	0.263	0.170	0.723	0	0	0	1
Haptophytes-6-like	0.728	0.240	0	0.007	0.379	0.336	0	0	0	1

Other stations	Chl_c3	Chlc_1-2	Peri	But-fuco	Fuco	Hex-fuco	Allo	Lut	Chl_b	Chl_a
Prasinophytes	0	0	0	0	0	0	0	0.007	0.400	1
Chlorophytes	0	0	0	0	0	0	0	0.306	0.096	1
Cryptophytes	0	0.190	0	0	0	0	0.236	0	0	1
Diatoms-1	0	0.088	0	0	1.030	0	0	0	0	1
Diatoms-2	0.017	0.378	0	0	0.608	0	0	0	0	1
Dinoflagellates 1	0	0.238	0.695	0	0	0	0	0	0	1
Dinoflagellates 2	0.301	0.414	0	0.358	0.403	0.573	0	0	0	1
Haptophytes 6 like	0.418	0.280	0	0.010	0.189	1.063	0	0	0	1

Peri: peridinin; Fuco: fucoxanthin; Allo: alloxanthin; Lut: lutein.

4. Discussion

4.1 Community patterns at the regional scale

The early autumn phyto and protozooplankton community composition in Kong Håkon VII Hav was dominated by diatoms and other algae from the Chl *c* -lineage, which is typical for the open Southern Ocean (e.g., Buck and Garrison, 1983; Davidson et al., 2010; Kang and Fryxell, 1993; van Leeuwe et al., 2015; Nöthig et al., 2009; Peeken, 1997; Smetacek et al., 2004; Wright et al., 2010). Although the communities in the different sampling areas were largely similar (Fig. 6), Some differences in the relative abundance of the major taxa were observed between the sampling areas, which will be discussed in the sections below. Furthermore, also in relation to the main oceanographic variables, the different areas showed some separation in a CCA analysis (Fig. 7). In particular, Maud Rise and the station 53 can be considered more oceanic with, in general terms, higher temperatures and salinity and a deeper MLD. Silicic acid was present in lower concentrations in surface waters at Maud Rise (Kauko et al., 2021), likely due to drawdown by the phytoplankton bloom, but concentrations in the depth both at Maud Rise and the station 53 were higher than at Astrid Ridge and the 6° E transect, and may help to sustain blooms of this type with the dominance of a heavily silicified species (see also section 4.3).

When it comes to biodiversity, phytoplankton species richness was similar between the areas investigated. The Maud Rise bloom had lower diversity indices, which can be attributed to the dominance of *C. dicheata* during the bloom (Vallina et al., 2014) and hence is likely not reflecting persistent lower diversity at Maud Rise compared to the other areas – both species richness and evenness in abundances between species are components of biodiversity. The diversity index and species richness sampling area averages in our study were clearly higher than cluster averages in a community composition study conducted at 30° – 80° E in austral summer (Davidson et al., 2010), and the diversity indices were relatively high for the low biomass level compared to a global data compilation (Irigoien et al., 2004).

All in all, oOur pigment composition was very similar (though with lower maximum concentrations) than in athe study by Gibberd et al. (2013) that was conducted mainly at the prime meridian and the Weddell Sea in January – February one decade earlier. Surprisingly, including the haptophytes pigment type 6 ("type species"

463   coccolithophore *Gephyrocapsa huxleyi*, formerly known as *Emiliania huxleyi*; Bendif et al., 2019) gave better

464   results (lower error) in the preliminary CHEMTAX analysis than including the pigment type 8 (e.g.

465   *Phaeocystis*), and when including both pigment types, type 6 was clearly more prominent. However,

466   coccolithophores are not abundant this far south in the Southern Ocean (Balch et al., 2016; Saavedra-Pellitero et

467   al., 2014; Trull et al., 2018), which is confirmed by~~in~~ our microscopy analysis. A few stations in the flow

468   cytometry data may have had low abundances of coccolithophores (not shown; based on high side-scattering and

469   red fluorescence) but neither of these data indicated a strong presence of this group throughout the study.

470   Although blooms of *P. antarctica* are a prominent feature in the marginal ice zones of the Ross Sea (Arrigo et

471   al., 1999) and the Weddell Gyre (Vernet et al. 2019), *P. antarctica* or other prymnesiophytes were not abundant

472   in our microscopy samples. This is consistent with the observation that blooms of *P. antarctica* are generally

473   rare in the land-remote ACC (Smetacek et al. 2004) and further supported by the low contribution of *P.*

474   *antarctica* to bloom biomass in iron fertilization experiments conducted in the iron-limited Southern Ocean

475   (Boyd et al. 2008). Even the LOHAFEX iron fertilization experiment conducted in low silicate waters with a

476   significant seed population of small initial *P. antarctica* colonies did not result in a bloom of this species,

477   presumably because of strong top down control by copepod grazers (Schulz et al., 2018). Furthermore, blooms

478   of *P. antarctica* seem to coincide with the sea ice retreat and ice edge (Davidson et al., 2010; Kang and Fryxell,

479   1993; Vernet et al., 2019). Our sampling effort was conducted later in the season (i.e., early autumn, at the onset

480   of sea ice formation) and could therefore partly explain why the species was observed at low abundances. A

481   subsequent cruise along the 6° E transect area earlier in the season (in December 2020–January 2021) observed

482   higher abundances of *P. antarctica* (S. Moreau et al., unpublished data).

483   Given the low contribution of both coccolithophores and *P. antarctica*, we have called the pigment group we

484   included in the final CHEMTAX analysis as "Haptophytes-6 -like" to acknowledge that the exact identity of this

485   group is unclear and can contain other types of algae that have similar pigment ratios than the haptophyte 6

486   group. The microscopy analysis indicated that the majority of the flagellates were different types of unidentified

487   flagellates in the size group 3 to 7 µm (note however that this group may and likely did also contain

488   heterotrophic flagellates). It should also be noted that due to the similarity in pigments and pigment ratios, this

489   pigment group will also contain silicoflagellates and chrysophytes. The former have a characteristic appearance

490   and should have been reliably identified in the microscopy samples, thus their share in the pigment group should

491   be correspondingly low as in the microscopy abundances. Unidentified chrysophytes on the contrary could have

492   formed a considerable share of this pigment group. Chrysophytes were regularly observed in our microscopy

493   samples, albeit not in high abundance. Unfortunately, pigment to Chl *a* ratio data are lacking for this group in the

494   Southern Ocean. It is also important to note that CHEMTAX is a statistical approach whose success depends on

495   the correct allocation of algal groups and pigment ratios. For unambiguous distinction between haptophytes and

496   dinoflagellates-2 additional pigments, such as other fucoxanthin derivatives, are needed (see e.g. Mendes et al.,

497   2018). In the lack of those, concurrent microscopy analysis is essential for confirming the algal groups present.

498   ~~Cryptophytes, that were relatively abundant among flagellates in the microscopy samples, also contain similar~~

499   ~~pigments to haptophytes, but due to the low concentrations of their marker pigment alloxanthin they do not show~~

500   ~~up strongly in the CHEMTAX results. The discrepancies might be partly explained with the relatively small~~

501   ~~volume filtered (typically 1 L) for HPLC samples during this study, potentially leading to underestimation of~~

502   ~~pigments that are present in trace amounts. Thus, we recommend a higher filtration volume for further studies.~~

503 ~~All in all, our pigment composition was very similar (though with lower maximum concentrations) than in the~~
504 ~~study by Gibberd et al. (2013) that was conducted mainly at the prime meridian and the Weddell Sea in January~~
505 ~~– February one decade earlier.~~

506 Finally, picophytoplankton was not abundant in the area compared to nanophytoplankton – maximum
507 picophytoplankton abundance was 15 % of maximum nanophytoplankton abundance, and only at certain
508 stations, a distinct picophytoplankton occurrence was observed in the FCM biplots. The absence of coccoid
509 cyanobacteria in the area contributes to low picophytoplankton abundance. Likewise, Rembauville et al. (2017)
510 observed low picophytoplankton contribution (<20 % contribution to phytoplankton carbon) in the Indian sector
511 in the Southern Ocean based on bio-optical observations from biogeochemical Argo floats, however the study
512 area was further north than ours (around 50° S).

513 **4.2 Vertical patterns**

514 Some of the data types and analyses indicated that the phytoplankton communities differed along the depth
515 gradient, in addition to the spatial variability discussed in the next sections. Besides differences in biomass or
516 abundances (e.g., at Astrid Ridge the highest abundances were located in the upper 40 m), the species richness
517 was significantly lower below 40 m. In the cluster analysis (Fig. 6~~5~~), a separation along sampling depth gradient
518 was visible in the figure (most notably separating the 25 m and 75 m depth categories), though further statistical
519 tests did no~~²~~t indicate large differences between communities at different depths. These patterns seem to suggest
520 that the phytoplankton communities above and below the MLD (the average for all the stations was 36 ±13 m,
521 Kauko et al., 2021) differed to some degree. As species richness correlated positively with biomass (Fig. 6d),
522 which is a typical global pattern up to certain biomass level (Vallina et al., 2014), it is not surprising that species
523 richness was lower at depth when surface biomass is typically higher. However, if other abundance patterns
524 contributed to the depth separation was not easy to detect, as the species counts for the most abundant taxa in
525 depth categories (Fig. A6 and A7) did not seem to differ to a great degree from the whole station or area
526 averages (Fig. 2). A study from the Indian sector of the Southern Ocean concluded that phytoplankton
527 communities at the deep Chl *a* maximum were not fundamentally different from surface mixed layer
528 communities (Gomi et al., 2010), similarly to a study conducted between 30 and 80° E (Davidson et al., 2010).
529 Moreover, the distinct sub-surface communities dominated by large diatoms found in the Southern Ocean are
530 suggested to be linked to upstream surface blooms (Baldry et al., 2020).

531 At Maud Rise, vertical patterns were less clear as it seemed that the surface bloom was sinking based, e.g., on
532 relatively high Chl *a* concentrations at depth and below the MLD (Kauko et al., 2021) and dampened
533 diadinoxanthin vertical patterns compared to the other areas (Fig. 8f). This indicates that cells deeper in the water
534 column had recently been exposed to upper water column light conditions. Furthermore, the diatom community
535 at 100 m depth (at station 110) was dominated by *C. dichaeta*, whereas at 70 m at the same station the diatom
536 community was more diverse (Fig. A8). There could be a somewhat separate community below the MLD (60 m
537 at this station; Kauko et al., 2020), having access to more iron than the surface community and therefore thriving
538 there (Baldry et al., 2020), which the sinking surface bloom could be "passing by" and then again dominating at
539 100 m depth. However, to properly resolve the vertical patterns, repeated sampling of different depths is needed,
540 in addition to the snapshot picture provided here.

4.3 *Chaetoceros dichaeta* blooms associated with natural iron fertilization

The different analyses – microscopic identification and pigments (especially fucoxanthin patterns and CHEMTAX results) – all show that a diatom bloom occurred at Maud Rise and station 53. We describe the observed phytoplankton patterns as a bloom based on a bloom phenology study (conducted with remote-sensing data) that showed that the average Chl *a* concentration during the blooms and the bloom amplitude in this area are mainly in the order of 0.5-1.5 mg Chl *a* m^{-3} (Fig. 6c and 11c in Kauko et al., 2021). We visited the study area late in the growing season (in late March), therefore it can be anticipated that the Chl *a* concentrations earlier in the season were higher, and that the observed maximum concentrations of >0.5 mg Chl *a* m^{-3} indicated a seasonal phytoplankton bloom. The maximum diatom abundance was somewhat higher compared to a study in the north-western Weddell Sea in the same season (March): 1.9×10^6 cells L^{-1} in our study compared to 1.2×10^6 cells L^{-1} in Kang and Fryxell (1993).

Both blooms observed in the present study were dominated by *C. dichaeta,* which is an important and widespread species in the pelagic communities across the Southern Ocean (reviewed in Assmy et al., 2008). Maximum *C. dichaeta* abundance of 1.6×10^6 cells L^{-1} was again higher than in the above mentioned study (0.4 $\times 10^6$ cells L^{-1}; Kang and Fryxell, 1993). This species seemed to belong to the diatoms pigment type 2, which was the most abundant of all groups and had maximum values at station 53 and Maud Rise. Likewise, in the study by Wright et al. (2010) east of our study area (30° – 80° E) the diatom type 2 was more widespread than the type 1 (though not linked to *C. dichaeta* dominance; Davidson et al., 2010), contrary to large parts of the prime meridian area and the Weddell Sea (Gibberd et al., 2013).

The observed bloom type belongs to the typical ecosystem of the open ocean iron-depleted areas of the Southern Ocean, where a few large, heavily silicified species are the main bloom-forming species (Lafond et al., 2020; Lasbleiz et al., 2016; Smetacek et al., 2004). Grazing from copepods and protozoans exerts a strong selective pressure in these areas, and large diatom species with strong silicate armour and spines can more easily escape predation (Hansen et al., 1994; Irigoien et al., 2005; Löder et al., 2011; Pančić and Kiørboe, 2018; Smetacek et al., 2004). Indeed, small copepods (180–1000 µm) and protists were the main zooplankton groups in the area and more abundant at Maud Rise than in the other sampling areas (corresponding data for station 53 are lacking; Kauko et al., 2021). Furthermore, amongst the diatoms characteristic of the iron-limited ACC, *C. dichaeta* seems to be quite responsive to elevated iron levels as it dominated blooms induced by the iron fertilization experiments EIFEX and SOFeX-South conducted in high silicate waters of the Southern Ocean during late austral summer (Assmy et al., 2013; Coale et al., 2004).

The observed phytoplankton community type is in contrast to iron-replete near-coastal areas where blooms are dominated by smaller and often spore-forming neritic diatoms e.g. from the genus *Thalassiosira* and the subgenus *Hyalochaete* within the genus *Chaetoceros* that can realize fast growth rates (Armand et al., 2008; Lasbleiz et al., 2016; Quéguiner, 2013; Smetacek et al., 2004). Species belonging to these genera were observed in our samples, but only in low abundances. Although there are regional differences in bloom magnitude and, likely, iron input in our study area (Kauko et al., 2021), the iron input does not seem to be sufficient and persistent enough to sustain the coastal diatom communities characteristic of the iron-replete areas of the Southern Ocean. In this context also the inoculum is important, that is, coastal diatom species are likely to

579 have low seeding abundance in oceanic waters at the start of the growth season, especially the spore forming

580 taxa that tend to overwinter as resting spores on the seafloor. Indeed, the spore forming diatom *Chaetoceros*

581 *debilis* responded with exponential growth to iron fertilization in the EisenEx experiment in the polar frontal

582 zone of the ACC but remained a minor component of the iron-induced diatom bloom because it started with a

583 very low seed population (Assmy et al. 2007). Changes in the spatial extent of the iron-replete productive system

584 and the iron-deplete HNLC system are reflected in diatom frustules preserved in Southern Ocean sediments

585 covering the last glacial and interglacial time periods. During the more iron-rich glacial periods resting spores of

586 the above mentioned *Chaetoceros* species dominated while the typical HNLC diatom *F. kerguelensis* dominated

587 sediments representative of the interglacial period with less iron input to the Southern Ocean (Abelmann et al.,

588 2006).

589 The blooms in our area were likely fuelled by upwelling-induced natural iron fertilization: at Maud Rise, the sea

590 mount topography is suggested to lead to upwelling of nutrients (von Berg et al., 2020; Jena and Pillai, 2020;

591 Kauko et al., 2021; de Steur et al., 2007), whereas in the area represented by station 53 wind patterns create

592 suitable upwelling conditions and supply the area with additional, deep iron (Moreau et al., in prep.). Carbon

593 export to the deep sea is typically low in the HNLC areas of the Southern Ocean while silica export is high due

594 to the heavily silicified frustules of the dominant HNLC diatom taxa (Assmy et al., 2013; Lafond et al., 2020;

595 Smetacek et al., 2004). On the other hand, significant carbon export from open-ocean fertilized blooms has been

596 observed (Smetacek et al., 2012) and attributed to mass mortality and aggregation of chain-forming oceanic

597 *Chaetoceros* species, particularly *C. dichaeta* (Assmy et al., 2013). In our study, the vertical Chl *a* profiles show

598 that at Maud Rise the biomass, as Chl *a* concentration above 0.01 mg m^{-3}, seemed to be sinking to approximately

599 300 m depth at the time of sampling (Kauko et al., 2021). Krill (which would be an important grazer of these

600 large and spiny colonies; Smetacek et al., 2004) was not observed in notable abundances at Maud Rise during

601 the cruise (Kauko et al., 2021), which may indicate lower grazing pressure on the bloom and support vertical

602 export as the main loss term. Indeed, fluxes of labile organic matter to the seafloor are elevated at Maud Rise

603 compared to the surrounding waters (Sachs et al., 2009). On the contrary, at station 53 grazing presumably by

604 krill played an important role for the bloom fate (Moreau et al., in prep.).

605 In addition to the diatom dominance, larger nanophytoplankton (Nanophytoplankton 2 in the FCM results) were

606 a notable component of the community at Maud Rise and station 53 (unlike in the other sampling areas). None of

607 the flagellate groups identified with microscopy correlated well with these results so the identity is unknown,

608 although in the average abundance results choanoflagellates showed higher abundance in these areas compared

609 to the others. Lastly, ciliates also showed patterns that were seemingly connected to the blooms and/or the

610 nanophytoplankton patterns, namely the larger share of tintinnid ciliates at Maud Rise and station 53.

611 **4.4 Dominance of pennate diatoms at Astrid Ridge**

612 Astrid Ridge and station 54 differed from the other sampling areas most notably by the more prominent role of

613 pennate diatoms (56 to 72 % of total diatom abundance). Phytoplankton abundance was in general much lower at

614 Astrid Ridge and station 54 than at Maud Rise, but diatoms were still more abundant than flagellates. The

615 phytoplankton community at Astrid Ridge was likely in a post bloom situation (Kauko et al., 2021). Also in this

616 area many of the dominant species fit into the concept of large, heavily silicified diatoms of the iron-deplete

617 areas (see discussion in the previous section; Smetacek et al., 2004), and *C. dichaeta* was also an important

618 species here. In terms of average abundance in all Astrid Ridge samples, the six most abundant taxa were the

619 pennate diatoms *Pseudo-nitzschia* spp., *Fragilariopsis nana*, *F. kerguelensis* and *Thalassiothrix antarctica* and

620 the centric diatoms *Thalassiosira* spp. and *C. dichaeta*.

621 Pennate diatoms are typically dominant in sea ice (Hop et al., 2020; van Leeuwe et al., 2018; Leu et al., 2015;

622 Poulin et al., 2011). This was also true for our study, where two ice cores sampled along the 6° E transect

623 showed strong dominance of pennate diatoms (≤95 % of diatom abundance; Fig. A14~~3~~). Furthermore, out of the

624 20 dominant diatom species or genera in the ice cores and at Astrid Ridge (average of the samples down to 100

625 m), 12 were shared between these two habitats (Table B3~~2~~; see the table also for ice core method descriptions). It

626 is however difficult to say whether the sea ice communities influenced the phytoplankton community

627 composition, or vice versa, as species exchange between the habitats occurs both during sea ice melt and sea ice

628 formation (Hardge et al., 2017). Contribution from sea ice to the planktonic communities was observed in spring

629 e.g. at the West Antarctic Peninsula (van Leeuwe et al., 2020) especially for flagellate species (van Leeuwe et

630 al., 2022), and in the Weddell Sea (Garrison et al., 1987), and was also suggested to be continuous along the ice

631 edge in the Weddell Sea (Ackley et al., 1979). However, cells from the sea ice do not necessarily grow and form

632 a bloom in the water column (e.g., van Leeuwe et al., 2022; Ligowski et al., 1992). ~~, or if the s~~Sea ice on the

633 other hand can reflect~~ed~~ the water column community because forming sea ice traps algal cells from the water

634 (Garrison et al., 1983), after which~~but with some~~ species succession towards ice specialists can occur (Kauko et

635 al., 2018)~~, as species exchange between the habitats occurs both during sea ice melt and sea ice formation~~

636 ~~(Hardge et al., 2017)~~. If the former was the case here, the later sea ice retreat at Astrid Ridge compared to many

637 of the other sampling areas (Kauko et al., 2021) could introduce algae from the sea ice at a later stage in the

638 growing season and possibly partly explain the dominance of pennate diatoms in this area. Due to the long sea

639 ice period, sea ice algae could also have a prominent sediment seed bank in the area, which could introduce cells

640 higher up in the water column through local current processes such as the strong tidal currents in this area

641 (Kauko et al., 2021). This topic thus requires further study and is interesting also in the light of any possible

642 co~~a~~stal to offshore gradients.

643 Astrid Ridge was most thoroughly sampled from all the sampling areas with a large number of CTD stations and

644 samples, with some variation seen within this area. In particular a few stations on the western part of Astrid

645 Ridge showed distinct features, including the highest picophytoplankton abundances and peridinin

646 concentrations of the entire sampling area. Future studies concentrating on ~~the detailed~~ current or food web

647 patterns in this area could indicate which processes contributed to these observations. However, when the

648 different parts of Astrid Ridge (southern, northern, western and eastern parts of the cross transect) were marked

649 in the cluster analysis using microscopy counts (figures not shown), no clear patterns emerged, and the sub-areas

650 were mixed.

651 **4.5 A flagellate-dominated post-bloom community**

652 Both FCM, pigment and microscopy data indicated that flagellates and the smaller nanophytoplankton were an

653 important component of the phytoplankton community at the 6° E transect. According to the microscopy data,

654 flagellates numerically dominated over diatoms, and the observed marker pigments pointed towards a diverse

flagellate community. Except cryptophytes, flagellates remained to a large degree unidentified in the microscopy samples, but pigment data showed that algae from the Chl *c*- lineage were most abundant. These could have been haptophytes and possibly in addition chrysophytes (see Discussion section 4.1). Chl *b* containing algae were present in low concentrations.

The 6° E transect area, similarly to Astrid Ridge, typically experiences summer blooms, and the low biomass and abundances during this cruise likely point to a post-bloom situation (Kauko et al., 2021). Indeed, the importance of flagellates and pico- and nanophytoplankton is thought to be the typical situation e.g. in the Weddell Gyre (Vernet et al., 2019) or in the Southern Ocean in general (Buma et al., 1990; Detmer and Bathmann, 1997; Smetacek et al., 2004) outside the bloom periods, during which larger cells, mainly diatoms, dominate. The abundance of nanophytoplankton in our FCM samples was very similar to the suggested "background concentration" of $2–4 \times 10^6$ cells L^{-1} for the Southern Ocean (Detmer and Bathmann, 1997). Previous studies from Wright et al. (2010) and Davidson et al. (2010) observed somewhat further east of our study area (30° – 80° E) that the northern areas with most advanced blooms and likely depleted iron concentrations were dominated by nanoflagellates, and suggested that krill grazing contributed to the community composition as they are ineffective in feeding on the smaller organisms, as also pointed out by other studies (Granéli et al., 1993; Kopczynska, 1992). Kauko et al. (2021) hypothesized that blooms in our study area were at least partly terminated by krill grazing, as macronutrient concentrations in the upper water column were still sufficient to support phytoplankton production during the cruise (i.e., after the peak bloom), and short-term incubations indicated minimal iron limitation in the southern cruise area (Singh et al., in prep.).

Although station 53 was close to the 6° E transect, it showed a different relative community composition, which could be a result of the different bloom phase. The station 53 area typically has a late bloom according to a phenology analysis using satellite Chl *a* remote sensing data (Kauko et al., 2021) and was also during the cruise in an earlier bloom phase than the surrounding areas. ~~These two areas were also separated by an oceanographic front (Moreau et al., in prep.).~~ It can be speculated that the 6° E transect area had earlier experienced a *C. dichaeta* dominated bloom similar to Maud Rise and station 53 just north of this transect, as *C. dichaeta* had fairly high relative abundance (21 %) among diatoms along the 6° E transect.

There was possibly a south to north gradient visible in the diatom community along the 6° E transect (Fig. A15~~4~~). The relative abundance of *C. dichaeta* increased at the northernmost station, i.e., towards station 53, whereas the relative abundance of e.g. *F. nana* decreased. Additionally, lutein and hex-fuco showed higher pigment to Chl *a* ratios in the southern part of the transect. At the coast, several oceanographic features and processes can affect iron sources and the phytoplankton growth environment: the Antarctic Slope Current, glacial melt-related processes, shallower bottom topography and the occurrence of latent heat polynyas (e.g. Arrigo and van Dijken, 2003; Dinniman et al., 2020; Dong et al., 2016). Differences between onshore and offshore communities have been observed east of the study area (between 30 and 80° E; Davidson et al., 2010). Future studies where sampling very close to the coast is possible will give further insights into the community composition in these areas. Due to heavy sea ice conditions, it was not possible to reach the coast during this cruise.

5. Conclusions

In this study, we have explored the phytoplankton community composition in a poorly studied area east of the prime meridian in the Southern Ocean, in the Kong Håkon VII Hav. The results indicate that the area has a typical open-ocean community composition with large, heavily silicified diatoms dominating~~forming the~~ blooms. These species traits are, according to the literature, a long-term evolutionary response to the heavy grazing pressure exerted by the micro- and mesozooplankton in the Southern Ocean. Furthermore, seasonal succession and bloom phase differences likely contributed to differences between the sampling areas, with post-bloom areas having a higher relative contribution by flagellates. Grazing (especially by krill) on bloom-forming species had likely shaped the community composition. The transient diatom blooms overlay a more stable flagellate-dominated background community.

The blooms described here were likely fuelled by natural iron fertilization driven by topography and wind-driven upwelling. Open ocean blooms triggered by local iron input cannot rival the more productive coastal systems of the Southern Ocean but enhance carbon export and feed a significant krill subpopulation. These results thus indicate that there exists a "middle ground" between the iron-replete coastal blooms and the iron-deplete status of the HNLC areas: oceanic blooms that are formed by some of the HNLC diatoms, particularly *C. dichaeta*, with important implications for the strength of the biological carbon pump and transfer to higher trophic levels in these areas. Compared to the neritic diatoms of the more productive coastal areas, *C. dichaeta* is a slow growing species, but within the diatoms characteristic of the HNLC areas it is among the faster growing ones, responding strongly to artificial (and natural) iron fertilization and contributing to carbon export. Thus, within this group, *C. dichaeta* can be characterized as a bloom-former and carbon sinker.

It is important to note that while the main groups of the phytoplankton community were revealed by the pigment data, the resolution of pigment data is not high enough to differentiate between, for instance, different diatoms and delineate the patterns discussed above. Therefore, microscopy data or other imaging techniques are needed to determine microphytoplankton to species level in order to fully understand the community composition. It is also noteworthy that the pigment approach may not capture a large part of the dinoflagellate community with a peridinin-based pigment type, as in our study the majority of dinoflagellates belonged to the genus *Gymnodinium*, which contains similar pigments to e.g. diatoms and haptophytes and no peridinin (Jeffrey et al., 2011). In addition, non-pigment containing heterotrophic species call for different approaches to identify this important group. Finally, the haptophyte-type pigment group requires other types of analyses to be properly identified. A possible solution for future studies could be a combination with 18S rRNA-sequencing, for a better interpretation of the various target groups.

This is the first thorough characterization of phytoplankton community composition in the area, studying the early autumn season. Future studies will show how it relates to the different seasons such as the early bloom phase in spring and whether seasonal succession can be seen in the community composition. In addition, the very near coast and coastal polynyas could not be sampled during this study and could potentially differ in their community composition, and future sampling can offer further insights into possible north-south gradients.

6. Data availability

The data presented in this study can be found in online repositories (Norwegian Polar Data Centre, data.npolar.no) in Moreau et al. (2020) and Kauko et al. (2022).

7. Author contributions

HMK planned the study, analysed the data and wrote the first manuscript draft. SM, HMK, TRK and AS planned and carried out the field work. HMK and AS analysed the FCM samples. PA contributed with expert knowledge. IP processed the pigment samples data and guided on the CHEMTAX analysis. MR and JW analysed the microscopy samples. GB arranged the FCM analysis and processed the data. All authors contributed to the manuscript writing.

8. Competing interest

The authors declare that they have no conflict of interest.

9. Acknowledgements

10. Appendices

Appendix A. Supplementary figures.

752

Figure A1: A summary plot from the *anosim* analysis (testing differences between the sampling areas in species abundances after the NMDS analysis). Range of dissimilarities in the different areas (2-6: station 53, station 54, Astrid Ridge, the 6° E transect and Maud Rise, respectively).

756
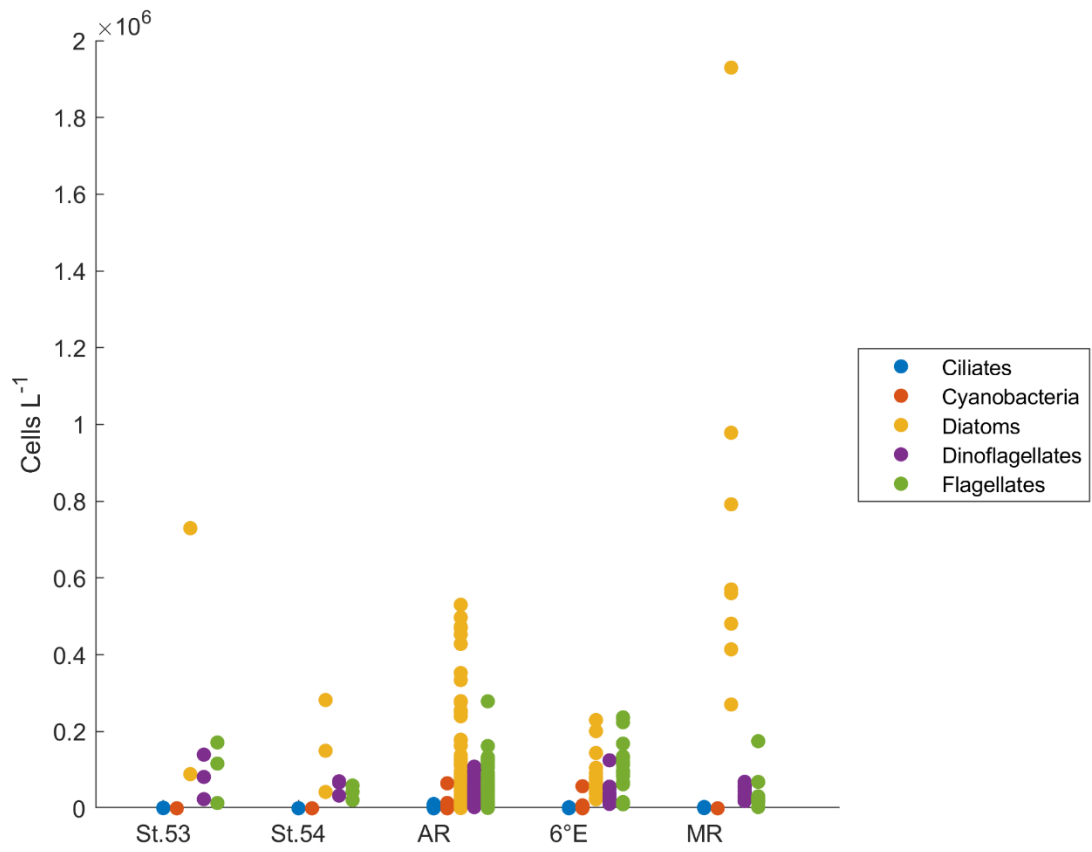
Figure A2: Protist abundance in all samples in the different sampling areas based on microscopy. St.53=station 53, St.54=station 54, AR=Astrid Ridge, 6°E= 6° E transect, MR=Maud Rise.
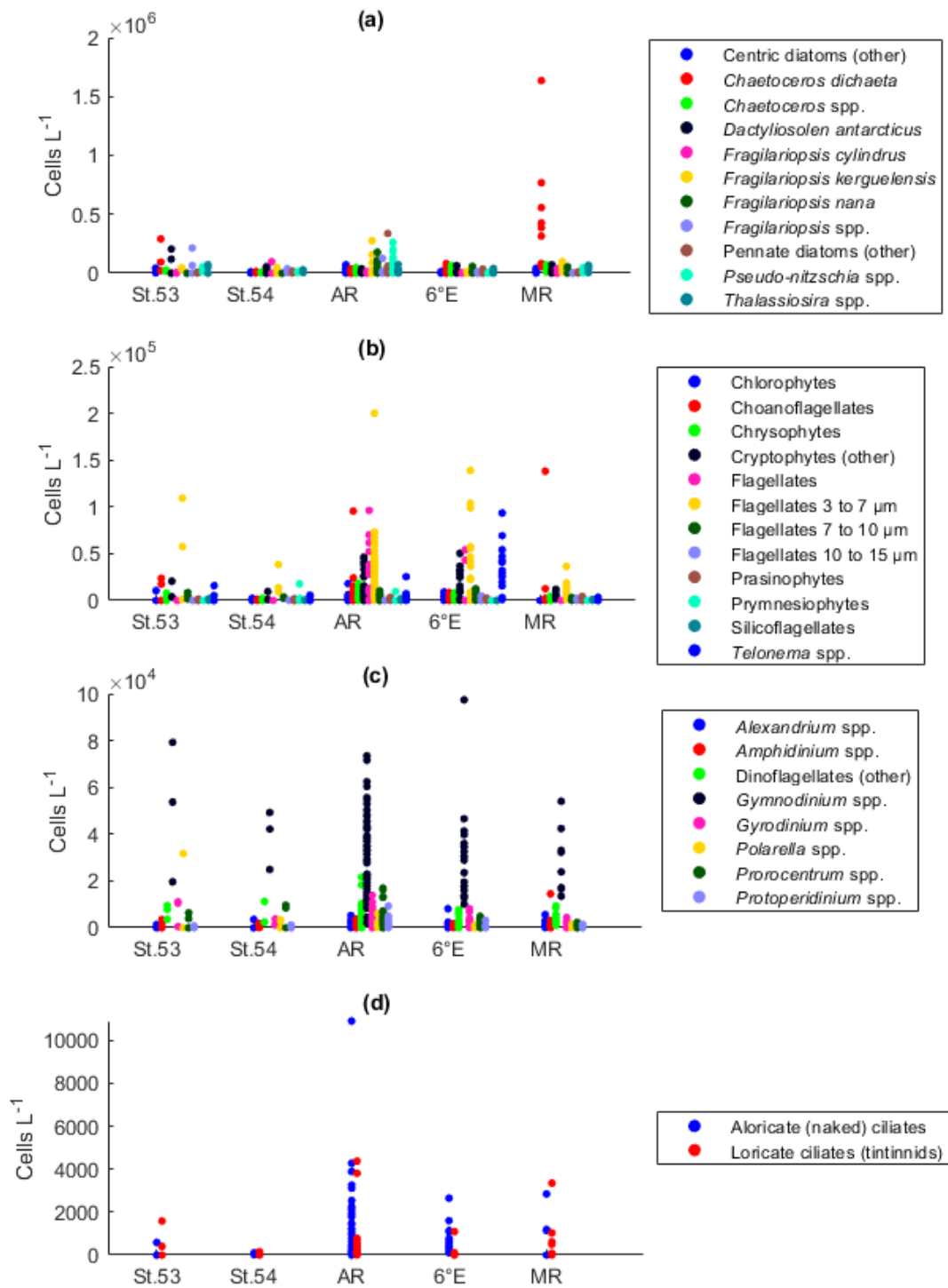
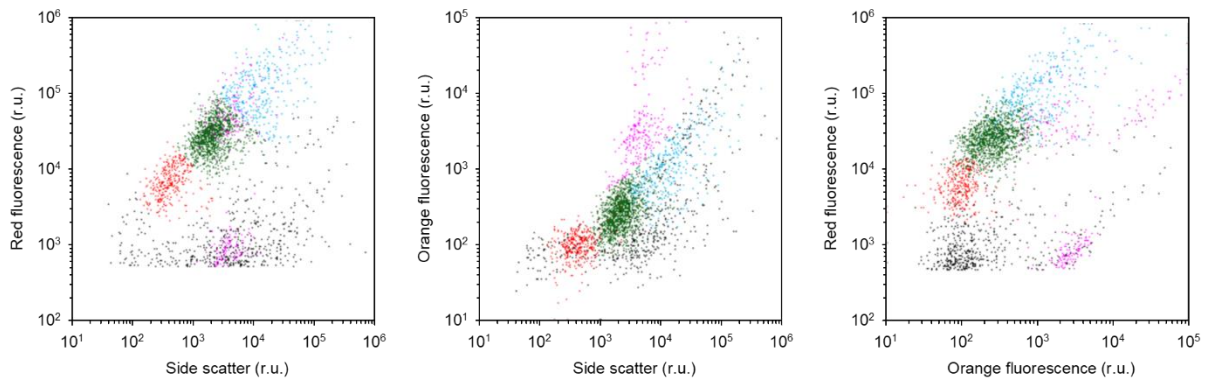**Figure A3: Protist abundance in all samples in the different sampling areas (based on microscopy) for (a) diatoms, (b) flagellates, (c) dinoflagellates and (d) ciliates. St.53=station 53, St.54=station 54, AR=Astrid Ridge, 6°E= 6° E transect, MR=Maud Rise.**
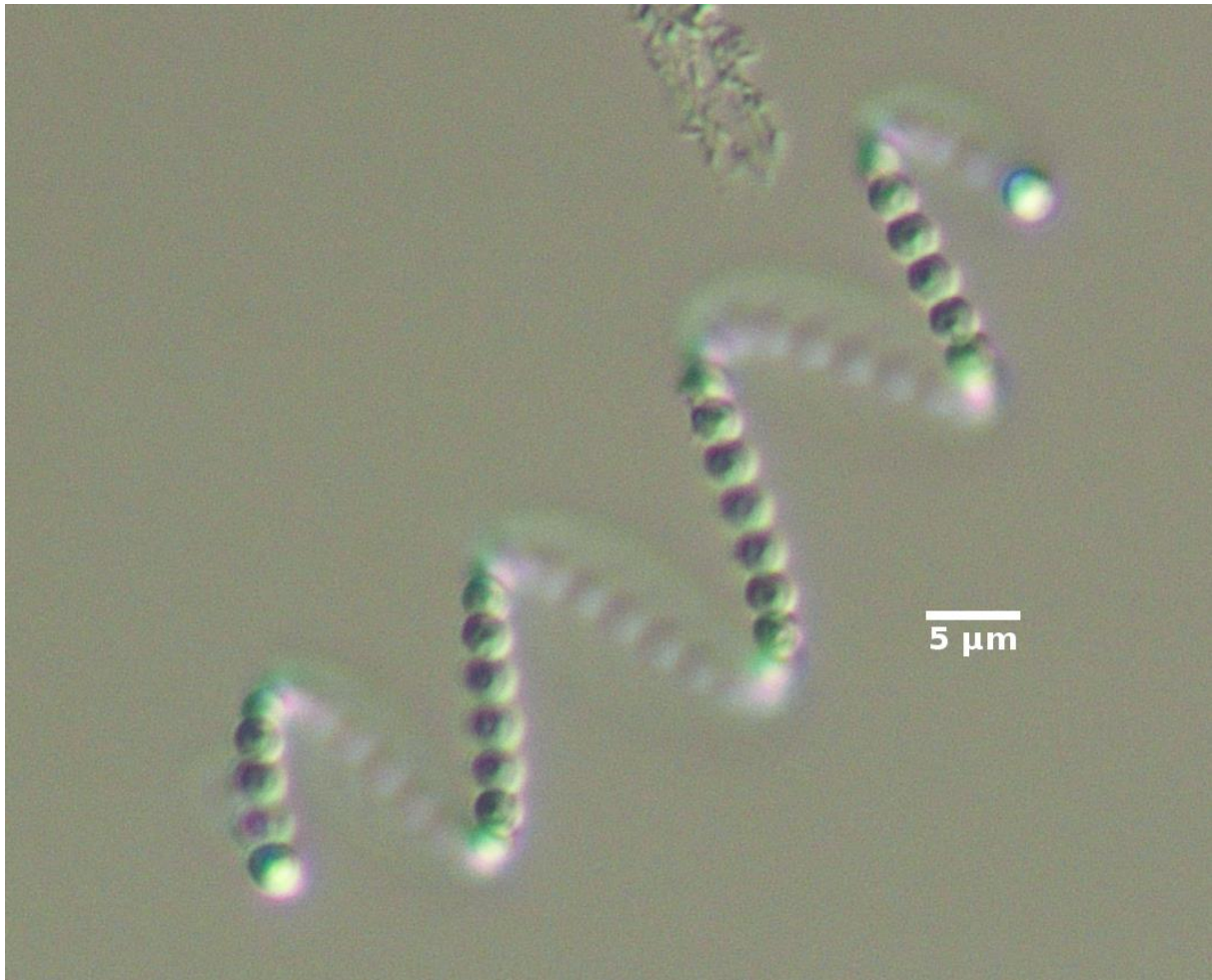
763

764   **Figure A4: Filamentous blue-green algae cf. *Anabaena* sp..**

765

766   **Figure A5: Scatter plots indicating the position of the different phytoplankton populations in the cytograms.**
767   **Picophytoplankton, Nanophytoplankton 1 and Nanophytoplankton 2 were discriminated based on chlorophyll red**
768   **autofluorescence versus side scatter (red, green and blue dots respectively). Possible cyanobacteria and cryptophytes**
769   **were in addition recognized based on their orange autofluorescence (violet dots). The example shown is from CTD**
770   **station 61 at 40 m depth. Axis are in relative units (r.u.).**
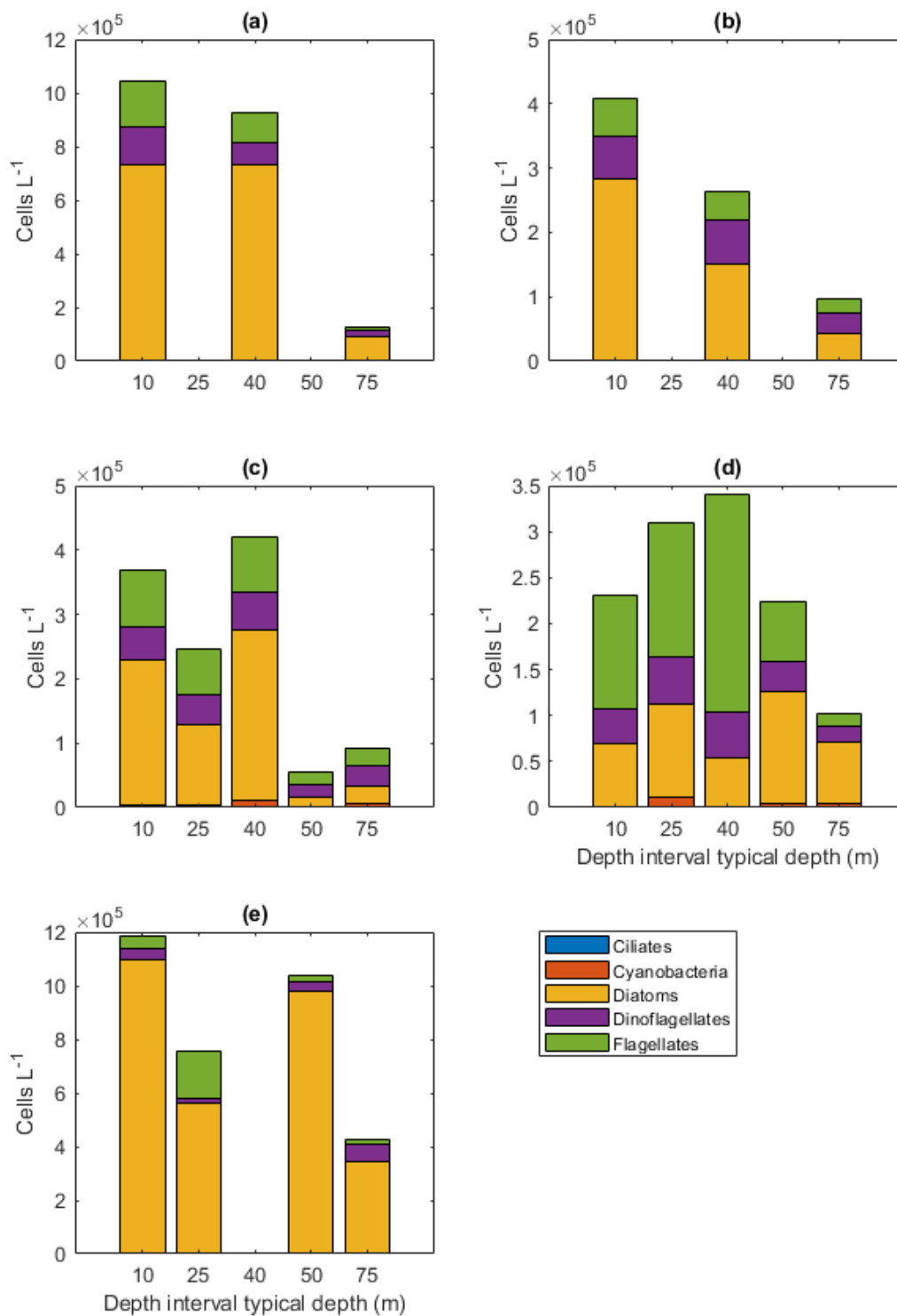
Figure A6: Protist abundances in the different sampling areas averaged per depth interval for (a) station 53, (b) station 54, (c) Astrid Ridge, (d) 6° E transect and (e) Maud Rise. Depth intervals (with typical sampling depth in brackets): 5-10 (10); 25-35 (25), 35-45 (40), 50-60, 65-85 (75) m.
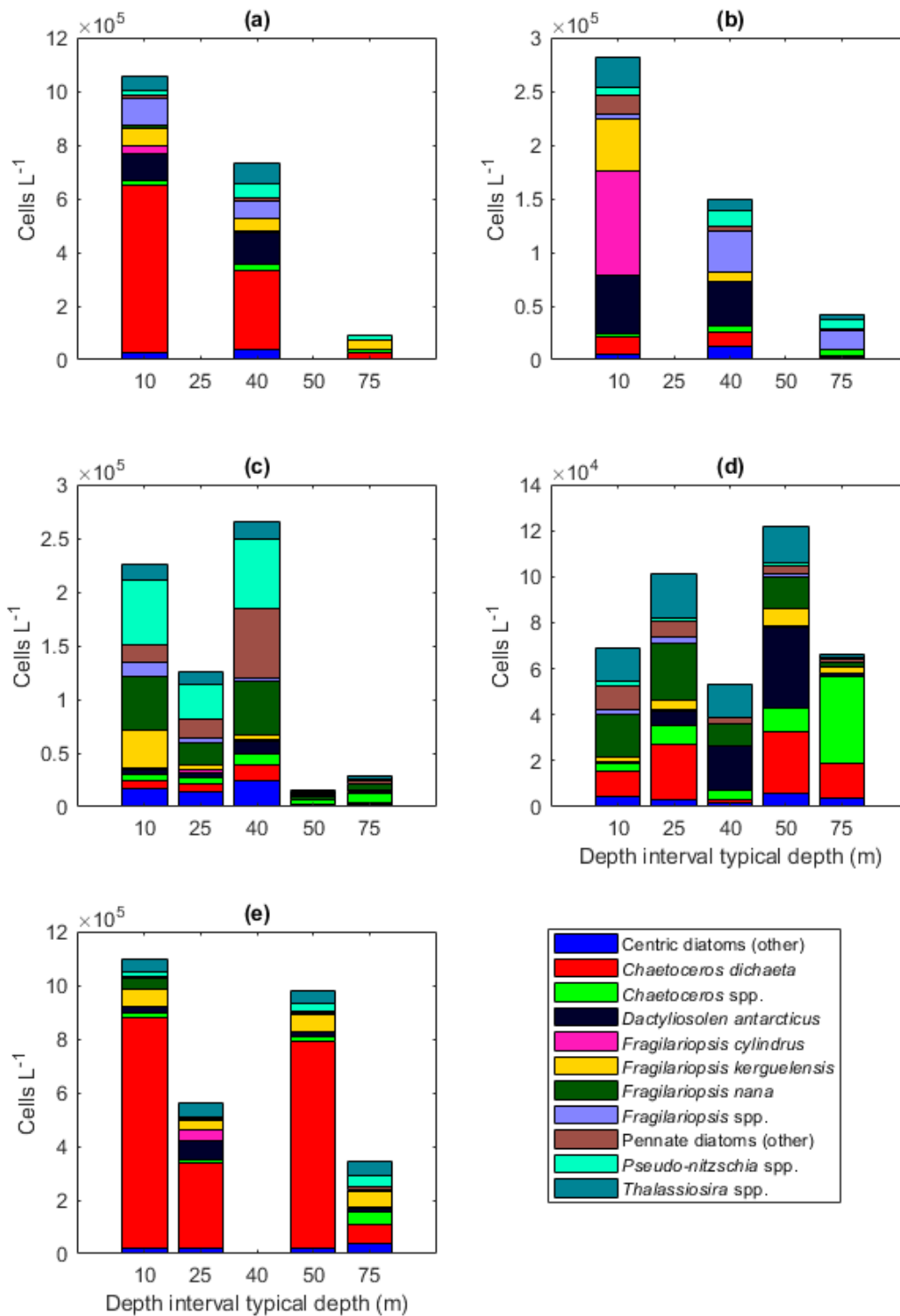
Figure A7: Diatom abundance in the different sampling areas averaged per depth interval for (a) station 53, (b) station 54, (c) Astrid Ridge, (d) 6° E transect and (e) Maud Rise. Depth intervals (with typical sampling depth in brackets): 5-10 (10); 25-35 (25), 35-45 (40), 50-60, 65-85 (75) m.
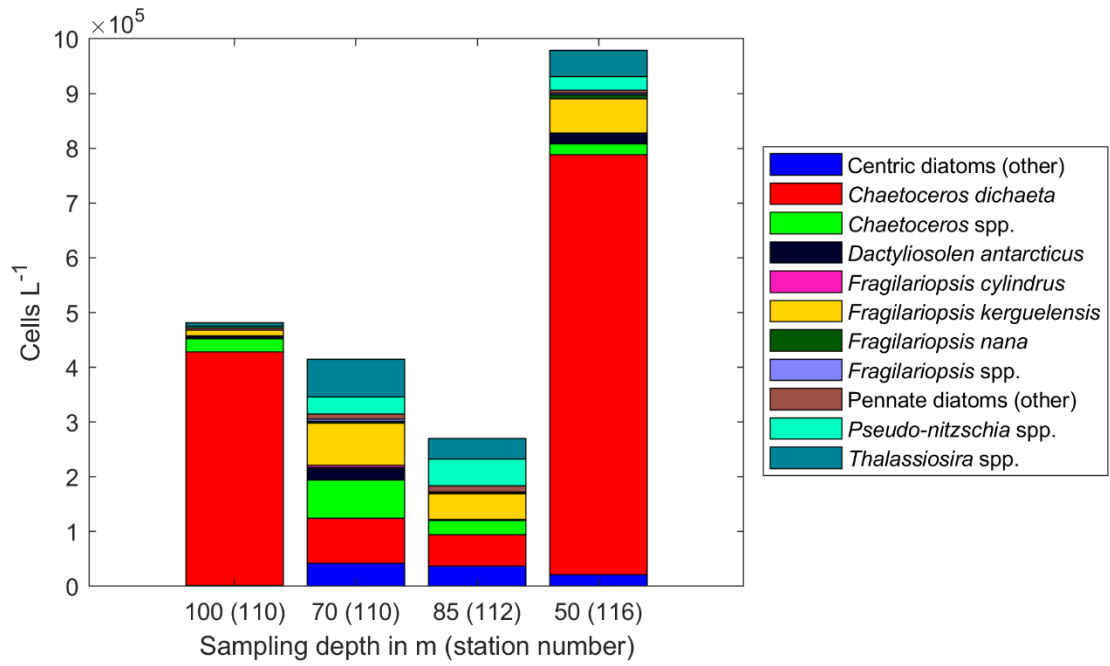
Figure A8: Diatom abundance in available deep samples at Maud Rise. Bars are marked with the sampling depth in meters and the station number in brackets.
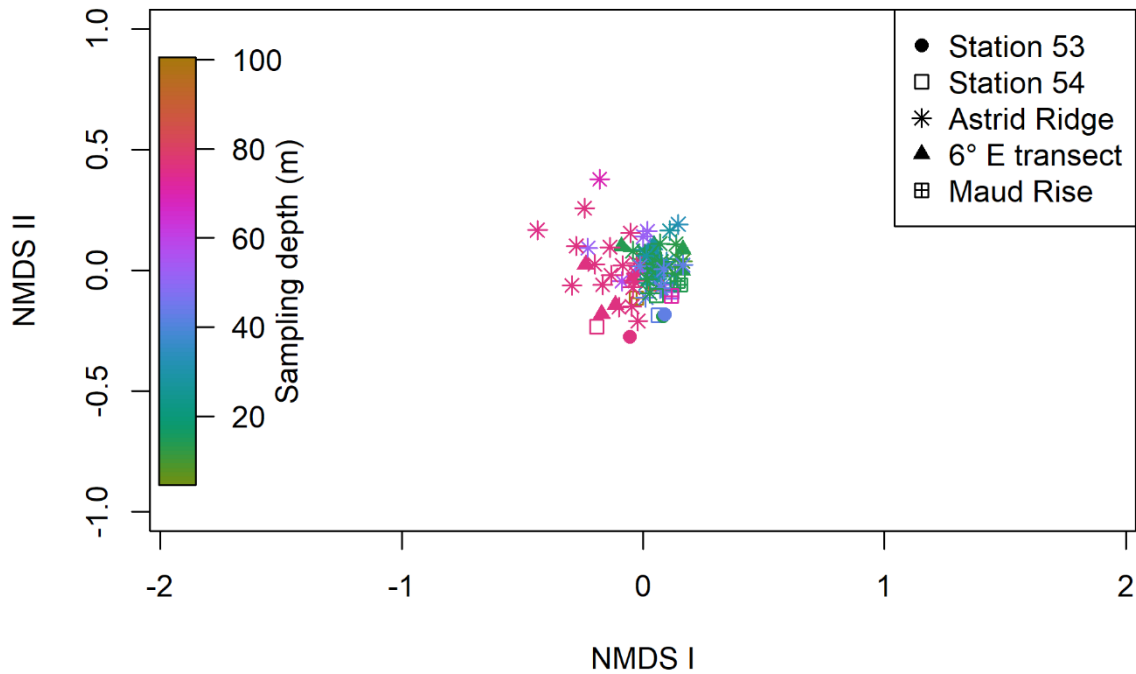
Figure A9: NMDS clustering using presence-absence data.

784
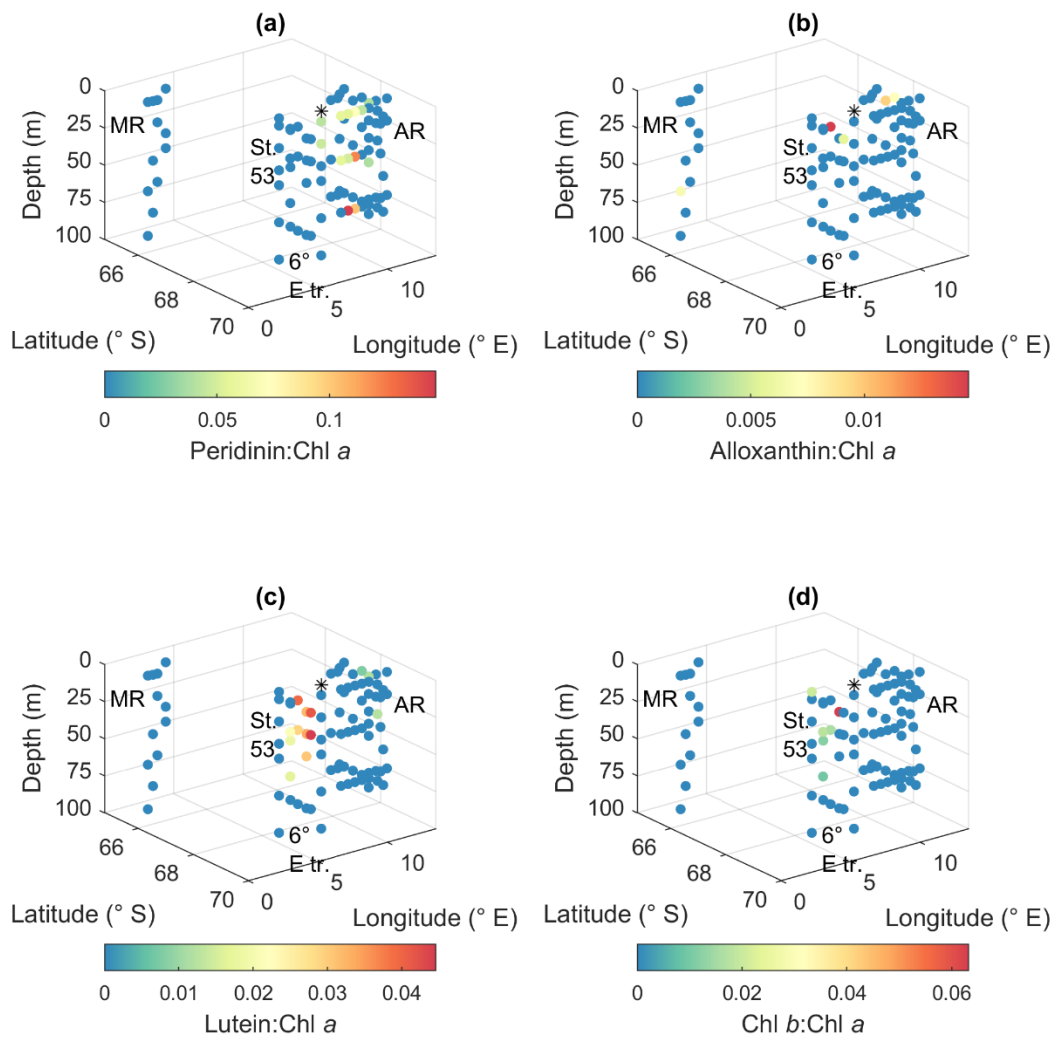
Figure ~~9~~A10: Ratios of algal pigments to Chl _a_ for (a) peridinin, (b) alloxanthin, (c) lutein and (d) Chl _b_. MR=Maud Rise, St. 53=station 53, AR=Astrid Ridge, 6° E tr.= 6° E transect. Station 54 is marked with a black asterisk.

787

(d)

(e)

(f)

790
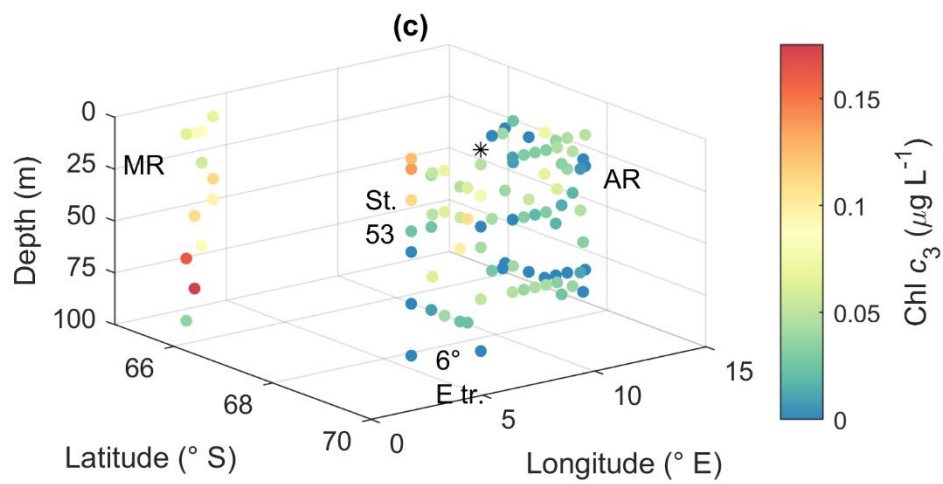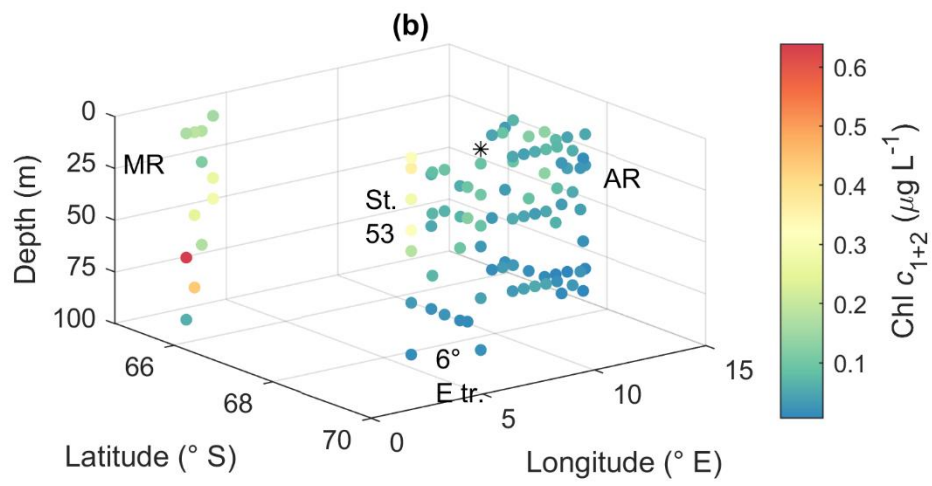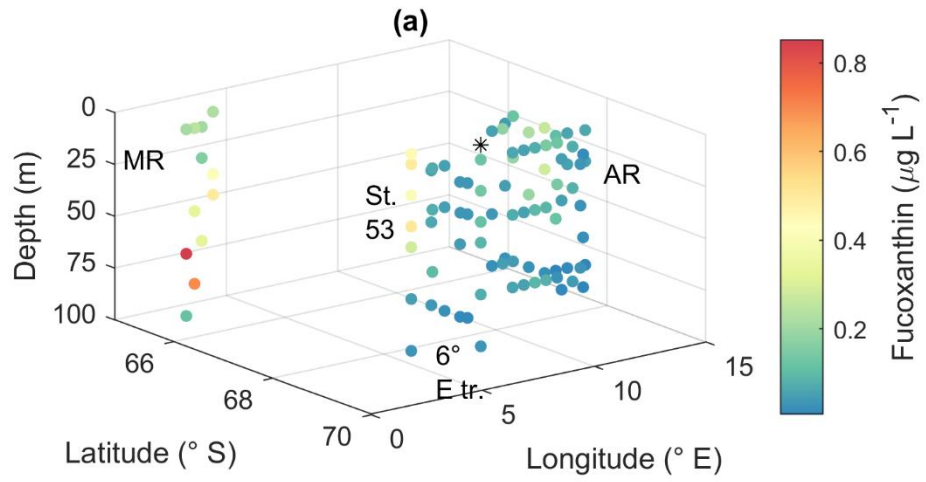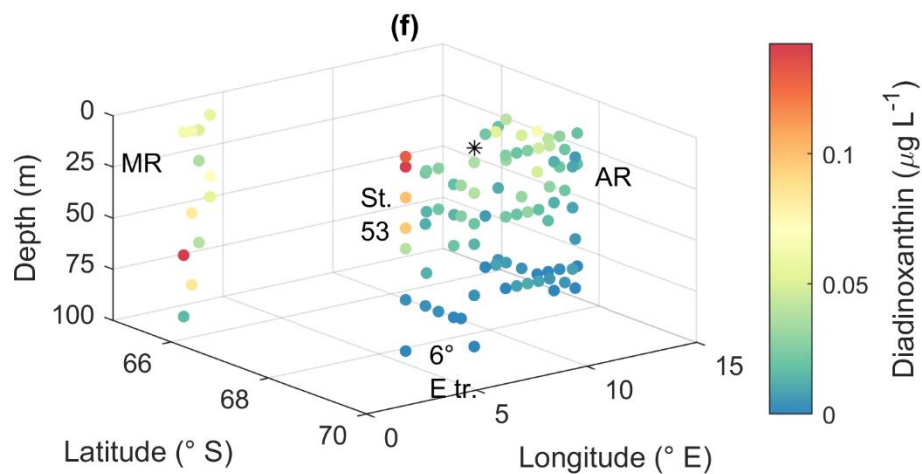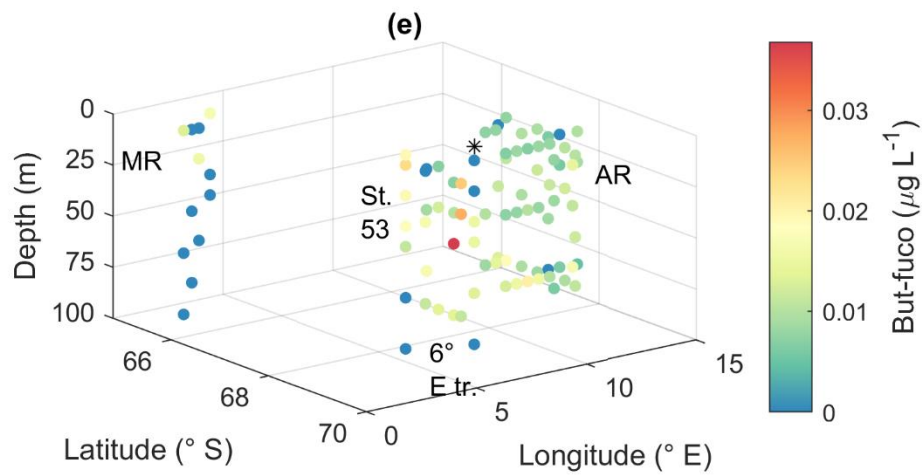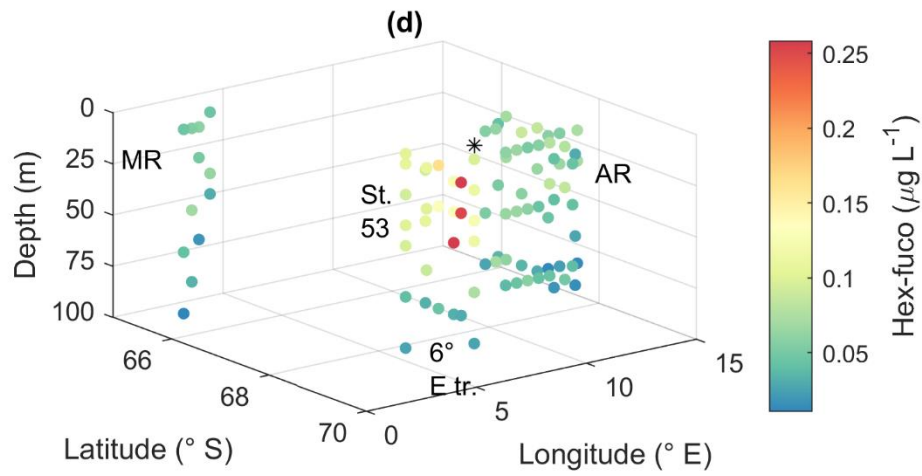
Figure A1<u>1</u>~~0~~: Pigment concentrations of (a) fucoxanthin, (b) Chl c_{1+2}, (c) Chl c_3, (d) hex-fuco, (e) but-fuco and (f)
diadinoxanthin. MR=Maud Rise, St. 53=station 53, AR=Astrid Ridge, 6° E tr.= 6° E transect. Station 54 is marked
with a black asterisk.

(a)

(b)

(c)

(d)

794
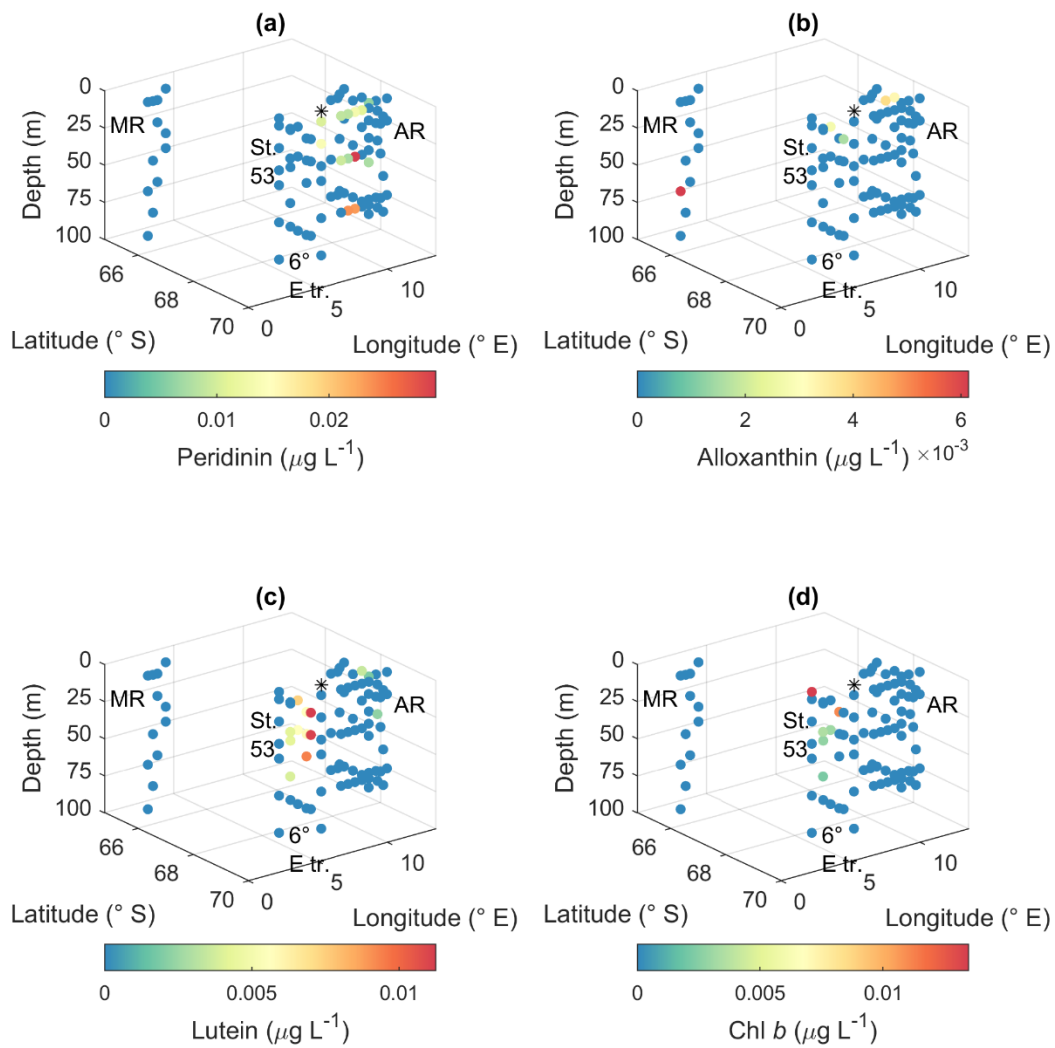
Figure A12̶1̶: Pigment concentrations of (a) peridinin, (b) alloxanthin, (c) lutein and (d) Chl *b*. MR=Maud Rise, St. 53=station 53, AR=Astrid Ridge, 6° E tr.= 6° E transect. Station 54 is marked with a black asterisk.

797

798
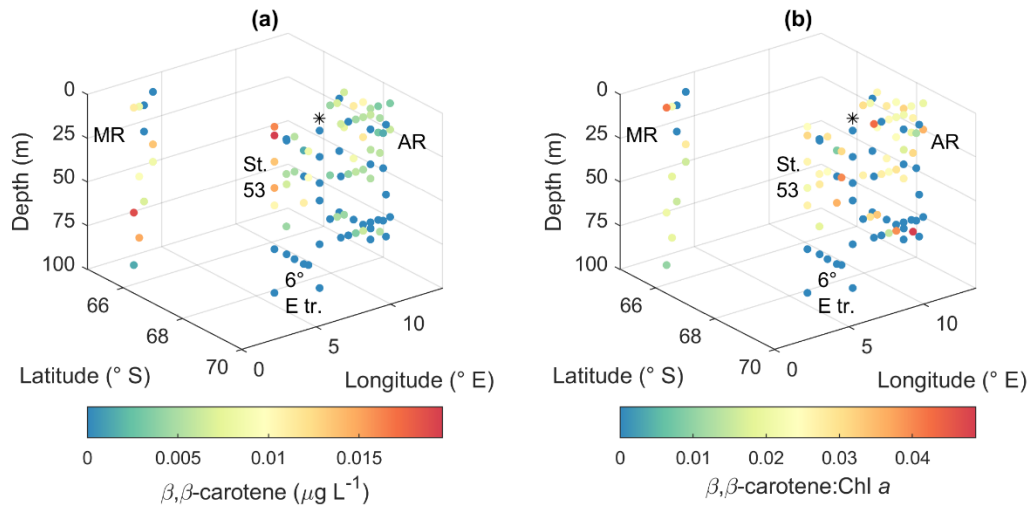
Figure A1~~3~~2: (a) β ,β-carotene concentration and (b) ratio of β,β-carotene to Chl a. MR=Maud Rise, St. 53=station 53, AR=Astrid Ridge, 6° E tr.= 6° E transect. Station 54 is marked with a black asterisk.

801
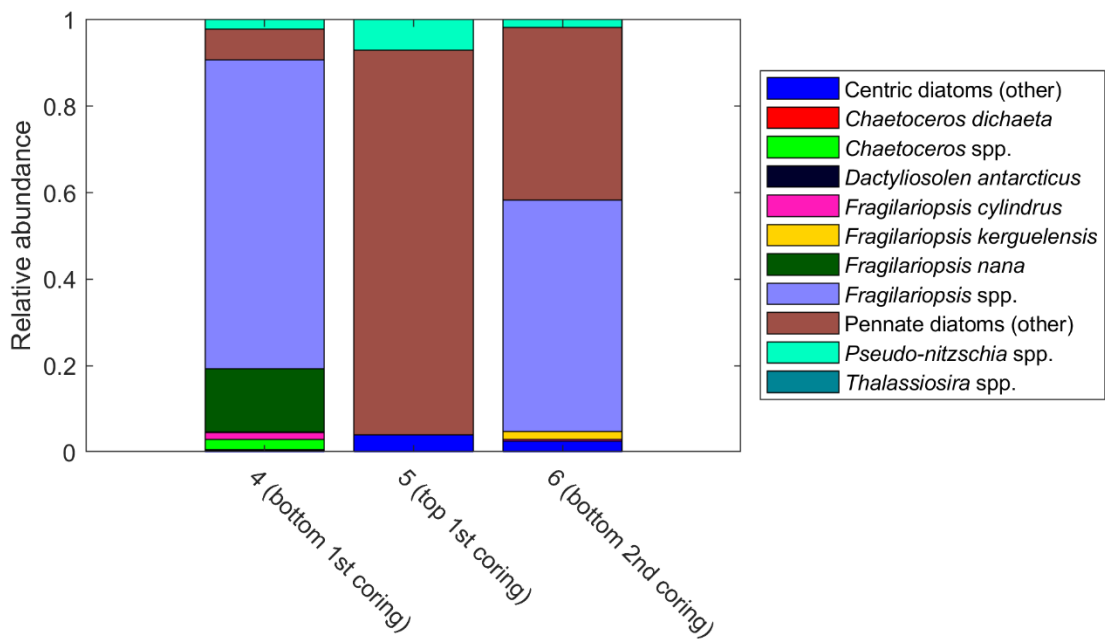
Figure A1~~4~~3: Relative diatom abundance in ice core samples. The colours pink to cyan comprise pennate diatoms. The bars are marked with sample numbers and ice core section explanations. See Table B2 for method descriptions.
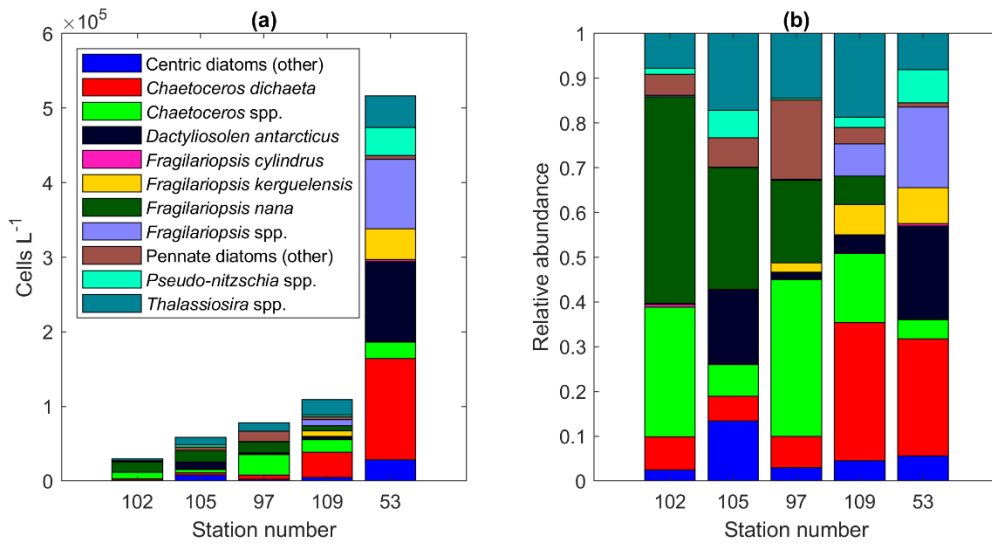
Figure A154: (a) Diatom abundance and (b) relative abundance in the south-north transect at 6° E including the station 53 just north of the transect (average abundances per station).

807 **Appendix B. Supplementary tables.**

808 **Table B1.** All taxa identified in the CTD station samples down to 100 m (in total 87 samples). For median abundance 2, only the samples where the species/taxon was
809 observed were taken into account (i.e., zero abundances do not contribute to the median value).

810

Class/group	Species/taxon	Number of samples observed in	Median abundance 1 (cells L^{-1})	Median abundance 2 (cells L^{-1})	Station 53	Station 54	Astrid Ridge	6° E transect	Maud Rise
Bacillariophyceae	*Actinocyclus* sp.	1	0	2411			x		
Bacillariophyceae	*Actinocyclus actinochilus*	19	0	95	x		x	x	x
Bacillariophyceae	*Actinocyclus curvatulus*	3	0	1404			x		x
Bacillariophyceae	*Asteromphalus* spp.	34	0	293			x	x	x
Bacillariophyceae	*Asteromphalus hyalinus*	51	297	2119	x	x	x	x	x
Bacillariophyceae	*Asteromphalus parvulus*	50	302	1113	x	x	x	x	x
Bacillariophyceae	*Auricula compacta*	7	0	378			x		x
Bacillariophyceae	*Banquisia belgicae*	36	0	373	x		x	x	x
Bacillariophyceae	*Chaetoceros* spp.	55	1261	4558	x	x	x	x	x
Bacillariophyceae	*Chaetoceros affinis*	1	0	7798			x		
Bacillariophyceae	*Chaetoceros atlanticus*	33	0	866	x	x	x	x	x
Bacillariophyceae	*Chaetoceros atlanticus f. bulbosus*	42	0	510	x		x	x	x
Bacillariophyceae	*Chaetoceros bulbosus*	32	0	213	x	x	x	x	x
Bacillariophyceae	*Chaetoceros castracanei*	50	151	368			x	x	x
Bacillariophyceae	*Chaetoceros concavicornis*	1	0	2133			x		
Bacillariophyceae	*Chaetoceros convolutus*	1	0	3562	x				
Bacillariophyceae	*Chaetoceros cryophilus*	3	0	830			x		x
Bacillariophyceae	*Chaetoceros curvatus*	41	0	257		x	x	x	x
Bacillariophyceae	*Chaetoceros decipiens*	1	0	3059	x				

48

Bacillariophyceae	*Chaetoceros densus*	1	0	1029	x				
Bacillariophyceae	*Chaetoceros dichaeta*	75	4594	6398	x	x	x	x	x
Bacillariophyceae	*Chaetoceros flexuosus*	1	0	872		x			
Bacillariophyceae	*Chaetoceros neglectus*	4	0	7600	x		x		
Bacillariophyceae	*Chaetoceros simplex*	20	0	2291			x	x	
Bacillariophyceae	*Chaetoceros socialis*	24	0	1078	x	x	x	x	x
Bacillariophyceae	*Corethron* spp.	17	0	134			x	x	x
Bacillariophyceae	*Corethron inerme*	4	0	795	x		x		
Bacillariophyceae	*Corethron pennatum*	63	415	817	x	x	x	x	x
Bacillariophyceae	*Coscinodiscophycidae*	10	0	647	x		x	x	x
Bacillariophyceae	*Coscinodiscus* sp.	2	0	4509		x	x		
Bacillariophyceae	*Cylindrotheca closterium*	84	1387	1395	x	x	x	x	x
Bacillariophyceae	*Dactyliosolen antarcticus*	46	172	8756	x	x	x	x	x
Bacillariophyceae	*Dactyliosolen fragilissimus*	1	0	8312	x				
Bacillariophyceae	*Dactyliosolen tenuijunctus*	51	172	670	x	x	x	x	x
Bacillariophyceae	*Entomoneis* spp.	6	0	119			x	x	
Bacillariophyceae	*Entomoneis paludosa*	35	0	402			x	x	x
Bacillariophyceae	*Eucampia antarctica*	22	0	384	x		x	x	
Bacillariophyceae	*Fragilariopsis* spp.	70	792	1153	x	x	x	x	x
Bacillariophyceae	*Fragilariopsis curta*	1	0	22493		x			
Bacillariophyceae	*Fragilariopsis cylindrus*	38	0	1309	x	x	x	x	x
Bacillariophyceae	*Fragilariopsis kerguelensis*	63	1771	6323	x	x	x	x	x
Bacillariophyceae	*Fragilariopsis nana*	71	10683	17244			x	x	x
Bacillariophyceae	*Fragilariopsis rhombica*	32	0	1720	x	x	x	x	x
Bacillariophyceae	*Fragillaria* spp.	2	0	1600			x	x	
Bacillariophyceae	*Guinardia* spp.	2	0	10059			x		x
Bacillariophyceae	*Guinardia cylindrus*	44	76	368	x	x	x	x	x
Bacillariophyceae	*Guinardia flaccida*	1	0	584			x		
Bacillariophyceae	*Haslea* spp.	72	792	1118	x	x	x	x	x

Class	Species								
Bacillariophyceae	*Haslea trompii*	1	0	1664			x		
Bacillariophyceae	*Haslea vitrea*	2	0	354					x
Bacillariophyceae	*Leptocylindrus mediterraneus*	33	0	195	x		x	x	x
Bacillariophyceae	*Membraneis challengeri*	25	0	396	x	x	x	x	x
Bacillariophyceae	*Navicula* spp.	60	179	399	x	x	x	x	x
Bacillariophyceae	*Navicula criophila*	1	0	1583	x				
Bacillariophyceae	*Navicula directa var. directa*	1	0	86			x		
Bacillariophyceae	*Navicula transitans*	1	0	109			x		
Bacillariophyceae	*Nitzschia longissima*	41	0	333			x	x	x
Bacillariophyceae	*Odontella* sp.	1	0	778			x		
Bacillariophyceae	*Odontella weissflogii*	1	0	176			x		
Bacillariophyceae	Pennales	59	302	757		x	x	x	x
Bacillariophyceae	Phaeoceros	4	0	516	x		x	x	
Bacillariophyceae	*Plagiotropus gaussii*	1	0	938			x		
Bacillariophyceae	*Proboscia* spp.	12	0	221	x	x	x		x
Bacillariophyceae	*Proboscia alata*	61	169	378	x	x	x	x	x
Bacillariophyceae	*Proboscia inermis*	29	0	172	x	x	x	x	x
Bacillariophyceae	*Proboscia truncata*	6	0	315			x		
Bacillariophyceae	*Pseudo-nitzschia* spp.	78	1474	1887	x	x	x	x	x
Bacillariophyceae	*Pseudo-nitzschia heimii*	28	0	3392	x	x	x	x	
Bacillariophyceae	*Pseudo-nitzschia lineola*	13	0	1245	x	x	x	x	
Bacillariophyceae	*Pseudo-nitzschia turgidula*	1	0	1105				x	
Bacillariophyceae	*Pseudo-nitzschia turgiduloides*	1	0	2010			x		
Bacillariophyceae	*Rhizosolenia* spp.	25	0	165	x	x	x	x	x
Bacillariophyceae	*Rhizosolenia delicatula*	1	0	792	x				
Bacillariophyceae	*Rhizosolenia hebetata*	3	0	396	x		x		
Bacillariophyceae	*Rhizosolenia hebetata f. semispina*	19	0	137	x	x	x	x	x
Bacillariophyceae	*Rhizosolenia imbricata*	25	0	218	x	x	x	x	x
Bacillariophyceae	*Rhizosolenia simplex*	2	0	534			x		

Bacillariophyceae	*Synedropsis* spp.	36	0	1505			x	x	x
Bacillariophyceae	*Thalassiosira* spp.	80	7296	9321	x	x	x	x	x
Bacillariophyceae	*Thalassiosira frenguelli*	1	0	28817	x				
Bacillariophyceae	*Thalassiosira gracilis*	11	0	6560	x	x	x		x
Bacillariophyceae	*Thalassiosira nordenskioeldii*	1	0	804			x		
Bacillariophyceae	*Thalassiosira oliveriana*	1	0	396			x		
Bacillariophyceae	*Thalassiosira perpusilla*	1	0	19418			x		
Bacillariophyceae	*Thalassiothrix* spp.	4	0	458					x
Bacillariophyceae	*Thalassiothrix antarctica*	14	0	491	x	x	x	x	x
Bacillariophyceae	*Trachyneis aspera*	1	0	1180			x		
Bacillariophyceae	*Trichotoxon reinboldii*	6	0	384	x	x			x
Bacillariophyceae	*Tropidoneis* sp.	1	0	7619			x		
Chlorophyceae	Chlorophyceae	1	0	10479	x				
Choanoflagellatea	*Bicosta spinifera*	15	0	1210			x	x	
Choanoflagellatea	*Choanoflagellatea*	41	0	2310	x	x	x	x	x
Choanoflagellatea	*Monosiga* sp.	1	0	3251			x		
Choanoflagellatea	*Monosiga marina*	13	0	2376	x		x	x	x
Choanoflagellatea	*Parvicorbicula socialis*	5	0	23577	x		x		x
Chrysophyceae	Chrysophyceae	63	2140	3670	x	x	x	x	x
Ciliophora	*Amphorides laackmanni*	8	0	175			x		
Ciliophora	*Balanion* spp.	27	0	165			x	x	
Ciliophora	Ciliophora	53	105	348	x		x	x	x
Ciliophora	*Didinium* spp.	2	0	198			x		
Ciliophora	*Lohmanniella oviformis*	20	0	188			x	x	x
Ciliophora	*Mesodinium pulex*	2	0	190		x	x		
Ciliophora	*Mesodinium rubrum*	4	0	179	x	x	x		
Ciliophora	Oligotrichida	1	0	174				x	
Ciliophora	*Pelagostrombidium* spp.	10	0	131		x	x		x
Ciliophora	*Salpingella costata*	39	0	165	x	x	x	x	x

Ciliophora	Strombidiidae	1	0	101			x		
Ciliophora	*Strombidium* spp.	10	0	121			x	x	
Ciliophora	*Strombidium conicum*	25	0	174			x	x	
Ciliophora	Tintinnidae	8	0	268			x		x
Ciliophora	*Tintinnopsis* sp.	1	0	109				x	
Ciliophora	*Uronema marinum*	1	0	1046				x	
Cryptophyceae	Cryptophyceae	44	1014	4497		x	x	x	x
Cryptophyceae	Cryptophyceae 3 to 7 µm	65	2279	3361	x	x	x	x	x
Cryptophyceae	Cryptophyceae 7 to 10 µm	50	1132	3565	x	x	x	x	x
Cryptophyceae	Cryptophyceae 10 to 20 µm	10	0	1685			x	x	x
Cryptophyceae	*Teleaulax* spp.	10	0	1280			x	x	x
Cryptophyceae	*Teleaulax amphioxeia*	1	0	10849			x		
Cryptophyceae	*Telonema* spp.	59	1205	3052	x	x	x	x	x
Dictyochophyceae	*Dictyocha speculum*	51	109	274	x	x	x	x	x
Dinophyceae	*Alexandrium* spp.	20	0	2154	x	x	x	x	x
Dinophyceae	*Amphidinium* spp.	15	0	411		x	x	x	x
Dinophyceae	*Amphidinium crassum*	3	0	1180			x	x	
Dinophyceae	*Amphidinium hadai*	33	0	804	x	x	x	x	x
Dinophyceae	*Amphidinium longum*	1	0	1631			x		
Dinophyceae	Amphidomataceae	3	0	2310	x	x	x		
Dinophyceae	Dinophyceae	23	0	2175	x	x	x	x	x
Dinophyceae	Dinophyceae 10 to 20 µm	22	0	1543			x	x	x
Dinophyceae	Dinophyceae 20 to 30 µm	11	0	1623		x	x	x	
Dinophyceae	Dinophyceae 30 to 40 µm	3	0	1180			x		
Dinophyceae	*Dinophysis* sp.	1	0	2455	x				
Dinophyceae	*Diplopsalis lenticula*	1	0	3749		x			
Dinophyceae	Gymnodiniales	5	0	1623			x	x	x
Dinophyceae	Gymnodiniales 10 to 20 µm	3	0	1087		x		x	
Dinophyceae	Gymnodiniales 20 to 30 µm	5	0	1608	x		x		

Dinophyceae	Gymnodiniales 30 to 40 µm	2	0	2298			x		
Dinophyceae	*Gymnodinium* spp.	69	2738	3361	x	x	x	x	x
Dinophyceae	*Gymnodinium galeatum*	57	1305	2936	x	x	x	x	x
Dinophyceae	*Gymnodinium gracilentum*	58	1167	2438	x	x	x	x	x
Dinophyceae	*Gymnodinium wulffii*	1	0	1066			x		
Dinophyceae	*Gymnodinium* spp. below 10 µm	78	4436	4839	x	x	x	x	x
Dinophyceae	*Gymnodinium* spp. 10 to 20 µm	86	15176	15309	x	x	x	x	x
Dinophyceae	*Gymnodinium* spp. 20 to 30 µm	53	1105	2455	x	x	x	x	x
Dinophyceae	*Gymnodinium* spp. 30 to 40 µm	4	0	1089			x	x	
Dinophyceae	*Gyrodinium* spp.	24	0	1595	x	x	x	x	x
Dinophyceae	*Gyrodinium fusiforme*	1	0	1132		x			
Dinophyceae	*Gyrodinium* spp. 10 to 20 µm	37	0	2360	x		x	x	x
Dinophyceae	*Gyrodinium* spp. 20 to 30 µm	37	0	1631	x	x	x	x	x
Dinophyceae	*Gyrodinium* spp. 30 to 40 µm	3	0	2310			x		
Dinophyceae	*Gyrodinium* spp. 40 to 50 µm	2	0	2052			x		
Dinophyceae	*Heterocapsa* spp.	2	0	1632	x		x		
Dinophyceae	*Heterocapsa triquetra*	1	0	2420			x		
Dinophyceae	*Lessardia elongata*	11	0	1109	x	x	x	x	x
Dinophyceae	Peridiniales	16	0	2262			x	x	
Dinophyceae	*Polarella* spp.	11	0	1492	x	x	x	x	x
Dinophyceae	*Polarella glacialis*	7	0	1305			x		
Dinophyceae	*Preperidinium perlatum*	9	0	1139		x	x	x	
Dinophyceae	*Pronoctiluca pelagica*	5	0	1404				x	x
Dinophyceae	*Prorocentrum* spp.	6	0	3865			x		
Dinophyceae	*Prorocentrum balticum*	1	0	6654			x		
Dinophyceae	*Prorocentrum minimum*	50	1087	2279	x	x	x	x	x
Dinophyceae	*Protoperidinium* spp.	45	82	1070	x	x	x	x	x
Dinophyceae	*Protoperidinium bipes*	3	0	198			x	x	
Dinophyceae	*Protoperidinium smithii*	3	0	1180			x		

Class	Species								
Dinophyceae	*Protoperidinium unipes*	1	0	1270			x		
Dinophyceae	*Torodinium* sp.	1	0	1631			x		
Eukaryote indetermined	Eukaryote indetermined	29	0	3527		x	x	x	x
Eukaryote indetermined	Eukaryote indetermined 3 to 7 µm	62	9753	17889		x	x	x	x
Eukaryote indetermined	Eukaryote indetermined 7 to 10 µm	6	0	2387		x	x	x	
Eukaryote indetermined	Eukaryote indetermined 10 to 20 µm	2	0	1582			x		x
Eukaryote indetermined	Spore	19	0	1180			x	x	x
Flagellates	Biflagellate	11	0	11416			x	x	
Flagellates	Biflagellate 3 to 7 µm	63	4265	6180	x	x	x	x	x
Flagellates	Biflagellate 10 to 15 µm	1	0	2218					x
Flagellates	Biflagellate heterotrophic 3 to7 µm	1	0	8409		x			
Flagellates	Flagellate	14	0	24026			x	x	
Flagellates	Flagellate 3 to 7 µm	73	14421	19507	x	x	x	x	x
Flagellates	Flagellate 7 to 10 µm	37	0	3109	x	x	x	x	x
Flagellates	Flagellate 10 to 15 µm	2	0	1053				x	x
Flagellates	Fourflagellate	1	0	2335				x	
Flagellates	Fourflagellate 3 to 7 µm	8	0	2712	x		x	x	
Flagellates	Uniflagellate	5	0	3262				x	x
Flagellates	Uniflagellate 3 to 7 µm	24	0	3228			x	x	x
Flagellates	Uniflagellate 7 to 10 µm	3	0	1519			x	x	
Flagellates	Uniflagellate 10 to 15 µm	1	0	4869				x	
Prasinophyceae	Prasinophyceae	1	0	1310	x				
Prasinophyceae	*Pterosperma* spp.	24	0	1552	x	x	x	x	x
Prokaryota	Filamentous blue-green algae cf. *Anabaena* sp.	15	0	6765			x	x	
Prymnesiophyceae	*Phaeocystis antarctica*	3	0	9628		x	x		
Pyramimonadophyceae	*Pyramimonas* spp.	35	0	2263		x	x	x	

811

812 **Table 1B2 Initial pigment to Chl a ratios used in the CHEMTAX analysis and the final ratio matrices for each cluster**
813 **(average of the 6 best performing runs of the second step; see Methods).**

Initial ratios	Chl_c3	Chlc_1-2	Peri	But-fuco	Fuco	Hex-fuco	Allo	Lut	Chl_b	Chl_a
Prasinophytes	0	0	0	0	0	0	0	0.0066	0.55	1
Chlorophytes	0	0	0	0	0	0	0	0.23	0.15	1
Cryptophytes	0	0.17	0	0	0	0	0.21	0	0	1
Diatoms-1	0	0.09	0	0	1.04	0	0	0	0	1
Diatoms-2	0.016	0.22	0	0	0.83	0	0	0	0	1
Dinoflagellates-1	0	0.23	0.82	0	0	0	0	0	0	1
Dinoflagellates-2	0.04	0.12	0	0.06	0.19	0.18	0	0	0	1
Haptophytes-6-like	0.18	0.18	0	0.005	0.23	0.47	0	0	0	1

Final ratios

Maud Rise	Chl_c3	Chlc_1-2	Peri	But-fuco	Fuco	Hex-fuco	Allo	Lut	Chl_b	Chl_a
Prasinophytes	0	0	0	0	0	0	0	0.006	0.533	1
Chlorophytes	0	0	0	0	0	0	0	0.239	0.157	1
Cryptophytes	0	0.163	0	0	0	0	0.191	0	0	1
Diatoms-1	0	0.101	0	0	0.624	0	0	0	0	1
Diatoms-2	0.187	0.561	0	0	0.974	0	0	0	0	1
Dinoflagellates-1	0	0.221	0.714	0	0	0	0	0	0	1
Dinoflagellates-2	0.100	0.284	0	0.227	0.588	0.304	0	0	0	1
Haptophytes-6-like	0.495	0.809	0	0.003	0.557	0.404	0	0	0	1

Astrid Ridge surface	Chl_c3	Chlc_1-2	Peri	But-fuco	Fuco	Hex-fuco	Allo	Lut	Chl_b	Chl_a
Prasinophytes	0	0	0	0	0	0	0	0.006	0.507	1
Chlorophytes	0	0	0	0	0	0	0	0.260	0.153	1
Cryptophytes	0	0.179	0	0	0	0	0.211	0	0	1
Diatoms-1	0	0.112	0	0	1.232	0	0	0	0	1
Diatoms-2	0.015	0.324	0	0	0.429	0	0	0	0	1
Dinoflagellates-1	0	0.219	0.802	0	0	0	0	0	0	1
Dinoflagellates-2	0.031	0.209	0	0.142	0.256	0.576	0	0	0	1
Haptophytes-6-like	0.943	0.392	0	0.012	0.502	0.795	0	0	0	1

Astrid Ridge deep	Chl_c3	Chlc_1-2	Peri	But-fuco	Fuco	Hex-fuco	Allo	Lut	Chl_b	Chl_a
Prasinophytes	0	0	0	0	0	0	0	0.007	0.475	1
Chlorophytes	0	0	0	0	0	0	0	0.220	0.136	1
Cryptophytes	0	0.156	0	0	0	0	0.226	0	0	1
Diatoms-1	0	0.088	0	0	1.014	0	0	0	0	1
Diatoms-2	0.016	0.276	0	0	0.463	0	0	0	0	1
Dinoflagellates-1	0	0.233	0.765	0	0	0	0	0	0	1
Dinoflagellates-2	0.035	0.219	0	0.263	0.170	0.723	0	0	0	1
Haptophytes-6-like	0.728	0.240	0	0.007	0.379	0.336	0	0	0	1

Other stations	Chl_c3	Chlc_1-2	Peri	But-fuco	Fuco	Hex-fuco	Allo	Lut	Chl_b	Chl_a
Prasinophytes	0	0	0	0	0	0	0	0.007	0.400	1
Chlorophytes	0	0	0	0	0	0	0	0.306	0.096	1
Cryptophytes	0	0.190	0	0	0	0	0.236	0	0	1
Diatoms-1	0	0.088	0	0	1.030	0	0	0	0	1
Diatoms-2	0.017	0.378	0	0	0.608	0	0	0	0	1
Dinoflagellates-1	0	0.238	0.695	0	0	0	0	0	0	1
Dinoflagellates-2	0.301	0.414	0	0.358	0.403	0.573	0	0	0	1
Haptophytes-6-like	0.418	0.280	0	0.010	0.189	1.063	0	0	0	1

814

815 *Peri: peridinin; Fuco: fucoxanthin; Allo: alloxanthin; Lut: lutein.*

816

817 **Table B32.** Comparison of the 20 most abundant diatom species between sea ice samples and Astrid Ridge

818 samples. Species name in bold textGreen colour indicates presence in both areas.

Ice samples (most abundant diatoms)	Average abundance (all samples; cells L^{-1})		Astrid Ridge (most abundant diatoms)	Average abundance (samples down to 100 m; cells L^{-1})
Fragilariopsis **spp.**	782601		*Pseudo-nitzschia* **spp.**	30105
Fragilariopsis nana	152180		*Fragilariopsis nana*	27081
Cylindrotheca closterium	53846		*Fragilariopsis kerguelensis*	13004
Pseudo-nitzschia **spp.**	25263		*Thalassiosira* spp.	8164
Eucampia antarctica	21718		*Thalassiothrix antarctica*	6068
Chaetoceros **spp.**	19298		*Chaetoceros dichaeta*	5954
Fragilariopsis cylindrus	16473		*Dactyliosolen tenuijunctus*	5823
Haslea **spp.**	11706		*Cylindrotheca closterium*	4436
Synedropsis **spp.**	9547		*Fragilariopsis* **spp.**	4389
Pennales	7604		*Dactyliosolen antarcticus*	3731
Navicula spp.	4949		*Chaetoceros* **spp.**	3164
Chaetoceros socialis	4365		**Pennales**	1656
Entomoneis paludosa	3201		*Haslea* **spp.**	1646
Fragilariopsis kerguelensis	2855		*Synedropsis* **spp.**	1330
Dactyliosolen tenuijunctus	2828		*Asteromphalus hyalinus*	1269
Banquisia belgicae	2466		*Fragilariopsis cylindrus*	1267
Chaetoceros curvatus	2341		*Corethron pennatum*	1235
Fragilariopsis rhombica	2341		*Pseudo-nitzschia heimii*	1199
Corethron pennatum	2328		*Pseudo-nitzschia lineola*	1133
Odontella spp.	1540		*Thalassiosira gracilis*	1113

819

820 *Two ice floes were sampled along the 6° E transect (the first one on 26.3.2019 at 68.9135° S and 6.0217° E, and*

821 *the second one on 27.3.2019 at 68.4392° S and 5.9135° E). Ice algal taxonomy and abundance samples were*

822   *taken from in total 3 ice core sections: a 10 cm bottom section and an 8.5 cm top section from the 18.5 cm thick*

823   *ice core at the first ice floe, and a 10 cm bottom section from the 93,5 cm thick ice core at the second ice floe. A*

824   *Kovacs 9 cm corer was used, and the ice samples were melted without the addition of filtered sea water in*

825   *darkness and room temperature, and processed as soon as the melting was complete.*

826

11. References

Abelmann, A., Gersonde, R., Cortese, G., Kuhn, G. and Smetacek, V.: Extensive phytoplankton blooms in the Atlantic sector of the glacial Southern Ocean, Paleoceanography, 21, PA1013, doi:10.1029/2005PA001199, 2006.

Ackley, S. F., Buck, K. R. and Taguchi, S.: Standing crop of algae in the sea ice of the Weddell Sea region, Deep Sea Res., 26(3), 269–281, doi:10.1016/0198-0149(79)90024-4, 1979.

Anderson, M. J. and Walsh, D. C. I.: PERMANOVA, ANOSIM, and the Mantel test in the face of heterogeneous dispersions: What null hypothesis are you testing?, Ecol. Monogr., 83(4), 557–574, doi:10.1890/12-2010.1, 2013.

Armand, L. K., Cornet-Barthaux, V., Mosseri, J. and Quéguiner, B.: Late summer diatom biomass and community structure on and around the naturally iron-fertilised Kerguelen Plateau in the Southern Ocean, Deep. Res. Part II Top. Stud. Oceanogr., 55(5–7), 653–676, doi:10.1016/j.dsr2.2007.12.031, 2008.

Arrigo, K. R. and van Dijken, G. L.: Phytoplankton dynamics within 37 Antarctic coastal polynya systems, J. Geophys. Res., 108(8), C83271, doi:10.1029/2002jc001739, 2003.

Arrigo, K. R., Robinson, D. H., Worthen, D. L., Dunbar, R. B., DiTullio, G. R., VanWoert, M. and Lizotte, M. P.: Phytoplankton community structure and the drawdown of nutrients and CO2 in the Southern Ocean, Science (80-.)., 283(5400), 365–367, doi:10.1126/science.283.5400.365, 1999.

Assmy, P., Hernández-Becerril, D. U. and Montresor, M.: Morphological variability and life cycle traits of the type species of the diatom genus Chaetoceros, C. dichaeta, J. Phycol., 44(1), 152–163, doi:10.1111/j.1529-8817.2007.00430.x, 2008.

Assmy, P., Smetacek, V., Montresor, M., Klaas, C., Henjes, J., Strass, V. H., Arrieta, J. M., Bathmann, U., Berg, G. M., Breitbarth, E., Cisewski, B., Friedrichs, L., Fuchs, N., Herndl, G. J., Jansen, S., Krägefsky, S., Latasa, M., Peeken, I., Röttgers, R., Scharek, R., Schüller, S. E., Steigenberger, S., Webb, A. and Wolf-Gladrow, D.: Thick-shelled, grazer-protected diatoms decouple ocean carbon and silicon cycles in the iron-limited Antarctic Circumpolar Current, Proc. Natl. Acad. Sci. U. S. A., 110(51), 20633–20638, doi:10.1073/pnas.1309345110, 2013.

Balch, W. M., Bates, N. R., Lam, P. J., Twining, B. S., Rosengard, S. Z., Bowler, B. C., Drapeau, D. T., Garley, R., Lubelczyk, L. C., Mitchell, C. and Rauschenberg, S.: Factors regulating the Great Calcite Belt in the Southern Ocean and its biogeochemical significance, Global Biogeochem. Cycles, 30, 1199–1214, doi:10.1002/2016GB005414, 2016.

Baldry, K., Strutton, P. G., Hill, N. A. and Boyd, P. W.: Subsurface chlorophyll-a maxima in the Southern Ocean, Front. Mar. Sci., 7, 671, doi:10.3389/fmars.2020.00671, 2020.

Bendif, E. M., Nevado, B., Wong, E. L. Y., Hagino, K., Probert, I., Young, J. R., Rickaby, R. E. M. and Filatov, D. A.: Repeated species radiations in the recent evolution of the key marine phytoplankton lineage Gephyrocapsa, Nat. Commun., 10, 4234, doi:10.1038/s41467-019-12169-7, 2019.

862 von Berg, L., Prend, C. J., Campbell, E. C., Mazloff, M. R., Talley, L. D. and Gille, S. T.: Weddell Sea

863 phytoplankton blooms modulated by sea ice variability and polynya formation, Geophys. Res. Lett., 47,

864 e2020GL087954, doi:10.1029/2020GL087954, 2020.

865 Blain, S., Quéguiner, B., Armand, L., Belviso, S., Bombled, B., Bopp, L., Bowie, A., Brunet, C., Brussaard, C.,

866 Carlotti, F., Christaki, U., Corbière, A., Durand, I., Ebersbach, F., Fuda, J. L., Garcia, N., Gerringa, L., Griffiths,

867 B., Guigue, C., Guillerm, C., Jacquet, S., Jeandel, C., Laan, P., Lefèvre, D., Lo Monaco, C., Malits, A., Mosseri,

868 J., Obernosterer, I., Park, Y. H., Picheral, M., Pondaven, P., Remenyi, T., Sandroni, V., Sarthou, G., Savoye, N.,

869 Scouarnec, L., Souhaut, M., Thuiller, D., Timmermans, K., Trull, T., Uitz, J., Van Beek, P., Veldhuis, M.,

870 Vincent, D., Viollier, E., Vong, L. and Wagener, T.: Effect of natural iron fertilization on carbon sequestration in

871 the Southern Ocean, Nature, 446(7139), 1070–1074, doi:10.1038/nature05700, 2007.

872 Buck, K. R. and Garrison, D. L.: Protists from the ice-edge region of the Weddell Sea, Deep Sea Res., 30(12),

873 1261–1277, doi:10.1016/0198-0149(83)90084-5, 1983.

874 Buma, A. G. J., Treguer, P., Kraaij, G. W. and Morvan, J.: Algal pigment patterns in different watermasses of

875 the Atlantic sector of the Southern Ocean during fall 1987, Polar Biol., 11(1), 55–62, doi:10.1007/BF00236522,

876 1990.

877 Chierici, M. and Fransson, A.: Nutrient data (nitrate, phosphate and silicate) in the eastern Weddell gyre, Kong

878 Haakon VII Hav, and the coast of Dronning Maud Land in the Atlantic sector of the Southern Ocean in March

879 2019, , doi:10.21335/NMDC-1503664923, 2020.

880 Coale, K. H., Johnson, K. S., Chavez, F. P., Buesseler, K. O., Barber, R. T., Brzezinski, M. A., Cochlan, W. P.,

881 Millero, F. J., Falkowski, P. G., Bauer, J. E., Wanninkhof, R. H., Kudela, R. M., Altabet, M. A., Hales, B. E.,

882 Takahashi, T., Landry, M. R., Bidigare, R. R., Wang, X., Chase, Z., Strutton, P. G., Friederich, G. E., Gorbunov,

883 M. Y., Lance, V. P., Hilting, A. K., Hiscock, M. R., Demarest, M., Hiscock, W. T., Sullivan, K. F., Tanner, S. J.,

884 Gordon, R. M., Hunter, C. N., Elrod, V. A., Fitzwater, S. E., Jones, J. L., Tozzi, S., Koblizek, M., Roberts, A. E.,

885 Herndon, J., Brewster, J., Ladizinsky, N., Smith, G., Cooper, D., Timothy, D., Brown, S. L., Selph, K. E.,

886 Sheridan, C. C., Twining, B. S. and Johnson, Z. I.: Southern Ocean iron enrichment experiment: carbon cycling

887 in high- and low-Si waters, Science (80-.)., 304(5669), 408–414, doi:10.1126/science.1089778, 2004.

888 Davidson, A. T., Scott, F. J., Nash, G. V., Wright, S. W. and Raymond, B.: Physical and biological control of

889 protistan community composition, distribution and abundance in the seasonal ice zone of the Southern Ocean

890 between 30 and 80°E, Deep. Res. Part II Top. Stud. Oceanogr., 57(9–10), 828–848,

891 doi:10.1016/j.dsr2.2009.02.011, 2010.

892 Deppeler, S. L. and Davidson, A. T.: Southern Ocean phytoplankton in a changing climate, Front. Mar. Sci., 4,

893 40, doi:10.3389/fmars.2017.00040, 2017.

894 Detmer, A. E. and Bathmann, U. V.: Distribution patterns of autotrophic pico- and nanoplankton and their

895 relative contribution to algal biomass during spring in the Atlantic sector of the Southern Ocean, Deep. Res. Part

896 II Top. Stud. Oceanogr., 44(1–2), 299–320, doi:10.1016/S0967-0645(96)00068-9, 1997.

897 Dinniman, M. S., St-Laurent, P., Arrigo, K. R., Hofmann, E. E. and van Dijken, G. L.: Analysis of iron sources

898   in Antarctic Continental Shelf waters, J. Geophys. Res. Ocean., 125(5), e2019JC015736,

899   doi:10.1029/2019JC015736, 2020.

900   Dong, J., Speer, K. and Jullion, L.: The Antarctic Slope Current near 30° E, J. Geophys. Res. Ocean., 121, 1051–

901   1062, doi:10.1038/175238c0, 2016.

902   Edler, L. and Elbrächter, M.: The Utermöhl method for quantitative phytoplankton analysis, in Microscopic and

903   Molecular Methods for Quantative Phytoplankton analysis, edited by B. Karlson, C. Cusack, and E. Bresnan, pp.

904   13–20, Intergovernmental Oceanographic Commission of UNESCO, Paris., 2010.

905   Garrison, D. L., Ackley, S. F. and Buck, K. R.: A physical mechanism for establishing algal populations in frazil

906   ice, Nature, 306, 363–365, 1983.

907   Garrison, D. L., Buck, K. R. and Fryxell, G. A.: Algal assemblages in Antarctic pack ice and in ice-edge

908   plankton, J. Phycol., 23(4), 564–572, doi:10.1111/j.1529-8817.1987.tb04206.x, 1987.

909   Gibberd, M. J., Kean, E., Barlow, R., Thomalla, S. and Lucas, M.: Phytoplankton chemotaxonomy in the

910   Atlantic sector of the Southern Ocean during late summer 2009, Deep. Res. Part I Oceanogr. Res. Pap., 78, 70–

911   78, doi:10.1016/j.dsr.2013.04.007, 2013.

912   Gomi, Y., Fukuchi, M. and Taniguchi, A.: Diatom assemblages at subsurface chlorophyll maximum layer in the

913   eastern Indian sector of the Southern Ocean in summer, J. Plankton Res., 32(7), 1039–1050,

914   doi:10.1093/plankt/fbq031, 2010.

915   Granéli, E., Granéli, W., Rabbani, M. M., Daugbjerg, N., Fransz, G., Roudy, J. C. and Alder, V. A.: The

916   influence of copepod and krill grazing on the species composition of phytoplankton communities from the Scotia

917   Weddell sea - An experimental approach, Polar Biol., 13(3), 201–213, doi:10.1007/BF00238930, 1993.

918   Hansen, B., Bjornsen, P. K. and Hansen, P. J.: The size ratio between planktonic predators and their prey,

919   Limnol. Oceanogr., 39(2), 395–403, doi:10.4319/lo.1994.39.2.0395, 1994.

920   Hardge, K., Peeken, I., Neuhaus, S., Lange, B. A., Stock, A., Stoeck, T., Weinisch, L. and Metfies, K.: The

921   importance of sea ice for exchange of habitat-specific protist communities in the Central Arctic Ocean, J. Mar.

922   Syst., 165, 124–138, doi:10.1016/j.jmarsys.2016.10.004, 2017.

923   Hattermann, T. and de Steur, L.: Southern Ocean Ecosystem cruise 2019 conductivity-temperature-depth (CTD)

924   data [Data set], Norwegian Polar Institute, https://data.npolar.no/dataset/bb2a91df-b2e7-48e3-8855-

925   d61d516d15c3, 2022.

926   Higgins, H. W., Wright, S. W. and Schlüter, L.: Quantative interpretation of chemotaxonomic pigment data, in

927   Phytoplankton Pigments - Characterization, Chemotaxonomy and Applications in Oceanography, edited by S.

928   Roy, C. A. LLewellyn, E. S. Egeland, and G. Johnsen, pp. 257–313, Cambridge University Press, New York.,

929   2011.

930   Hop, H., Vihtakari, M., Bluhm, B. A., Assmy, P., Poulin, M., Gradinger, R., Peeken, I., von Quillfeldt, C.,

931   Olsen, L. M., Zhitina, L. and Melnikov, I. A.: Changes in sea-ice protist diversity with declining sea ice in the

932   Arctic Ocean from the 1980s to 2010s, Front. Mar. Sci., 7, 243, doi:10.3389/fmars.2020.00243, 2020.

933 Irigoien, X., Hulsman, J. and Harris, R. P.: Global biodiversity patterns of marine phytoplankton and
934 zooplankton, Nature, 429(6994), 863–867, doi:10.1038/nature02593, 2004.

935 Irigoien, X., Flynn, K. J. and Harris, R. P.: Phytoplankton blooms: A "loophole" in microzooplankton grazing
936 impact?, J. Plankton Res., 27(4), 313–321, doi:10.1093/plankt/fbi011, 2005.

937 Jeffrey, S. W., Wright, S. W. and Zapata, M.: Microalgal classes and their signature pigments, in Phytoplankton
938 Pigments - Characterization, Chemotaxonomy and Applications in Oceanography, edited by S. Roy, C. A.
939 LLewellyn, E. S. Egeland, and G. Johnsen, pp. 3–77, Cambridge University Press, Cambridge., 2011.

940 Jena, B. and Pillai, A. N.: Satellite observations of unprecedented phytoplankton blooms in the Maud Rise
941 polynya, Southern Ocean, Cryosphere, 14(4), 1385–1398, doi:10.5194/tc-14-1385-2020, 2020.

942 Kang, S. H. and Fryxell, G. A.: Phytoplankton in the Weddell Sea, Antarctica: composition, abundance and
943 distribution in water-column assemblages of the marginal ice-edge zone during austral autumn, Mar. Biol.,
944 116(2), 335–348, doi:10.1007/BF00350024, 1993.

945 Kauko, H. M., Olsen, L. M., Duarte, P., Peeken, I., Granskog, M. A., Johnsen, G., Fernández-Méndez, M.,
946 Pavlov, A. K., Mundy, C. J. and Assmy, P.: Algal colonization of young Arctic sea ice in Spring, Front. Mar.
947 Sci., 5, 199, doi:10.3389/fmars.2018.00199, 2018.

948 Kauko, H. M., Moreau, S. and Hattermann, T.: Southern Ocean Ecosystem cruise 2019 vertical in situ
949 chlorophyll a profiles [Data set], , doi:10.21334/npolar.2021.5e510f85, 2020.

950 Kauko, H. M., Hattermann, T., Ryan-Keogh, T., Singh, A., de Steur, L., Fransson, A., Chierici, M., Falkenhaug,
951 T., Hallfredsson, E. H., Bratbak, G., Tsagaraki, T., Berge, T., Zhou, Q. and Moreau, S.: Phenology and
952 environmental control of phytoplankton blooms in the Kong Håkon VII Hav in the Southern Ocean, Front. Mar.
953 Sci., 8, 623856, doi:10.3389/fmars.2021.623856, 2021.

954 Kauko, H. M., Moreau, S., Rózańska, M. and Wiktor, J. M.: Southern Ocean Ecosystem cruise 2019
955 phytoplankton taxonomy and abundance [Data set], , doi:10.21334/npolar.2022.283e500c, 2022.

956 Kopczynska, E. E.: Dominance of microflagellates over diatoms in the Antarctic areas of deep vertical mixing
957 and krill concentrations, J. Plankton Res., 14(8), 1031–1054, doi:10.1093/plankt/14.8.1031, 1992.

958 Lafond, A., Leblanc, K., Legras, J., Cornet, V. and Quéguiner, B.: The structure of diatom communities
959 constrains biogeochemical properties in surface waters of the Southern Ocean (Kerguelen Plateau), J. Mar. Syst.,
960 212, 103458, doi:10.1016/j.jmarsys.2020.103458, 2020.

961 Lasbleiz, M., Leblanc, K., Armand, L. K., Christaki, U., Georges, C., Obernosterer, I. and Quéguiner, B.:
962 Composition of diatom communities and their contribution to plankton biomass in the naturally iron-fertilized
963 region of Kerguelen in the Southern Ocean, FEMS Microbiol. Ecol., 92(11), fiw171,
964 doi:10.1093/femsec/fiw171, 2016.

965 van Leeuwe, M. A. and Stefels, J.: Effects of iron and light stress on the biochemical composition of Antarctic
966 Phaeocystis sp. (Prymnesiophyceae). II. Pigment composition, J. Phycol., 34(3), 496–503, doi:10.1046/j.1529-
967 8817.1998.340486.x, 1998.

van Leeuwe, M. A., Kattner, G., van Oijen, T., de Jong, J. T. M. and de Baar, H. J. W.: Phytoplankton and pigment patterns across frontal zones in the Atlantic sector of the Southern Ocean, Mar. Chem., 177, 510–517, doi:10.1016/j.marchem.2015.08.003, 2015.

van Leeuwe, M. A., Tedesco, L., Arrigo, K. R., Assmy, P., Campbell, K., Meiners, K. M., Rintala, J.-M., Selz, V., Thomas, D. N. and Stefels, J.: Microalgal community structure and primary production in Arctic and Antarctic sea ice: A synthesis, Elem. Sci. Anthr., 6, 4, doi:10.1525/elementa.267, 2018.

van Leeuwe, M. A., Webb, A. L., Venables, H. J., Visser, R. J. W., Meredith, M. P., Elzenga, J. T. M. and Stefels, J.: Annual patterns in phytoplankton phenology in Antarctic coastal waters explained by environmental drivers, Limnol. Oceanogr., 65(7), 1651–1668, doi:10.1002/lno.11477, 2020.

van Leeuwe, M. A., Fenton, M., Davey, E., Rintala, J.-M., Jones, E. M., Meredith, M. P. and Stefels, J.: On the phenology and seeding potential of sea-ice microalgal species, Elem. Sci. Anthr., 10, 1, doi:10.1525/elementa.2021.00029, 2022.

Leu, E., Mundy, C. J., Assmy, P., Campbell, K., Gabrielsen, T. M., Gosselin, M., Juul-Pedersen, T. and Gradinger, R.: Arctic spring awakening – Steering principles behind the phenology of vernal ice algal blooms, Prog. Oceanogr., 139, 151–170, doi:10.1016/j.pocean.2015.07.012, 2015.

Ligowski, R., Godlewski, M. and Łukowski, A.: Sea ice diatoms and ice edge planktonic diatoms at the nothern limit of the Weddell Sea pack ice, Proc. NIPR Symp. Polar Biol., 5, 9–20, 1992.

Löder, M. G. J., Meunier, C., Wiltshire, K. H., Boersma, M. and Aberle, N.: The role of ciliates, heterotrophic dinoflagellates and copepods in structuring spring plankton communities at Helgoland Roads, North Sea, Mar. Biol., 158(7), 1551–1580, doi:10.1007/s00227-011-1670-2, 2011.

Mackey, M. D., Mackey, D. J., Higgins, H. W. and Wright, S. W.: CHEMTAX - A program for estimating class abundances from chemical markers: Application to HPLC measurements of phytoplankton, Mar. Ecol. Prog. Ser., 144(1–3), 265–283, doi:10.3354/meps144265, 1996.

Van den Meersche, K., Soetaert, K. and Middelburg, J. J.: A Bayesian compositional estimator for microbial taxonomy based on biomarkers, Limnol. Oceanogr. Methods, 6(5), 190–199, doi:10.4319/lom.2008.6.190, 2008.

Mendes, C. R. B., Tavano, V. M., Kerr, R., Dotto, T. S., Maximiano, T. and Secchi, E. R.: Impact of sea ice on the structure of phytoplankton communities in the northern Antarctic Peninsula, Deep. Res. Part II Top. Stud. Oceanogr., 149(December 2017), 111–123, doi:10.1016/j.dsr2.2017.12.003, 2018.

Moreau, S., Kauko, H. M., Ryan-Keogh, T., Singh, A. and Bratbak, G.: Southern Ocean Ecosystem cruise 2019 biogeochemistry [Data set], , doi:10.21334/npolar.2021.28fbddd2, 2020.

Nöthig, E.-M., Assmy, P., Klaas, C. and Scharek, R.: Phyto-and protozooplankton in polar waters, in Biological Studies in Polar Oceans: Exploration of Life in Icy Waters, edited by G. Hempel and I. Hempel, pp. 65–73, Wirtschaftsverlag NW, Bremerhaven, Germany., 2009.

Ogundare, M. O., Fransson, A., Chierici, M., Joubert, W. R. and Roychoudhury, A. N.: Variability of sea-air carbon dioxide flux in Autumn across the Weddell Gyre and offshore Dronning Maud Land in the Southern

Ocean, Front. Mar. Sci., 7, 614263, doi:10.3389/fmars.2020.614263, 2021.

Oksanen, J., Blanchet, F. G., Friendly, M., Kindt, R., Legendre, P., McGlinn, D., Minchin, P. R., O'Hara, R. B., Simpson, G. L., Solymos, P., Stevens, M. H. H., Szoecs, E. and Wagner, H.: vegan: Community Ecology Package, [online] Available from: https://cran.r-project.org/package=vegan, 2017.

Le Paih, N., Hattermann, T., Boebel, O., Kanzow, T., Lüpkes, C., Rohardt, G., Strass, V. and Herbette, S.: Coherent seasonal acceleration of the Weddell Sea boundary current system driven by upstream winds, J. Geophys. Res. Ocean., 125, e2020JC016316, doi:10.1029/2020jc016316, 2020.

Pančić, M. and Kiørboe, T.: Phytoplankton defence mechanisms: traits and trade-offs, Biol. Rev., 93(2), 1269–1303, doi:10.1111/brv.12395, 2018.

Peeken, I.: Photosynthetic pigment fingerprints as indicators of phytoplankton biomass and development in different water masses of the Southern Ocean during austral spring, Deep. Res. Part II Top. Stud. Oceanogr., 44(1–2), 261–282, doi:10.1016/S0967-0645(96)00077-X, 1997.

Pollard, R. T., Salter, I., Sanders, R. J., Lucas, M. I., Moore, C. M., Mills, R. A., Statham, P. J., Allen, J. T., Baker, A. R., Bakker, D. C. E., Charette, M. A., Fielding, S., Fones, G. R., French, M., Hickman, A. E., Holland, R. J., Hughes, J. A., Jickells, T. D., Lampitt, R. S., Morris, P. J., Nédélec, F. H., Nielsdóttir, M., Planquette, H., Popova, E. E., Poulton, A. J., Read, J. F., Seeyave, S., Smith, T., Stinchcombe, M., Taylor, S., Thomalla, S., Venables, H. J., Williamson, R. and Zubkov, M. V.: Southern Ocean deep-water carbon export enhanced by natural iron fertilization, Nature, 457(7229), 577–580, doi:10.1038/nature07716, 2009.

Poulin, M., Daugbjerg, N., Gradinger, R., Ilyash, L., Ratkova, T. and von Quillfeldt, C.: The pan-Arctic biodiversity of marine pelagic and sea-ice unicellular eukaryotes: A first-attempt assessment, Mar. Biodivers., 41(1), 13–28, doi:10.1007/s12526-010-0058-8, 2011.

Quéguiner, B.: Iron fertilization and the structure of planktonic communities in high nutrient regions of the Southern Ocean, Deep. Res. Part II Top. Stud. Oceanogr., 90, 43–54, doi:10.1016/j.dsr2.2012.07.024, 2013.

R Core Team: R: A language and environment for statistical computing, 2017.

Rembauville, M., Briggs, N., Ardyna, M., Uitz, J., Catala, P., Penkerc'h, C., Poteau, A., Claustre, H. and Blain, S.: Plankton assemblage estimated with BGC-Argo floats in the Southern Ocean: Implications for seasonal successions and particle export, J. Geophys. Res. Ocean., 122(10), 8278–8292, doi:10.1002/2017JC013067, 2017.

Roy, S., LLewellyn, C. A., Egeland, E. S. and Johnsen, G., Eds.: Phytoplankton Pigments - Characterization, Chemotaxonomy and Applications in Oceanography, 1. edition., Cambridge University Press, Cambridge., 2011.

Sachs, O., Sauter, E. J., Schlüter, M., Rutgers van der Loeff, M. M., Jerosch, K. and Holby, O.: Benthic organic carbon flux and oxygen penetration reflect different plankton provinces in the Southern Ocean, Deep. Res. Part I Oceanogr. Res. Pap., 56(8), 1319–1335, doi:10.1016/j.dsr.2009.02.003, 2009.

Schulz, I., Montresor, M., Klaas, C., Assmy, P., Wolzenburg, S., Gauns, M., Sarkar, A., Thiele, S., Wolf-Gladrow, D., Naqvi, W. and Smetacek, V.: Remarkable structural resistance of a nanoflagellate-dominated

plankton community to iron fertilization during the Southern Ocean experiment LOHAFEX, Mar. Ecol. Prog. Ser., 601, 77–95, doi:10.3354/meps12685, 2018.

Smetacek, V., Assmy, P. and Henjes, J.: The role of grazing in structuring Southern Ocean pelagic ecosystems and biogeochemical cycles, Antarct. Sci., 16(4), 541–558, doi:10.1017/S0954102004002317, 2004.

Smetacek, V., Klaas, C., Strass, V. H., Assmy, P., Montresor, M., Cisewski, B., Savoye, N., Webb, A., D'Ovidio, F., Arrieta, J. M., Bathmann, U., Bellerby, R., Berg, G. M., Croot, P., Gonzalez, S., Henjes, J., Herndl, G. J., Hoffmann, L. J., Leach, H., Losch, M., Mills, M. M., Neill, C., Peeken, I., Röttgers, R., Sachs, O., Sauter, E., Schmidt, M. M., Schwarz, J., Terbrüggen, A. and Wolf-Gladrow, D.: Deep carbon export from a Southern Ocean iron-fertilized diatom bloom, Nature, 487(7407), 313–319, doi:10.1038/nature11229, 2012.

de Steur, L., Holland, D. M., Muench, R. D. and Mcphee, M. G.: The warm-water "'Halo'" around Maud Rise: Properties, dynamics and impact, Deep Sea Res. I, 54, 871–896, doi:10.1016/j.dsr.2007.03.009, 2007.

Saavedra-Pellitero, M., Baumann, K.-H., Flores, J.-A. and Gersonde, R.: Biogeographic distribution of living coccolithophores in the Pacific sector of the Southern Ocean, Mar. Micropaleontol., 109, 1–20, 2014.

Tran, S., Bonsang, B., Gros, V., Peeken, I., Sarda-Esteve, R., Bernhardt, A. and Belviso, S.: A survey of carbon monoxide and non-methane hydrocarbons in the Arctic Ocean during summer 2010, Biogeosciences, 10(3), 1909–1935, doi:10.5194/bg-10-1909-2013, 2013.

Tréguer, P., Bowler, C., Moriceau, B., Dutkiewicz, S., Gehlen, M., Aumont, O., Bittner, L., Dugdale, R., Finkel, Z., Iudicone, D., Jahn, O., Guidi, L., Lasbleiz, M., Leblanc, K., Levy, M. and Pondaven, P.: Influence of diatom diversity on the ocean biological carbon pump, Nat. Geosci., 11(1), 27–37, doi:10.1038/s41561-017-0028-x, 2018.

Trull, T. W., Passmore, A., Davies, D. M., Smit, T., Berry, K. and Tilbrook, B.: Distribution of planktonic biogenic carbonate organisms in the Southern Ocean south of Australia: A baseline for ocean acidification impact assessment, Biogeosciences, 15(1), 31–49, doi:10.5194/bg-15-31-2018, 2018.

Vallina, S. M., Follows, M. J., Dutkiewicz, S., Montoya, J. M., Cermeno, P. and Loreau, M.: Global relationship between phytoplankton diversity and productivity in the ocean, Nat. Commun., 5, 4299, doi:10.1038/ncomms5299, 2014.

Venables, W. N. and Ripley, B. D.: Modern applied statistics with S, 4. edition., Springer, New York., 2002.

Vernet, M., Geibert, W., Hoppema, M., Brown, P. J., Haas, C., Hellmer, H. H., Jokat, W., Jullion, L., Mazloff, M., Bakker, D. C. E., Brearley, J. A., Croot, P., Hattermann, T., Hauck, J., Hillenbrand, C.-D., Hoppe, C. J. M., Huhn, O., Koch, B. P., Lechtenfeld, O. J., Meredith, M. P., Naveira Garabato, A. C., Nöthig, E.-M., Peeken, I., van der Loeff, M. M. R., Schmidtko, S., Schröder, M., Strass, V. H., Torres-Valdés, S. and Verdy, A.: The Weddell Gyre, Southern Ocean: Present knowledge and future challenges, Rev. Geophys., 57(3), 623–708, doi:10.1029/2018RG000604, 2019.

Wright, S.: Chemtax version 1.95 for calculating the taxonomic composition of phytoplankton populations, , Accessed: 2020-11-27, doi:10.4225/15/59fff1c5ea8fc, 2008.

1073 Wright, S. W., van den Enden, R. L., Pearce, I., Davidson, A. T., Scott, F. J. and Westwood, K. J.:

1074 Phytoplankton community structure and stocks in the Southern Ocean (30-80°E) determined by CHEMTAX

1075 analysis of HPLC pigment signatures, Deep. Res. Part II Top. Stud. Oceanogr., 57(9–10), 758–778,

1076 doi:10.1016/j.dsr2.2009.06.015, 2010.

1077 Zapata, M., Jeffrey, S. W., Wright, S. W., Rodríguez, F., Garrido, J. L. and Clementson, L.: Photosynthetic

1078 pigments in 37 species (65 strains) of Haptophyta: Implications for oceanography and chemotaxonomy, Mar.

1079 Ecol. Prog. Ser., 270, 83–102, doi:10.3354/meps270083, 2004.

1080